STEADY-STATE VISCOPLASTIC ANALYSIS OF METAL FLOW DURING COLD DRAWING

By

VASUDEVA PRASAD RAVI

Bachelor of Engineering

Osmania University

Hyderabad, India

1988

Submitted to the Faculty of the
Graduate College of the
Oklahoma State University
in partial fulfillment of
the requirements for
the Degree of
MASTER OF SCIENCE
May, 1992

STEADY-STATE VISCOPLASTIC ANALYSIS OF

METAL FLOW DURING COLD DRAWING

Thesis Approved:

Y. C. Shin 4/21/92

Thesis Adviser

Don A. Lucca 4/21/92

James K. Good 4/22/92

Thomas C. Collins

Dean of the Graduate College

PREFACE

The three-dimensional finite-element method is applied to the metal forming process of drawing rectangular bars from rectangular billets. The rigid-viscoplastic formulation is modified to incorporate the steady-state nature of the drawing process.

Various methods of analysis of the drawing process are summarized. Application of the three-dimensional finite element method to other forming process like forging, rolling and extrusion are reviewed. Also presented is the finite element method applied to the analysis of steady-state processes.

Simulations were performed under various conditions of the process parameters such as drawing velocity, die-workpiece interface friction, die angle, and area reduction. Velocity distributions, steady-state drawing loads, die-pressure distribution, flow stress, average stresses, effective strain-rates and principle stresses predicted for different simulation conditions are compared. The results are then discussed to gain insight into the mechanics of metal deformation during drawing.

The author wishes to express his deepest gratitude and sincere appreciation to his advisor, Dr. Yuh-Cheng Shiau for his exceptional guidance, encouragement and warm personal care throughout the present investigations. The author is also grateful to Dr. Don A. Lucca and Dr. J. K. Good for reviewing the manuscript and for their helpful suggestions.

He also wishes to thank his parents for their endless encouragement, patience and support. Thanks are also due to his colleagues and friends for their valuable discussions and their help in preparing the manuscript.

Research support from ALCOA Technical Center and National Center for Super Computing Applications are gratefully acknowledged. Thanks are also due to National Standard Company for providing samples of drawn wire for microstructural studies.

TABLE OF CONTENTS

Chapter Page

LIST OF FIGURES

Figure Page

CHAPTER I

INTRODUCTION

With escalating energy and labor costs, near net-shape forming has become the most competitive manufacturing method. Not only do costs favor forming, but technological requirements have increased in importance as specifications have tightened to suit more exacting operational conditions. Traditionally, the characteristics of wrought products have been strength and long fatigue life. But now, in addition, high quality surface finish, high dimensional accuracy, precise shape and consistent composition, are all economically attainable by forming, i.e without recourse to metal removal operations. The analysis of forming processes poses a range of complex problems in continuum mechanics and heat transfer. Numerical, computer based methods for the analysis of forming processes have recently started to make important contributions. By means of deformation analysis, die designers can obtain necessary information such as die-cavity filling, stress, strain and forming loads. These methods of analysis are capable of evaluating the effects of process parameters, so that die designers can find an optimum process and its associated conditions.

Of the various numerical, computer based methods, the finite element method (FEM) has become an indispensable and powerful tool for process modeling. Many industrial forming processes like cold drawing are three dimensional in nature. Thus the development of finite element programs with three dimensional analysis capability has been one of the recent research areas in process modeling. Further development of the FEM

approach is done in the present work by modifying the computer program 'Analysis of Large Plastic Incremental Deformation for Three Dimensional Forming (ALPID-3D)'.

This study provides a better understanding of metal deformation and therefore helps in optimizing process parameters to improve the dimensional accuracy, grain size distribution and corner filling of the rectangular cross section. For bars with a high aspect ratio, twisting is also often observed along the length direction as well as on the cross section. A better understanding of metal flow and die deformation facilitates the elimination or modification of some of the heat treatment and surface preparatory steps in the cold drawing process.

CHAPTER II

REVIEW OF THE DRAWING PROCESS

Introduction

Like most metal forming processes, drawing evolved through experience rather than by the application of scientific principles. However in the past four decades, the analytical approach has come to play a significant part in its further development. Of late, numerical methods are ever increasingly being used for understanding and developing more complicated real life drawing processes.

In the drawing process the cross-section area and/or shape of a rod, bar, tube or wire is reduced by pulling through a die with a tapered bore of required shape. Sufficient stresses (combination of tensile and compressive) are generated in the metal by the pull and the nip of the die for the drawn metal to deform plastically within the confines of the die. Products previously rolled, extruded, or fabricated, with a solid or hollow cross-section are drawn at velocities as high as several thousand feet per minute [Altan et al, 1983], [ASM Metals Hand Book, 1970]. The die geometry determines the final dimensions, cross-sectional area, and the reduction in area of the drawn product. The reduction in size attainable is limited by the pull that the wire/rod can sustain without breaking; hence, for large reductions, the process has to be usually repeated many times. This repetition is achieved by passing through consecutively located dies. But for a few exemptions like drawing of tungsten wire for lamp filaments, drawing is usually conducted at room temperature. After a number of drawn passes, annealing may be necessary to eliminate the

effects of strain hardening, that is, to reduce the flow stress and increase ductility before the drawing process is continued.

Larger drawn sections that cannot be wound as coils are called bars or rods. The deformation behavior of wires and rods is different only with regard to their geometries [Lange, 1985]. In drawing, the cross-section is usually round but can be a shape. A few examples of drawn shapes are illustrated in Fig. 2.1. In the cold drawing of shapes, the basic contour of the incoming shape is established by cold-rolling passes that are usually preceded by annealing. After rolling, the section shape is refined and reduced to close tolerances by cold drawing. A number of annealing steps may be needed in drawing of shapes too.

The reduction of cross-sectional area per pass, $r = (A_0 - A_1)/A_0$, where A_0, A_1 are the cross-sectional area at the entry and exit, respectively. The reduction is generally between 0.15 to 0.25 in drawing of fine wires, and between 0.20 to 0.45 in drawing coarser sizes. Drawing speeds range from 100 to 8000 ft/min, depending on size, metal and the particular pass of a continuous machine.

Most dies used in drawing are trumpet-shaped, but the curvature is so small that it can be neglected simplifying the die shape into a frustum of a cone as in Fig. 2.2. Deformation of metal takes place in the conical part of the die. Half die angles range from 2^{o} to 12^{o}. The entry to the die is bell shaped to help die lubrication. The cylindrical (or shaped) portion of the die exit preserves the operative size of the bore in the face of wear and does not play any part in plastic deformation. Its length usually varies from zero to about twice the wire diameters.

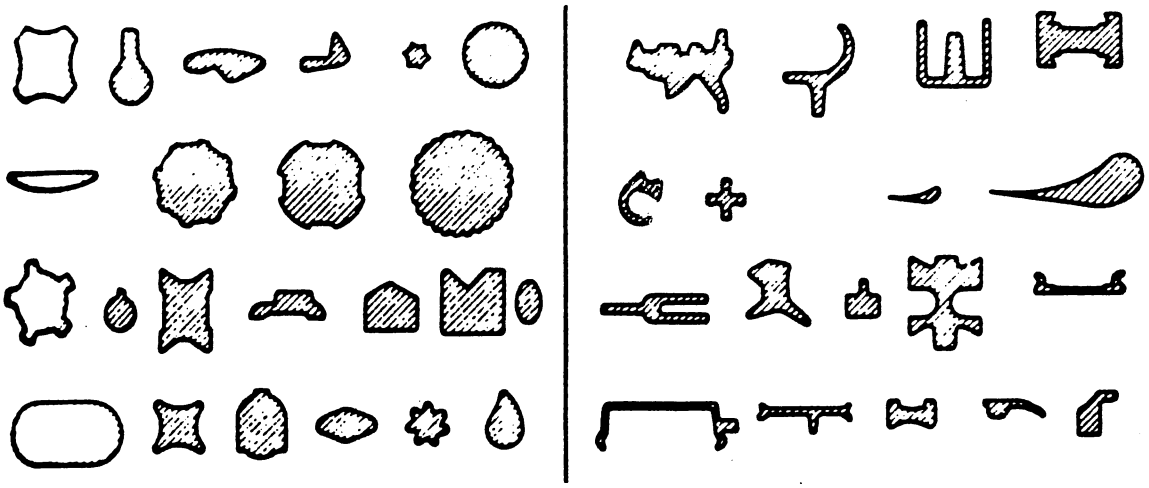

Profiles drawn from Square or Round Slabs

Profiles Requiring Prerolled Slab

Figure 2.1 Samples of Drawn Profiles [Lange, 1974]

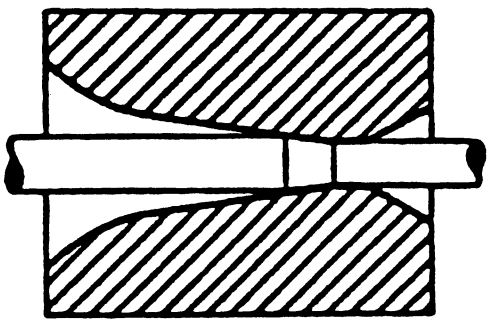

Figure 2.2 Wire Drawing Die

Material Flow, Stress, and Forces in Drawing

The assumption that deformation is homogeneous is applicable only under favorable friction conditions and for small strains. The greater the half die angle, the greater is the inhomogeneity of strain distribution across the section. The shape of the deformation zone (Fig. 2.3) has been experimentally established by Wistreich [1958], among others. The plastic zone is made visible by etching. This shape is confirmed by the slip-line theory [Hill and Tupper, 1948]. It is seen from Fig. 2.3 that the deformation zone is not bounded by straight lines, extends further on the tool surface, and is very small at the axis of the workpiece.

The stresses in drawing are explained here using the deformation zone predicted by the slip-line field. The deformation zone for frictionless strip drawing as obtained by the slip-line fields [Lange, 1985] is shown in Fig. 2.4. In plane-strain drawing the axial stress σ_z increases from the entry to the deformation zone toward the exit. It has its maximum (tensile) value at the entry on the drawing axis, and might become compressive near the tool surface. This pattern is observed in the Mohr's stress circles shown in Fig. 2.4. Due to the interaction between the applied tensile drawing forces and the reactive compressive stress on the tool surfaces, all possible stress conditions from biaxial tension to biaxial compression exist in drawing. As maximum values of axial stress σ_z (tensile) occur near the axis, cracks occur in this vicinity. In case of strip drawing, the radial stresses σ_r are highest (compressive) near the tool surface at both the entry and exit. The tangential stresses σ_t (compressive) are of the same order of magnitude and have a similar distribution as the radial stress.

Equivalent strain-rates $\dot{\bar{\varepsilon}}$ are especially high in three regions of the deformation zone, (1) around the drawing axis, (2) the material entry near the tool surface, and (3) the material exit near the tool surface. Across any cross-section the maximum strains occur

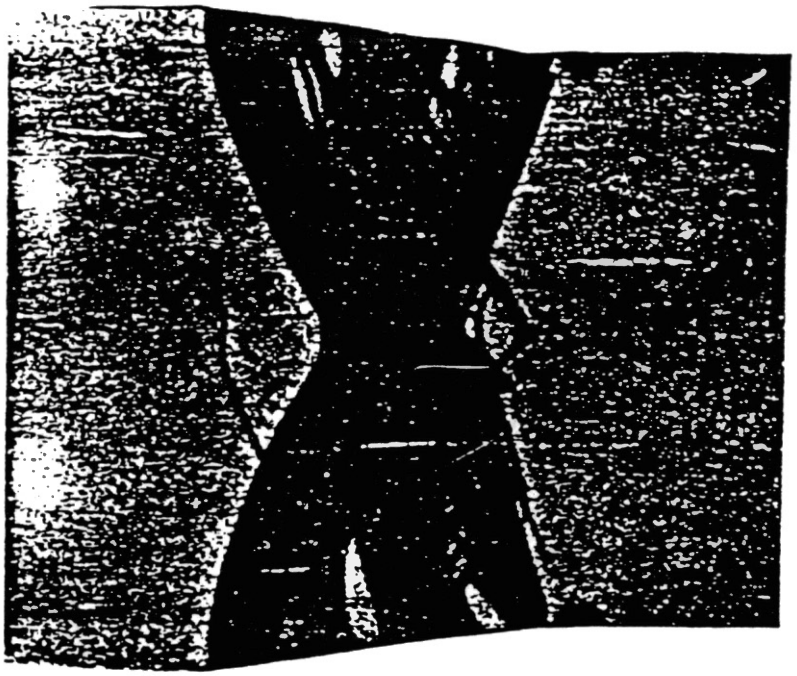

Figure 2.3 Shape of Deformed Zone in Drawing [Wistreich, 1958]

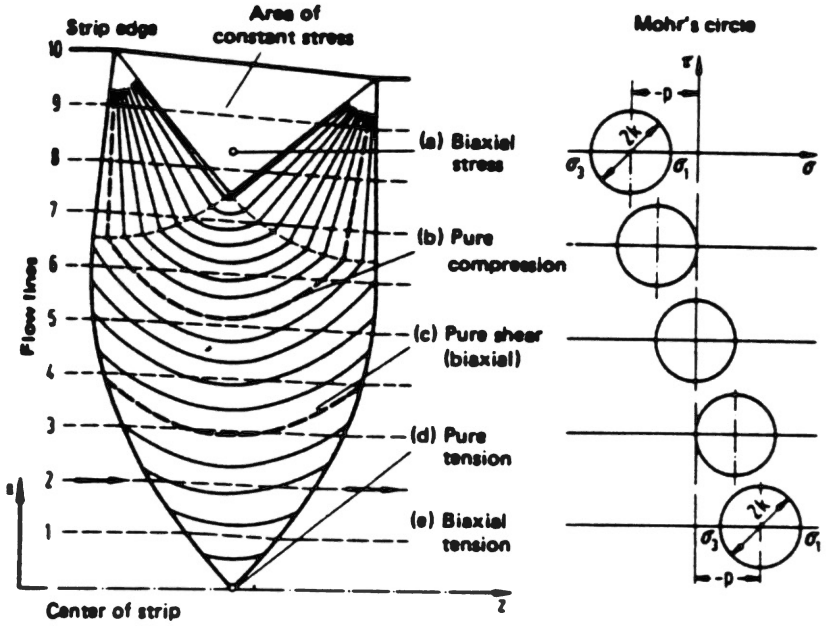

Figure 2.4 Deformation Zone in Plane-Strain Drawing Represented by Lines of Equal Average Pressure [Lange, 1985]

along the flow lines in these three regions. The lowest equivalent strains occur near the material axis. The equivalent strain-rate at these points represents the homogeneous deformation ratio. The equivalent strains increase towards the boundary. Therefore for a work-hardening material the hardness distribution along the section will show lower values near the axis and higher values near the boundary (surface). An increase in the coefficient of friction μ, moves the deformation zone towards the material entry and has the effect of increasing the the shear stress τ_{rz} near the tool surfaces.

The solution for the calculation of the force required for drawing can be written as [Schey, 1983]

$$P = \sigma_{fm}(1+\mu \cot\alpha)\, \phi\, \varepsilon = \sigma_{fm} Q \qquad (2.1)$$

where P is the force required for drawing, σ_{fm} the mean flow stress, ε the strain, μ is the coefficient of friction, α the half die angle, Q the pressure-multiplying factor and ϕ is determined experimentally. For wire drawing $\phi = 0.88 + 0.12$ h/L and for plane-strain drawing $\phi = 0.8 + 0.2$ h/L, where h is the mean workpiece diameter, and L the contact length. The drawing force consists of three components; (1) the force required for supplying the pure deformation work, which is proportional to the strain and the flow stress values, (2) the force required to overcome friction, which for a given reduction increases with increasing interface shear strength and decreases with increasing half die angle as this in turn decreases the sliding length, (3) the contribution of redundant work due to inhomogeneous deformation, which increases, as in other processes, with an increasing h/L ratio. For a given reduction, the ratio increases with increasing half die angle as L decreases. This results in the rise of the interface pressure at the entry and exit of the die.

Heat and Temperatures in Drawing

Deformation and friction are the two sources of heat during drawing. Most of the work expended in drawing is converted into heat. About 85-95% of the deformation work is converted to heat energy in the case of metals deformed below the recrystallization temperature (as in cold drawing). Due to the high speeds involved in drawing, the heat is often evolved within a millisecond or less. This results in high temperatures and steep temperature gradients. The mass of the die is small and is in continuous contact with the wire, making heating a serious problem. The temperature difference between the wire surface and the core results in harmful residual stresses. Temperature gradients in the boundary layers lead to different expansions over the cross-section of a wire, which in turn results in residual stresses also. In ferrous and other alloys, high temperatures may speed up age hardening, lowering the ductility of the drawn wire. The temperature increase ΔT of a volume element in the wire, assuming homogeneous deformation is given by

$$\Delta T = \sigma_{f,m} \ln \left(\frac{A_0}{A_1}\right) \frac{1}{c\rho} \tag{2.2}$$

where c is specific heat and ρ is density. From the above equation it can be seen that the temperature increase is dependent on the natural strain. The friction between the lubricant and the wire surface area along the deformation zone and the concentration of redundant work at the die surface contribute to further increase in temperature in the boundary areas. With increase of drawing velocity, less heat flows into the die compared to heat generated in the deformation zone. Surface temperatures along the deformation zone increase with increasing drawing velocity as shown in Fig. 2.5 (a). The temperature at the material boundary increases steeply when the material enters the deformation zone. The temperature flattens before increasing at the die exit. The temperature at the center of the bar does not vary very much with velocity. It should be noted that the frictional heat is constant for all

drawing velocities, but the frictional work is concentrated in a thinner layer near the boundary for higher drawing velocities due to the time dependence of heat conduction. The temperature profile across the wire cross-section at the die exit is shown in Fig. 2.5 (b). The temperature distribution in the die for a drawing speed of 1400 ft/min is shown in Fig. 2.6 [Ranger, 1957]. Steep gradients exist at the die entry and exit.

Die cooling is another important thermal aspect of drawing. The fraction of frictional heat entering the die at high drawing speeds is very small. The die inlet is at a lower temperature as it is cooled by the incoming wire.

Friction in Drawing

Friction in drawing is equivalent to a back tension and thus lowers the interface pressure, but at the expense of higher drawing forces. Frictional contributions increase with increasing interface shear strength for a given reduction and decrease with increasing half die angle because of a decrease in sliding length. Friction is usually assumed constant in the analysis of a drawing process for a given drawing condition. The force required to draw a wire through a die depends upon several factors, the two most important of which are the friction of the wire on the walls of the die and the resistance of the wire to plastic deformation. Numerous attempts have been made to determine the coefficient of friction in a drawing operation.

Davis and Dokos [1944] derived a mathematical formula relating the drawing force with the reduction in area using the maximum shear stress criterion.

$$\sigma_f = \frac{1+k}{k}\left\{ 3\Omega \ln\frac{A_o}{A_f} - \left(\frac{3\Omega}{k} - \sigma_o\right)\left[1 - \left(\frac{A_f}{A_o}\right)^k\right]\right\} + \sigma_1 \left(\frac{A_f}{A_o}\right)^k \qquad (2.3)$$

Where σ_f is the drawing stress, k is the ratio of coefficient of friction (μ) and the semi die angle (α), Ω is the coefficient of strain hardening in shear, σ_o is idealized yield stress, σ_1 is

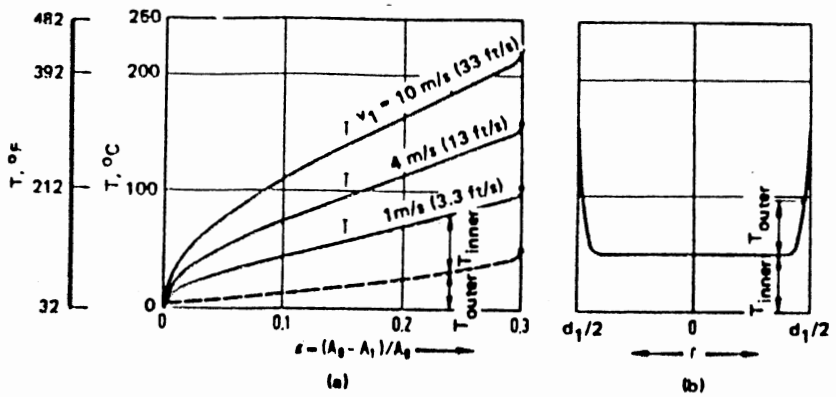

Figure 2.5 (a) Surface Temperature Along Deformation Zone at Different Velocities
(b) Temperature Profile at Material Exit [Lange, 1985]

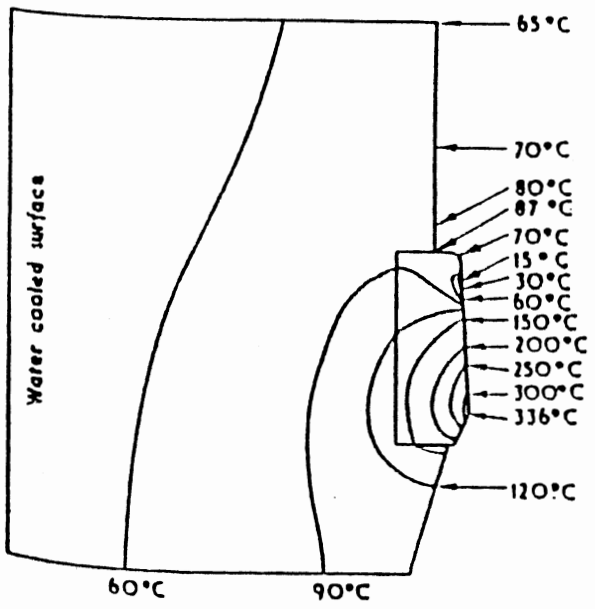

Figure 2.6 Temperature Distribution in Die at 1400 ft/min [Ranger, 1957]

stress at the boundary between elastic and plastic regions, A_o and A_f are the initial and final areas of wear. The formula considers the effects of strain hardening and the frictional effects at the die-wire interface. Maclellan [1948] suggested a means of determining μ on the basis of the measurement of the resultant axial reaction force (F) on the die and the resultant force (F_s) on one half of the die, in the plane perpendicular to the wire axis. From Fig. 2.7

$$F_s = \bar{\sigma}_n(A_o - A_f)(\cot\alpha - \mu) \tag{2.4a}$$

$$F = \bar{\sigma}_n(A_o - A_f)(1 + \mu\cot\alpha) \tag{2.4b}$$

where $\bar{\sigma}_n$ is the mean value of the normal stress between the wire and the die. It follows that,

$$\mu = \frac{F\cot\alpha - F_s}{F + F_s\cot\alpha} \quad \text{and} \quad \bar{\sigma}_n = \frac{F + F_s\cot\alpha}{(A_o - A_f)\,\mathrm{cosec}^2\alpha} \tag{2.5}$$

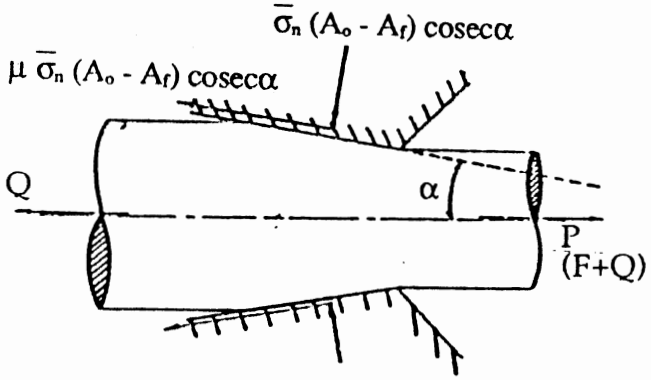

Figure 2.7 Forces Acting on a Wire

Some effects of frictional drag on the die are described below.

(1) The greater the actual reaction on the die due to the frictional drag, the smaller is the "deformation" component of the drawing force.

(2) The mean value of normal stress $\bar{\sigma}_n$ decreases with increasing μ.

(3) Eqn. (2.4a) gives the die splitting force, F_s as a function of $\bar{\sigma}_n$ and μ, and indicates that F_s should decrease with increasing μ. This arises from the fact that practical values of α make $\cot\alpha$ very much larger than any physically probable values of μ making $(\cot\alpha - \mu)$ independent of μ. F_s is thus approximately proportional to $\bar{\sigma}_n$ and should therefore decrease with increasing μ.

(4) The average shear stress at the interface, $\mu\bar{\sigma}_n$ increases with μ but at a slower rate. Thus a reduction in μ would reduce the interfacial shear stress and a correspondingly small reduction of the average wear.

(5) The pressure between wire and die is much more sensitive to friction than the drawing force.

Different experimental methods developed by several investigators for determining the coefficient of friction are described in the later sections.

Lubrication in Drawing

The method of lubrication used in a drawing operation generally depends on whether the surface finish is of importance or the order of the size reduction. To achieve good surface finish, solid friction or lubrication is more suitable. Hydrodynamic lubrication is the best choice when there is a large reduction in size of the wire. In hydrodynamic lubrication, the wire and die are completely and permanently separated throughout the running period. This can be achieved by feeding the lubricant into the die/wire interface at the pressure prevailing there. This reduces friction and dissipates the heat generated effectively.

As yet, the exact nature of the lubricants function in drawing is not well understood. This is due to the fact that the pressures are of the order of a few hundred thousand psi and that one of the surfaces is constantly moving away from the other. However, it is considered that at low speeds, boundary lubrication exists, and as the speed is increased an increasing proportion of the load is supported by fluid pressure. The friction rapidly decreases to a minimum and fluid lubrication is established.

Experiments [Wistreich, 1951] have shown that the film thickness is greater if a small die angle is employed and if the reduction is slight and the wire is soft. The film thickness in dry drawing are comparable to the surface roughness of the wire. The conditions are, however, unsteady and the presence of die particle debris attached to the wire causes continuous changes of the wire surface. This has been considered to cause a rapid sequence of formation and collapse of hydrodynamic films. The regime is intermediate between the true boundary and hydrodynamic state and is termed "quasi-hydrodynamic."

In dry drawing, the surface of the wire is coated with various lubricants, depending on its strength and frictional characteristics. A common lubricant is soap. The soap is picked up by the "pickled" wire as it goes through a box filled with soap powder.

In wet drawing, the dies and rods are completely immersed in a lubricant. Typical lubricants are oils and emulsions containing fatty or chlorinated additives, and various chemical compounds.

Wear in Drawing

Wear in drawing is caused by a combination of abrasion, adhesion, fatigue, corrosion, erosion, cavitation, or thermal effects. Of these the first three are the most active. The body abrasion is one of the most common forms of wear mechanism prevalent in wire drawing. Harper et al [1970] reported that wear increases as the lubricant ages, the aging causes the lubricant to be contaminated with particulate debris. They suggest that

lubricants that do not retain the dust in suspension be chosen or to apply ultrasonic vibrations, or add oxidizing agents to remove the dust particles. Adhesion is the primary cause of wear in tungsten carbide dies. In carbide dies, microscopic welding of the wire and the carbide binder can result in dislodgment of carbide grains. Thus adhesive wear depends both on the sticking or reactive tendency between the wire and the die constituents and the strength of interparticle bonding within the die. Ringing in dies is a form of grooving near the entry of the wire, the suppression of which might result in better die performance. Wistreich [1951, 1958] concluded from experiments that, generally, ringing is not caused by the abrasive action of a contaminated lubricant, but is the result of the steep stress gradients at the beginning of the working surface of the die. The plane of impingement of the wire on the die oscillates about a mean position because of irregularities of size and vibration of the wire. This causes a narrow zone of the die bore to be subjected to cyclic loading causing failure by fatigue. It leads to roughness and longitudinal grooving of the working surface of the die, resulting in the appearance of ridges on the wire. It can be reduced greatly by applying heavy back pull to the wire, and accurate alignment and elimination of vibration by guide pulleys.

In a typical die, wear occurs at three major points: (1) Severe wear at the point where the wire enters the die results in "ringing." The change in entry geometry changes the film thickness and thus the surface finish of the product. (2) Wear of the draw cone changes the geometry of operation and affects film thickness. (3) Wear of the die land is directly responsible for the loss of tolerances, and also affects the surface finish of the product. If wear of a wire is non-uniform, the wire acquires a non-circular profile.

The intensity of wear varies markedly along the die-wire interface, it is the least in the middle, more at the exit, and greatest at the entry. Papsdorf [1952] found that wear increases linearly with the length of the wire drawn. There is a phase of early rapid wear, which is attributed to the removal of the asperities in a new die, and an acceleration in the last stage, which is associated with heavy ringing.

Tools for Drawing

Proper tool design is the most important aspect of the drawing process, it is critical for the economic production of quality wire or bar. In most of the methods used for the cold drawing of rod, wire, and tubes of small diameter, the machines are designed such that the products are uncoiled, drawn, and then re-coiled. This process of uncoiling and recoiling is repeated at successive stations on multiple-die continuous machines.

The preparation of the part to be drawn consists of heat treatment, surface preparation, and pointing. These steps depend on the state of the part before drawing and on the requirements after drawing. On preparing the wire or rod to be drawn, it is coiled and placed on a payoff tray, stand or reel so as to permit easy unwinding of the stock. The pointed, leading end of the wire or bar is inserted through the drawing die and sized by a gripper attached to a powered cylindrical block or capstan. In case a liquid lubricant is used, the die is fully submerged in the lubricant. In the case of so-called dry machines, the die is mounted in an adapter within a box which contains grease, dry soap, oil, or other lubricants through which the stock must pass before reaching the die.

Drawing machines can be broadly classified into, (1) bull blocks, (2) dry-drawing continuous machines, and (3) drawbenches. Bull blocks are used extensively for breakdown, finishing, or sizing operations on large-diameter ferrous and nonferrous rod and wire. The production capacity of these machines is low compared to the continuous machines. The spindles of these machines are generally vertical, with the spindle blocks revolving in a horizontal plane. For large diameter stock this arrangement is sometimes reversed. Other modification such as a double deck arrangement to perform two drafts at a time, external air and internal water cooling of the block and riding-type block-stripping spiders for direct coiling and wire removal are available.

There are two types of continuous drawing machines; dry-drawing nonslip-type and wet-drawing slip-type. The dry-type are generally used for drawing ferrous metals and

the wet-type are generally used for nonferrous rod and wire, as well as fine ferrous wires. Four types of nonslip continuous machines are in use; accumulating-type, double-block accumulating-type, controlled-speed, and straight-through machines. The multiblock accumulating-type machine is equipped with electro-magnetic block clutches. High and low wire accumulation of the wire on individual blocks is sensed by photocells and appropriate block clutches are engaged and disengaged. A single direct-current motor drives a coupled line shaft that carries the clutches. The geometry of these machines imparts a twist to the wire with each revolution of the flyer (a sheave that revolves around the block). This might be undesirable for some applications. In the case of the double-block accumulating machines the two blocks are individually driven. In this, wire is transferred from the first drawing block by means of an intermediate flyer sheave which reverses the direction of the wire (without twisting it) onto a coiling block mounted immediately above the first drawing block. The wire is temporarily held in storage until it is needed by the second block. On the controlled speed machines, the wire follows an essentially flat path from block to block with a constant, unvarying amount of wire storage, without twisting or slipping. A tension arm between blocks, activated by a loop of the wire being drawn, regulates the speed of the adjustable-speed, direct-current motor on the preceding block. Straight-through machines do not have tension arms. For large workpieces the spindles are canted from the vertical axis to accommodate wire buildup on the blocks and to provide unimpended, straight entry into the succeeding die.

On the wet-drawing slip-type machines, the surface speed of the capstans, but for the final capstans, exceeds the speed of the wire being drawn, causing slip of the wire on the capstans. Even though very small reductions per pass can be achieved on these machines, bright surface finishes are produced.

The distinction between wire and rod (or bar) is somewhat arbitrary. The term wire generally refers to smaller-diameter products (< 5 mm, or 0.2 in.) that can be rapidly drawn on multiple-die machines. Larger-diameter products are referred to as rod or bar and

are usually drawn on single-die machines or benches that do not provide for the coiling of the drawn product. Fig. 2.8 shows an in-line drawing and straightening machine for producing cold-drawn bars from hot-rolled steel coils or bars. It has a fixed die box with a recirculating wet-die lubricating system. Drawing is accomplished with three moving grip slides; one slide for punch pointing before the die box and two opposed-motion drawing slides after the die box. The push-pointing grip runs twice as fast as the drawing grips in order to minimize production loss when push pointing. Straightening is done by one set each of vertical and horizontal straightening rollers, and a set of feed-out rolls.

Another commonly used machine for drawing bars is the draw bench (Fig. 2.9). They are long horizontal, high powered, rigidly built machines. The drawing bench essentially consists of a entry conveyor, a die stand, a carriage, and an exit rack. The entry side of the head is provided with a hydraulic pushing device. The pointed heads protruding through the die are grasped by a pneumatically operated grips on the carriage. The carriage is powered by a motor-driven chain of hydraulic piston to slide or roll along ways to pull the bar through the die. The upright head can hold as many as four dies to facilitate drawing of four bars at a time. On exiting the die the bar is released automatically by the carriage. The bar is then removed from the draw bench. The carriage is then rapidly returned to the die stand by a separately powered return system on chain benches or by means of a piston on hydraulic benches for drawing the next bar. At the start, the pulling speed is low but is quickly accelerated to a preset value.

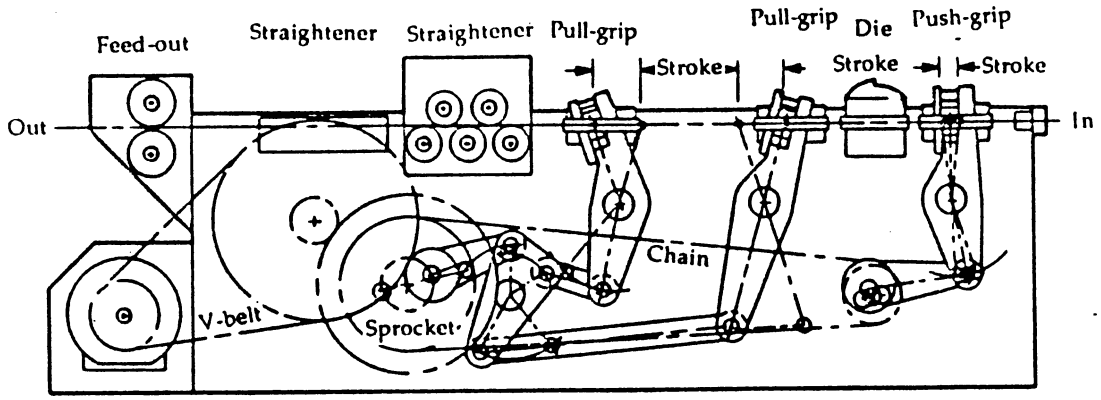

Figure 2.8 In-Line Drawing and Straightening Machine for Producing Cold-Drawn Bars from Hot-Rolled Steel Coils or Bars [Lange, 1985]

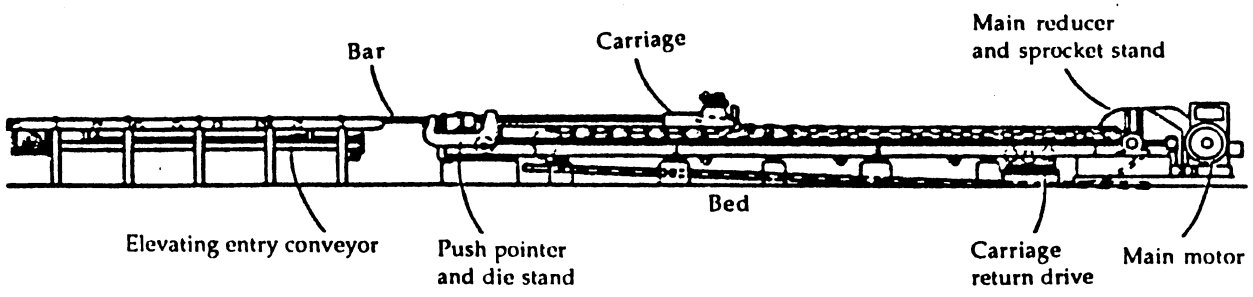

Figure 2.9 Typical Arrangement of a Drawbench for Producing Cold-Drawn Bars from Hot-Rolled Bars [Lange, 1985]

CHAPTER III

REVIEW OF THE METHODS OF ANALYSIS

Introduction

A number of analytical methods of varying degree of accuracy and complexity have been developed for assessing the various parameters of metal forming process. Some of these methods give local distributions. The basic methods of analysis usually employed in metal forming are uniform deformation energy method, slab method, slip-line method and upper-bound method. Uniform deformation method and slab method were introduced in the late 1920's. Uniform deformation method was introduced by Siebel [1932]. Sachs [1931] and Siebel introduced the slab method at about the same time. Hencky [1923] introduced the slip-line method in 1923. The upper-bound method was introduced by Johnson [1959] and Kudo [1958].

The basic characteristics of the plastic state of the material such as the condition of volume constancy, the yield criterion and flow stress relation have to be satisfied. As none of the solutions are perfect the solutions obtained by different methods may not result in identical answers. Hence the choice of the method must be made with care and the results should be applied with caution. In the following sections the four methods are briefly reviewed from the point of view of its applicability to the drawing process. Full discussion of these these techniques and the derivations of mathematical expressions can be found in books by, among others, Prager and Hodge [1951], Thomsen et al. [1965], Johnson and Mellor [1962], Johnson and Kudo [1962], and Avitzur [1968].

Uniform Deformation Energy Method

The uniform-deformation energy method is also called uniform-work method. In this method the deformation mechanism of the system is simplified that straining occurs only under maximum shearing stress or under principal stress. Friction is assumed not to affect the stress distribution and is taken into consideration by superimposing frictional effects on the system. The material is assumed to be real and may be affected by strain, strain-rate and temperature. This method is most useful for steady-state problems.

In the rest of this section, calculation of drawing stress by the uniform deformation energy method is discussed. Assuming uniform deformation and no friction at the die wall friction, from Fig. 3.1 the effective strain is given by

$$\bar{\varepsilon} = \ln\left(\frac{D_b}{D_a}\right)^2 \tag{3.1}$$

Now assuming that the yield stress is independent of work hardening and deformation speed, the drawing stress is equal to the internal specific energy given by

$$(\sigma_z)_{ave} = 2\,\bar{\sigma}_0 \ln\frac{D_b}{D_a} \tag{3.2}$$

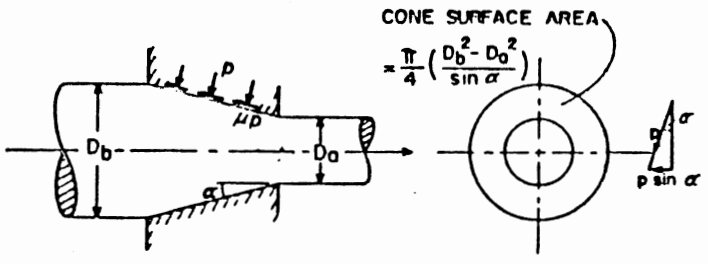

Figure 3.1 Schematic Diagram of Die Pressure and Friction Stresses in Wire Drawing

where $\bar{\sigma}_0$ is the initial yield strength of the metal. If the metal is not an ideal material, then $\bar{\sigma}$ must be integrated to calculate the average drawing stress, resulting in the integral form of the internal energy equation

$$(\sigma_z)_{ave} = \int_0^{\bar{\varepsilon} = \ln (D_b/D_a)^2} \bar{\sigma}\, d\bar{\varepsilon} \tag{3.3}$$

where the relationship between σ and ε must be known. To take friction at the die surface into consideration, the fraction of the drawing stress required to overcome friction given by

$$(\sigma_z)_f = \mu p \cos(\alpha) \frac{D_b^2 - D_a^2}{\sin\alpha} \frac{1}{D_a^2} \tag{3.4}$$

has to be superimposed on the drawing stress obtained in Eqn. (3.3). In the above equation p is the normal pressure on the die wall and α is the half die angle. Therefore the total drawing stress at constant σ is given by

$$(\sigma_z)_{ave} = \int_0^{\bar{\varepsilon}} \bar{\sigma}\, d\bar{\varepsilon} + \mu p \cot(\alpha) \frac{D_b^2 - D_a^2}{D_a^2} \tag{3.5}$$

$$= \bar{\sigma} \ln\left(\frac{D_b}{D_a}\right)^2 + \mu p \cot(\alpha) \left[\left(\frac{D_b}{D_a}\right)^2 - 1\right] \tag{3.6}$$

If α is assumed to be small, $\sigma_\theta = \sigma_r \approx -p$, and the yield condition is given by

$$p + \sigma_z = \bar{\sigma}_0 \tag{3.7}$$

and Eqn. (3.6) can be integrated for a constant $\bar{\sigma}$. Eqn. (3.6) can be written in the simplified form

$$(\sigma_z)_a = \bar{\sigma} \ln\left(\frac{D_b}{D_a}\right)^2 (1 + \mu \cot \alpha) \tag{3.8}$$

as suggested by Sachs and Van Horn [1940]. The Eqns. (3.6) and (3.8) can be modified to incorporate the effects of shear deformation, work hardening, and deformation speed.

Slab Analysis

The slab method of analysis is also referred to as Sache's method or equilibrium method or sometimes even as the stress method. In the slab analysis a representative volume element in the body of the material undergoing plastic deformation is isolated. The behavior of the isolated element as it moves along the working zone of the pass is then observed. In reality as the isolated element is an integral part of the whole material of the body, it must remain in the state of force equilibrium throughout its period of deformations. The behavior of the material can be analyzed from the behavior of the element by considering the equilibrium of forces acting on it at any instant of deformation.

In the rest of this section the calculation of the drawing stress by the slab method is discussed. Consider equilibrium of forces on the slab of length dz of Fig. 3.2. The resulting differential equation is given by,

$$\frac{d\sigma_z}{B\sigma_z - (1 + B)\bar{\sigma}} = 2\frac{dD}{D} \tag{3.9}$$

where $B = \mu \cot \alpha$ and α is considered to be small.

In the case where $\mu = 0$ and $\bar{\sigma}$ = constant Eqn. (3.9) becomes

$$\frac{d\sigma_z}{\bar{\sigma}} = -2\frac{dD}{D} \tag{3.10}$$

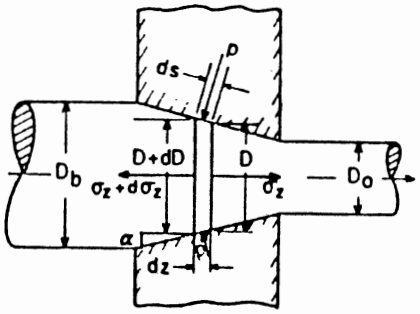

Figure 3.2 Equilibrium of Stresses on an Element of Infinitesimal Thickness During Wire Drawing

which on integration yields

$$\sigma_z = -2\bar{\sigma}(\ln D + C) \tag{3.11}$$

Introducing the boundary conditions

$$\sigma_z = 0 \quad \text{at} \quad D = D_b \tag{3.12}$$

permits determination of the constant $C = -\ln D_b$, which results in the drawing stress at any cross-section

$$\sigma_z = -2\bar{\sigma}\ln\frac{D}{D_b} \tag{3.13}$$

Substituting $D = D_a$ in Eqn. (3.13) required drawing stress can be expressed as

$$(\sigma_z)_a = 2\,\bar{\sigma}\,\ln\frac{D_b}{D_a} \tag{3.14}$$

The drawing stress of Eqn. (3.14) is again the specific energy of deformation as expected.

In case $\mu \neq 0$, $\bar{\sigma}$ = constant, the total drawing stress is given by

$$\sigma_z = \left[1 - \left(\frac{D_a}{D_b}\right)^{2B}\right]\left(\frac{1+B}{B}\right)\bar{\sigma} \tag{3.15}$$

Davis and Dokos [1944] suggested a solution taking the strain-hardening effect in wire drawing into account. Körber and Eichinger [1940] proposed a solution taking the rotational distortion of metal crystals during wire drawing into consideration. They suggested the introduction of an additional term, the so-called Körber and Eichinger effect into the wire drawing equations.

Slip-Line Analysis

Slip-line analysis is based on the physical observation that plastic flow occurs predominantly as a result of microscopic slip, on an atomic scale, along crystallographic planes. A large number of close-packed planes are present in polycrystalline metals. Slip is likely to occur along these planes if sufficient number of these are orientated in such a way that, on a macroscopic scale their direction coincides with that of the maximum shear stress. The directions of the maximum shear stress are the characteristic properties of the system. On establishing the directions of the maximum shear stress, the stress distribution over the entire deforming region and at the tool workpiece interface can be established. At the interface the loads exerted by the tools can be calculated. This method applies rigorously only to plane-strain deformations of rigid, perfectly plastic isotropic materials.

Also it does not account for strain-hardening, strain-rate, frictional and redundancy effects unless artificially modified.

The slip-line field for wire drawing as suggested by Hill and Tupper [1948] is shown in Fig. 3.3. Even though the model is two dimensional, the results can be applied as a first approximation to the cylindrical drawing. Here the calculation of the drawing stress by the slip-line method in the case where $\mu = 0$, $\bar{\sigma}$ = constatnt and back tension is absent is discussed.

In Fig. 3.3 let ADF and the lines of the same family represent the first shear lines (α-lines) and BEF and other lines of the same family be second shear lines (β-lines). Also let the mean pressure at point F be p_0. When back tension is absent, the boundary condition at ADF is given by

$$\int (p \cos\theta - k \sin\theta)\, ds = 0 \tag{3.16}$$

Thus the slip-line ADF cannot be drawn arbitrarily and must fit the condition given by Eqn. (3.16). Integration along the slip-line ADF, under the condition that $p + 2k$ = constant along this line and that at F, $p = p_0$, where $\theta = \pi/4$, gives

$$p = p_0 + \frac{k\pi}{2} - 2k\theta \tag{3.17}$$

Let the horizontal difference in distance between A and F along z be given by h, where the vertical distance is $D_b/2$; then along ADF we have

$$\int \sin\theta\, ds = h\,; \qquad \int \cos\theta\, ds = \frac{D_b}{2} \tag{3.18}$$

Substitution of Eqn. (3.17) into Eqn. (3.16) results in

$$\int (p_0 + \frac{k\pi}{2} - 2k\theta) \cos\theta \, ds - \int k \sin\theta \, ds = 0 \qquad (3.19)$$

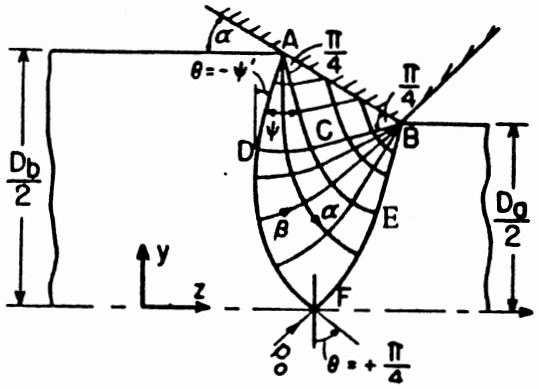

Figure 3.3 Possible Slip-Line Field in Plane-Strain Without Die Friction [Hill et al, 1948]

Now substituting Eqn. (3.18) into Eqn. (3.19) yields

$$p_0 + \frac{k\pi}{2} = \frac{2}{D_b} (kh + 2k \int \theta \cos\theta \, ds) \qquad (3.20)$$

along the straight slip-line AD the angle ψ' = constatnt, which determines $p = p_1$ = constant.

Introducing $\theta = -\psi'$ into Eqn. (3.17) determines p_1 along AD

$$p_1 = p_0 + \frac{k\pi}{2} + 2k\psi' \qquad (3.21)$$

Substituting Eqn. (3.20) into Eqn. (3.21), we obtain

$$p_1 = \frac{2}{D_b}\left(kh + 2k\int \theta \cos\theta \, ds\right) + 2k\psi' \tag{3.22}$$

where $\psi' = \alpha + \psi - \pi/4$. Thus for the point D the mean pressure is given by $p_D = p_1$. It is now possible to calculate the pressure at point B by going along the β (or second) slip-line DCB. Thus along the β slip-line from D to C the pressure increases from p_D to p_c and is given by

$$p_C = p_D - 2k(-\psi') - 2k\left(\alpha - \frac{\pi}{4}\right) \tag{3.23}$$

which is based on the relationship $p - 2k\theta$ = constant along a β slip-line.

Substituting Eqn. (3.22) into Eqn. (3.23) results in

$$\frac{p_c}{2k} = \frac{1}{D_b}\left(2\int \theta \cos\theta \, ds + h\right) + \frac{\pi}{4} - \alpha + 2\psi' \tag{3.24}$$

Within triangle ABC the slip-lines are straight lines, and therefore the stresses within this triangle are everywhere identical with those at C. It can be shown from the Mohr circle diagram that on the die wall the two principal stress are $p_c + k$ and $p_c - k$, which are uniformly distributed on the die surface. Hence the total force in the z direction is given by

$$(p_c + k)\,\overline{AB}\,\sin\alpha = (p_c + k)\,\frac{D_b - D_a}{2} \tag{3.25}$$

The drawing stress is then given by

$$(\sigma_z)_a = (p_C + k)\left(\frac{D_b}{D_a} - 1\right) \tag{3.26}$$

Substituting Eqn. (3.24) into (3.25) we obtain

$$(\sigma_z)_a = 2k\left[\frac{1}{D_b}\left(2\int \theta \cos\theta \, ds + h\right) + \left(\frac{1}{2} + \frac{\pi}{4} - \alpha + 2\psi\right)\right]\left(\frac{D_b}{D_a} - 1\right) \tag{3.27}$$

The integration of Eqn. (3.27) can be performed graphically.

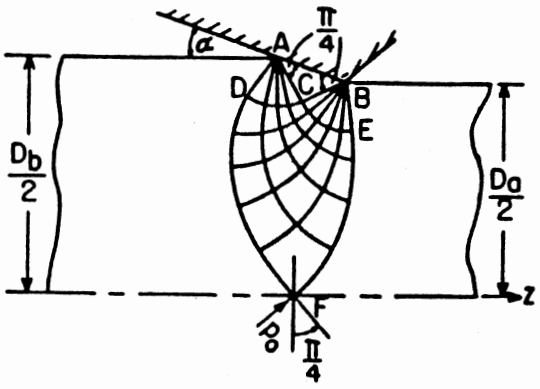

Figure 3.4 Alternate Slip-Line Field in Drawing in Plane-Strain Without Die Friction [Hill et al, 1948]

Another possible solution for the drawing problem is given by the slip-line net of the two-centered fan type which is shown in Fig. 3.4. This slip-line field can be drawn readily to fit the particular drawing conditions. The drawing stress can then be obtained in a manner similar to that in Fig. 3.3. Unlike Fig. 3.2, in Fig. 3.4 all the α-lines meet at A and all the β-lines meet at B.

The solution proposed by Hill and Tupper [1948] taking friction also into consideration is shown in the slip-line field of Fig. 3.5. The principal difference between Fig. 3.2 and Fig. 3.5 is that the slip-lines in ABC of Fig. 3.5 do not meet the wall at 45^0 and the circular arcs CD and CE no longer have equal radii.

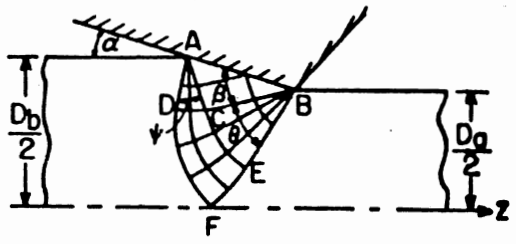

Figure 3.5 Slip-Line Field in Drawing in Plane-Strain With Die Friction [Hill et al, 1948]

Taking the increase in drawing stress due to the frictional force along the surface AB in the axial direction, the total drawing stress is given by

$$(\sigma_z)_a = (1 + \mu q \cot \alpha)\left(\frac{D_b}{D_a} - 1\right) q \qquad (3.28)$$

where q is the normal pressure on the die face.

Upper-Bound Analysis

This method is also called as limit analysis. The working region is divided into a number of zones. The particle velocity in each of the zones is continuous, but adjacent

zones can have different velocity distributions. As in the case of the velocity fields derived in the slip-line analysis, velocity discontinuity may occur only in the tangential components of velocity along the actual zone interfaces and the tool specimen boundaries. Discontinuities imply the presence of shear, and the existence of velocity distributions in each zone indicates the presence of plastic strain which in turn implies dissipation of energy. As energy governs change in shape, on computing the energy dissipated for a given velocity or strain-rate field, the magnitude of the external load required can be calculated. The power required to overcome the resistance of the worked material to deform and the power to compensate for the frictional effects produced by relative motion between the tool and the specimen constitute the total power required to perform a metal forming operation. A velocity field that minimizes the computed power is taken as the actual one.

In order to simplify calculations, the upper bound solution of plane-strain drawing is used as an approximate estimate of the tensile stress in wire drawing. Fig. 3.6(a) shows an assumed simple plane-strain deformation pattern on a meridian plane in drawing a wire of diameter D_b into a wire of reduced diameter D_a through a die having a half angle α.

The plane-strain drawing stress at the die exit without considering die friction is given by

$$(\sigma_z)_a = \bar{\sigma} \frac{2}{\sqrt{3}\, D_a} (\overline{OB}\ \mathbf{ob} + \overline{OA}\ \mathbf{oa}) \tag{3.29}$$

If the die assumed to be rough, the energy dissipated along the die surface be taken into account for finding the drawing stress, namely,

$$(\sigma_z)_a = \bar{\sigma} \frac{2}{\sqrt{3}\, D_a} (\overline{OB}\ \mathbf{ob} + \overline{OA}\ \mathbf{oa} + \overline{AB}\ \mathbf{ab}) \tag{3.30}$$

The best solution for the drawing stress, with or without friction, is obtained at the value of θ at which $(\sigma_z)_a$ is a minimum. For larger reductions a better upper-bound solution can be found for the velocity field with more than one triangle, as shown in Fig. 3.6(b). The average drawing stress without friction for $\theta = \psi + \alpha$, as proposed by Green [1952], is then given by

$$(\sigma_z)_a = \frac{2kn}{\sin \alpha} \left(y + \frac{1}{y} - 2 \cos \alpha\right) \tag{3.31}$$

where $y = (1 - r)^{1/2n}$ and r is the thickness reduction. The integer n is chosen for the least bound.

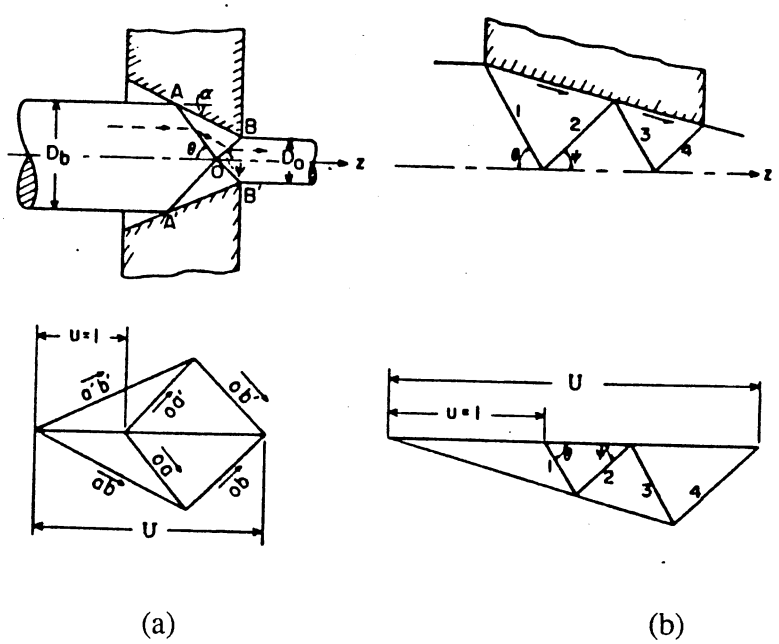

Figure 3.6 Upper-Bound Solutions for Drawing in Plane-Strain
(a) Discontinuous Velocity Field With One Triangle
(b) Discontinuous Velocity Field With Two Triangles

CHAPTER IV

FINITE ELEMENT APPROACH

Application of 3D-Finite Element Analysis to Metal Forming

Introduction

Many of the industrial forming processes are three dimensional in nature. The need to develop and/or improve three dimensional analysis methods which take into account all the aspects of such processes has been felt for some time. Several methods of analysis have been developed, with various degrees of approximations and idealizations. Of all the methods, the finite element method seems to be the most powerful for metal forming because of its flexibility, adaptability and accuracy. Most of the previous finite element computer calculations, for plastic and viscoplastic material were based on plane or axisymmetric deformations. The extension of the finite element method to solve three-dimensional problems is natural and is not new, particularly in the area of elasticity [Zienkiewicz 1977]. However, the analysis of three-dimensional metal forming problems by the finite element method is relatively recent. Large deformation elastic-plastic formulations require a large amount of computer time. The development of computer simulation programs with three-dimensional finite element analysis capabilities has been one of the recent research areas of process modelling. In the following sections applications of three-dimensional finite element method for the analysis of forging, rolling and extrusion are reviewed.

Forging

Park and Kobayashi [1984] performed three-dimensional analysis of block compression based on the rigid-viscoplastic formulation. The 8-node hexahedral isoparametric elements were used to discretize the variational form of the equilibrium equation. Simulations were performed for two friction (velocity dependent) conditions of m=0.1 and m=0.5. The workpiece material was annealed Al-1100. The final stage of compression was at 50% reduction in both the cases. The simulations showed that higher friction required more load and that the load difference between the two friction conditions becomes larger as the ram displacement increases. Also high friction conditions cause inhomogeneous deformation. These results compare well with experimental results. Park and Kobayashi [1984] also reported the compression of wedge-shaped blocks. In practice the compression of wedge-shaped blocks between two flat parallel dies is used for workability and microstructural studies in forging. The finite element program for this problem is more complex compared to block compression because it has to handle the determination of neutral regions at contact surfaces along with the occurrence of folding and lifting. The load-displacement curve was found to have jumps. These jumps occur because the contact area increases when folding takes place.

Surdon and Chenot [1987] presented a method for simulating three-dimensional deformation in hot forging. Their method is based on the viscoplastic finite element method with a viscoplastic friction law and also assumes an isothermal deformation. Simulations were performed for compression of cubic blocks and cylindrical blocks between flat platens. Discretization of the variational formulation was made with eight node hexahedral and six node prismatic isoparametric elements. The changes in the cross-sections and end surfaces for different friction conditions were found to agree with the experimental results.

A three dimensional finite element program called FORGE3 was used by Soyris et al [1988] to simulate the forging of a connecting rod. The striking feature of this work is that it shows that complex three-dimensional geometry forgings can be simulated without excluding the thermal effects. FORGE3 is based on the coupled thermo-viscoplastic analysis. The deformation and thermal analysis are done independently at each time step. In the processes like low speed aluminium forging, which are influenced by convection and the radiation on the free surfaces, the inclusion of the thermal analysis is critical.

The rigid-viscoplastic FEM formulation with 8-node hexahedral elements [Park and Kobayashi, 1984] was further developed into a three-dimensional FEM code ALPID-3D Park and Oh [1987]. ALPID-3D supports curved die surfaces and has a provision to automatically generate an initial guess solution. This code was validated among other things, by the simulation of simple forming processes of compression of circular and square rings. In practice ring compression is used for evaluating lubricants. Since this process is axisymmetric the solution obtained by ALPID-3D was compared with the axisymmetric prediction by ALPID-2D and was found to agree well. The mode of deformation of the square ring was found to agree with the experiments conducted by Aku et al [1967] and the collapse modes were compared with the experimental investigations of Andrews et al [1983]. Different collapse modes such as, (i) axisymmetric and sequential folding starting at one end of tube, (ii) bending of tube as a strut, etc. were identified by Andrews et al [1983] by axial crushing of tubes.

Rolling

In the rolling of thick plates, metal flow occurs in three dimensions. The rolled material is elongated in the rolling as well as spread in the lateral, or width direction. As the theory of rolling to deal with three dimensional deformation, but for a very few exceptions the studies on deformation in rolling have been experimental. Rolling of wide strips or plates involves width-to-thickness ratios of larger than about ten. In such

situations, spread in width is usually negligible and problems can be considered as plane-strain. However if the width-to-thickness ratio is less than about six, spread is appreciable and cannot be neglected. Although several researchers applied the finite element technique to solve the rolling problem, they also made the plane-strain assumption. Oh and Kobayashi [1975] analyzed three-dimensional deformation in rolling using an extremum principle for rigid, perfectly plastic materials. Other approaches taking the lateral spread in rolling into account are works by Kanazawa and Marceal [1978], Li and Kobayashi [1984] and Mori and Osakada [1982].

In Oh and Kobayashi [1975] theoretical solutions were obtained for single-pass rolling in terms of sideways spread, roll torque and the location of neutral points. To apply the extremum principle to metal-working process, the geometrical configuration of a plastically deforming body must be prescribed. Because of this, the application of the extremum principle to the problem of rolling is not straightforward, if spread in the width direction is to be considered in the analysis. The approximate method for the solution of the problem is as follows. First a class of surface shapes are assumed, then a velocity field which minimizes a functional for an assumed surface is determined. The minimization is done in the usual upper-bound method of assuming a class of velocity fields. Among the velocity fields thus determined, the steady-state velocity field is searched for, along with the surface shape. The results on spread and roll torque were in good agreement with those found by experiments.

The finite element method based on the flow formulations is applied in Li and Kobayashi [1984]. The solution of the original boundary value problem is obtained by solving the dual variational problem where the first order variation of the functional vanishes. The functional referred here is for rigid-plastic materials which obey the Von Mises yield criterion and its associated flow rule. The nonlinear algebraic equations (nodal velocities are unknowns) obtained by finite element discretization of the functional and applying the condition that it be stationary are solved by the Newton-Raphson iterative

method. The simplified eight-node elements (also called 'Two and a Half-D' brick element) are used to discretize the work piece. The simplified hexahedral elements are derived by taking one layer of elements in the direction normal to the plane of symmetry and assuming that the element sides which are initially normal to the plane remain normal during deformation. Two different element arrangements are possible in rolling depending on how the plane of symmetry is selected. The choice of the element arrangement depends on required information and possibly the rolling condition, such as width to thickness ratio. One of the most important advantages of using the simplified eight-node element is the reduction in the number of variables.

Three-dimensional finite element simulations of the rolling of a beam with the H-cross-section was simulated from beginning of the process until it becomes steady-state by Chen [1989]. This FEM program is called TARRIT (Three-dimensional Analysis of Rolling-process by Rigid-plastic Incremental Theory). The deformation of the material under the roll gap is very complex during rolling of shapes or sections because of the large non-uniform deformation occuring along the cross-section. Unlike the forging process, the specimen in rolling is driven by the frictional force between the specimen and work rolls. The frictional force between the specimen and work rolls is not high enough at the beginning stage of a simulation. Hence, a pulling or pushing velocity is applied to the head or tail of the work-piece, until sufficient frictional forces exist. The process is considered to have reached steady-state if the roll torque becomes stable in successive time increments. In the same paper, three-dimensional finite element analysis of ring rolling was also reported. Ring rolling is a specialized form of rolling process for manufacturing seamless rings. Ring rolling differs from conventional flat rolling in many ways like; workpiece has a curvature with a varying radius, diameters of the driving roll and the pressure roll are different, pressure roll is idle and advances to the driving roll side continuously, and metal flow is three dimensional. These differences indicate that it is not appropriate to apply the analytical method of the flat rolling process to ring rolling. The finite element code

"RING" developed for the analysis of ring rolling has a special method of updating. Two mesh systems are used, actually rotating mesh system (AMS) which is fixed to the workpiece and spatially fixed mesh system (SMS) which is fixed in space but changing its geometry according to that of AMS. The AMS stores all the information like the geometry of the workpiece, history of plastic deformation etc. The velocity field is calculated from the SMS and then interpolated to the nodes in the AMS.

Extrusion

Plane-strain or axisymmetric extrusion problems have been analyzed by numerous researchers using the finite element method. Yang et al [1984] employed the rigid-plastic finite element method to study the steady-state three-dimensional extrusion of non-circular sections such as elliptic and clover-leaf sections through curved dies. The penalty method, based on the rigid-plastic material model, is used to handle the incompressibility condition. The initial guess velocity fields are obtained by applying the upper-bound method for extrusion of non-circular sections. The work-hardening effect for the steady-state flow is incorporated by integrating the effective strain-rate along each stream line through interpolation by the least square method. The finite element code was validated by performing the computations for the extrusion of elliptic and clover-leaf sections. The results obtained were found to be in good agreement with experimental results.

Finite Element Analysis of Steady-State Processes

Introduction

Various reference systems can be used while formulating mathematical models for the simulation of forming processes. The most commonly used reference systems are; Eulerian, Lagrangian and Arbitrary Eulerian-Lagrangian (AEL).

In the Lagrangian formulation the reference system is attached to the body and hence leads to some mathematical complexities. The Lagrangian formulation of the finite element method results in the finite element mesh being connected to the material movement and deforms with the material. For large deformations there is a remarkable distortion in the mesh, and therefore needs regeneration (rezoning) whenever such distortion occurs. Also imposition of non-material-associated boundary conditions in steady-state processes becomes tedious.

In the Eulerian formulation the reference system, called the spatial reference system, is fixed in the space. In the Eulerian formulation of the finite element method the finite element mesh is fixed in the space. Because of this, as a body deforms the boundary of the body and the sides of the element may not coincide. This in turn makes it almost impossible to impose material associated boundary conditions.

To overcome the difficulties encountered in the pure Lagrangian and Eulerian formulations, the Arbitrary Lagrangian-Eulerian formulation which lies half-way between the two was developed. In the AEL formulation the reference system (mesh) is neither fixed in the space nor attached to the body. The mesh changes its position in a predetermined manner by imposing a velocity to all the points. As the new position of the mesh is computed based on a prescribed velocity, AEL formulation is also called the computational reference system.

The equilibrium (momentum balance) equations can be written as

$$\sigma_{ij,j} + b_i = \rho \dot{v}_i \tag{4.1}$$

where σ_{ij} is the stress tensor; v_i the velocity b_i the body force, and ρ the density. Material time derivative in the Lagrangian reference frame is related to spatial time derivative, in the Eulerian reference frame

$$\dot{v}_i = \frac{dv_i}{dt} = \frac{\partial v_i}{\partial t} + v_j\, v_{i,j} \tag{4.2a}$$

where the second term is the convective term. The equilibrium equations are identical in both Lagrangian and Eulerian reference frames if the problem is such that acceleration can be neglected (slow forming). In the case of an AEL reference frame

$$\dot{v}_i = \frac{\partial v_i}{\partial t} + (v_j - \bar{v}_j)\, v_{i,j} \tag{4.2b}$$

where $\bar{v}_j$ is the prescribed velocity of the AEL reference frame. The heat transfer equation for a Lagrangian reference frame is

$$\rho c_p \dot{T} = \nabla\cdot (k\nabla T) + q \tag{4.3a}$$

for an Eulerian reference frame

$$\rho c_p \left(\frac{\partial T}{\partial t} + v_i T_{,i}\right) = \nabla\cdot(k\nabla T) + q \tag{4.3b}$$

and for an AEL reference frame

$$\rho c_p \left[\frac{\partial T}{\partial t} + (v_i - \bar{v}_i) T_{,i}\right] = \nabla\cdot(k\nabla T) + q \tag{4.3c}$$

where c_p is the specific heat, k the thermal conductivity and q the energy dissipated by motion per unit volume and time. For a strain hardening material the flow stress depends not only on temperature and strain-rate but also on the effective strain $\bar{\varepsilon}$. The total effective strain-rate $\dot{\bar{\varepsilon}}$ is defined by velocity. In the Lagrangian reference frame

$$\frac{\partial \bar{\varepsilon}}{\partial t} = \dot{\bar{\varepsilon}} \tag{4.4a}$$

in the Eulerian reference frame

$$\frac{\partial \bar{\varepsilon}}{\partial t} + v_j \bar{\varepsilon}_{,j} = \dot{\bar{\varepsilon}} \tag{4.4b}$$

where $\dot{\bar{\varepsilon}}$ is the material time derivative. In the AEL reference frame

$$\frac{\partial \bar{\varepsilon}}{\partial t} + (v_j - \bar{v}_j) \bar{\varepsilon}_{,j} = \dot{\bar{\varepsilon}} \tag{4.4c}$$

where $\bar{v}_j$ is the prescribed velocity of the AEL reference frame.

Steady-state metal forming processes are often analyzed using a mesh fixed in space (Eulerian reference frame) as the process configuration does not change with time. As a result the time derivative terms in the Eqns. (4.2a), (4.3b) and (4.4b) disappear. The convective terms which occur in the Eulerian formulation lead to non-symmetric matrices which in turn cause associated numerical difficulties. Velocity is used as the primary field variable. For transient problems whose solutions depend on the loading history or strain history of the material, combined Eulerian-Lagrangian approaches are necessary [Schreurs, 1986]. Metals behave as viscous fluids under conditions such as high temperature and/or low forming speeds [Zienkiewicz, 1974] [Thompson, 1984]. The behavior of the metals begins to influence the flow at lower temperatures and faster speeds. A variety of problems related to plastic deformations and flow are presently being solved by applying the elasto-viscoplastic and viscoplastic flow approximations in conjunction with the finite element method.

Elasto-Viscoplastic Flow

For many applications the rigid plastic and viscoplastic flow approximations are valid, but for some applications neglecting elastic strains in the analysis can lead to erroneous results. Lynch [1969] presented a method for the finite element analysis of steady-state visco-elastic flow where he made use of an integrated constitutive equation to formulate the stiffness matrix. This formulation uses displacement as the field variable. Dawson [1978] presented a method for including the elastic strains in a steady-state, controlled volume, viscoplastic analysis. The field variable used is velocity. It is called the 'initial stress-rate method' because of its similarity with the initial-stress and initial-strain methods. In this approach, the stress and velocity fields associated with the convective terms in the constitutive equation are assumed known and placed in the right-hand side of the finite element equations for momentum. An iterative procedure is then used during which these terms are corrected until there is no discrepancy between the new stress distribution and the previous one. Variations are performed on velocity and pressure only.

As the derivative of stress is present in the constitutive equation, the governing equations for elasto-viscoplastic and viscoplastic flow are of higher order than those for Newtonian fluids. This requires that an additional boundary condition be specified for the state of stress. Shimazaki [1981] developed an algorithm to impose this boundary condition. They used the momentum and continuity equations to determine velocity and pressure assuming the stress constant. Then the stress was determined assuming velocity and pressure constant. These two calculations form an iterative loop and the iteration process is carried out until convergence is reached. This process is called the decoupled mixed method as momentum and continuity equations are decoupled from the constitutive equations.

Rigid Viscoplastic Flow

For plastic or viscoplastic materials in large deformation processes the elastic deformation can be considered to be negligible. Chen and Kobayashi [1972] and Zienkiewicz [1974] have both used such a formulation to investigate problems related to metal forming processes. For such problems the constitutive relations can be expressed [Zienkiewicz, 1974] in an Eulerian form linking the stresses and current strain-rates. As viscosity is now dependent on the current strain-rates it is identical to the flow of viscous, non-Newtonian incompressible fluid.

For a viscous, incompressible fluid the constitutive relation is of the form

$$\dot{\varepsilon}_{ij} = \frac{1}{2\mu}\sigma'_{ij} \tag{4.5}$$

where σ'_{ij} are the deviatoric components of stress and the scalar μ is the viscosity which can be a function of strain, strain-rate, and temperature. Metals have a well-defined plastic yield stress and μ is given by

$$\mu = \frac{\bar{\sigma} + \gamma \dot{\bar{\varepsilon}}^m}{3\dot{\bar{\varepsilon}}} \tag{4.6}$$

where $m < 1$, and $\bar{\sigma}$ the effective stress is a function of $\bar{\varepsilon}$, $\dot{\bar{\varepsilon}}$ and T. $\gamma = 0$ for ideal plastic metals and hence μ is given by

$$\mu = \frac{\bar{\sigma}}{3\dot{\bar{\varepsilon}}} \tag{4.7}$$

Therefore Eqn. (4.5) becomes

$$\dot{\varepsilon}_{ij} = \frac{3}{2}\frac{\dot{\bar{\varepsilon}}}{\bar{\sigma}}\sigma'_{ij} \tag{4.8}$$

The constitutive relation represented by Eqn. (4.8) is identical to the isotropic elastic relations for incompressible solids with strain-rates taking the place of strains. If dynamic forces are neglected the equilibrium equations of both solid and fluid are identical. Therefore elastic solutions can be identified for the same configurations as with those of viscous flow, provided displacements are interpreted as velocities and strains (infinitesimal) as strain-rates. This analogy is useful as all the methods capable of dealing with incompressible elastic materials in the context of solid mechanics become immediately available for the viscous flow problems.

Strain Calculation

For the transient processes, the effective strain-rates are integrated over the time for each element to determine the effective strains after a certain amount of deformation. For the analysis of a steady-state process, a technique is needed for determining the distributions of effective strain if the deforming material is a strain hardening material. The following method [Chen, 1979] [Yang, 1989] may be used to obtain the effective strain distribution.

In the finite element technique the strain-rates are obtained at the center of each finite element and the velocities at the nodes. The coordinates of these element centers and nodal points are also known. All values of effective strain-rate at the center points of finite elements may be projected to those on nodal points by the least square method. Consider two neighboring points P_i and P_{i+1} on a flow line. After checking to see which element the point P_i belongs to, velocity components V_i on the point P_i can be determined by linear interpolation. Depending on the type of elements and the co-ordinate system used,

methods can be devised to check, to which element a point on a flow line belongs. The next location P_{i+1} on the flow line is given by

$$P_{i+1} = P_i + \Delta t\, V_i \tag{4.9}$$

where Δt denotes the time increment. After checking to see which element the point P_{i+1} belongs to, the effective strain-rate on the point can be calculated by linear interpolation. The interpolated strain-rate is added incrementally to the value of effective strain at the previous location as follows:

$$\bar{\varepsilon}_{i+1} = \bar{\varepsilon}_i + \Delta t\, \dot{\bar{\varepsilon}}_{i+1} \tag{4.10}$$

Now a new grid system is made by the points on the selected flow lines. Finally, the effective strain at the center of an original finite element can be obtained through linear interpolation of the values on the new grid system.

Shimazaki [1981] obtained the values of the effective strain by applying the Galerkin's method to the material derivative of the following equation

$$\dot{\bar{\varepsilon}} = \frac{\partial \bar{\varepsilon}}{\partial t} + v_i \frac{\partial \bar{\varepsilon}}{\partial x_i} \tag{4.11}$$

where $\dot{\bar{\varepsilon}} = \sqrt{\frac{2}{3}\, \dot{\varepsilon}_{ij}\, \dot{\varepsilon}_{ij}}$ is obtained from the velocity field which has already been solved for.

CHAPTER V

ANALYSIS OF DRAWING

Basic Equations

The theory of plasticity deals with the time independent behavior of material adequately, but not with the time-dependent behavior. For the analysis of time-dependent behavior of material in the moderate range of temperature, the theory of plasticity is generalized to cases which include the strain-rate sensitivity. Assuming the isotropy, negligible elastic deformation and Huber-Mises yield criterion, the constitutive relation can be expressed as

$$\dot{\varepsilon} = \frac{3}{2}\frac{\dot{\bar{\varepsilon}}}{\bar{\sigma}}\sigma' \tag{5.1}$$

where σ' and $\dot{\varepsilon}$ are the deviatoric stress tensor and the strain-rate tensor, respectively. The effective stress $\bar{\sigma}$ and effective strain-rate $\dot{\bar{\varepsilon}}$ are defined by

$$\bar{\sigma} = \left(\frac{3}{2}\sigma'^{T}\sigma'\right)^{1/2} \tag{5.2}$$

$$\dot{\bar{\varepsilon}} = \left(\frac{2}{3}\dot{\varepsilon}^{T}\dot{\varepsilon}\right)^{1/2} \tag{5.3}$$

The effective stress (the flow stress) for a specific material is determined, by uniaxial tension or compression tests as a function of the strain, the strain-rate, and temperature such as

$$\bar{\sigma} = \bar{\sigma}(\bar{\varepsilon}, \dot{\bar{\varepsilon}}, T) \tag{5.4}$$

The deformation of a rigid-viscoplastic material obeying the constitutive relation, Eqn. (5.1), is associated with the following boundary value problems. Cartesian coordinate system is used throughout this work.

A body of volume, V, is considered with the traction, $\mathbf{f}^*$, prescribed on a part of the surface, S_F, and the velocity, $\mathbf{v}^*$, prescribed on the reminder of the surface, S_v. The deformation process is assumed as a static problem by neglecting the inertia effect and the body force. The stress, σ, and velocity field, $\mathbf{v}$, satisfy the following relations.

(1) equilibrium equations;

$$\nabla \cdot \sigma = 0 \tag{5.5}$$

(2) constitutive equations;

$$\dot{\varepsilon} = \frac{3}{2}\sigma' \dot{\lambda} = \frac{3}{2}\frac{\dot{\bar{\varepsilon}}}{\bar{\sigma}}\sigma' \tag{5.6a}$$

$$\bar{\sigma} = \bar{\sigma}(\bar{\varepsilon}, \dot{\bar{\varepsilon}}, T) \tag{5.6b}$$

(3) incompressibility condition;

$$\dot{\varepsilon}_v = \nabla \cdot \mathbf{v} = 0 \tag{5.7}$$

(4) strain-rate velocity relations;

$$\dot{\varepsilon} = \frac{1}{2}(\nabla \mathbf{v} + (\nabla \mathbf{v})^T) \tag{5.8}$$

(5) boundary conditions;

$$\sigma \mathbf{n} = \mathbf{f}^* \text{ on } S_F \tag{5.9a}$$

$$\mathbf{v} = \mathbf{v}^* \text{ on } S_v \tag{5.9b}$$

$\dot{\varepsilon}_v$ is the volumetric strain-rate, and **n** is the unit vector normal to the corresponding surface.

The unknowns for the solution of a quasi-static plastic deformation process are six stress components, six strain-rate components, and three velocity components. The governing equations are three equilibrium equations, six strain-rate velocity relations, and six constitutive equations derived from the flow rule. The boundary conditions are prescribed in terms of velocity and traction.

Since it is difficult to obtain a complete solution that satisfies all of the governing equations, various approximate methods (described in chapter 3) have been devised. The final equation can be obtained by the finite element method using the variational approach or the weighted residual method. To obtain the weak form of the equation the integrand of the first term of Eqn. (5.10a) is replaced with the deviatoric stress and the hydrostatic pressure, and the hydrostatic part with a large positive penalty function, K, in order to satisfy the incompressibility condition.

$$\int_V \sigma^T \delta\dot{\varepsilon}\, dV - \int_{S_F} \mathbf{f}\, \delta\mathbf{v}\, dS = 0 \tag{5.10a}$$

$$\int_V \sigma'^T \delta\dot{\varepsilon}\, dV + K\int_V \dot{\varepsilon}_v\, \delta\dot{\varepsilon}_v\, dV - \int_{S_F} \mathbf{f}\, \delta\mathbf{v}\, dS = 0 \tag{5.10b}$$

Finite Element Discretization

The weak form, Eqn (5.10b), originated from the equilibrium equations associated with the rigid-viscoplastic materials is valid over the entire volume, V. But it should also

be valid for any portion of the volume because the equilibrium equations should be satisfied at every point in the volume.

If volume V is divided into M elements interconnected at N nodal points, then Eqn. (5.10) can be written at the element level as

$$\sum_{e} \left(\int_{V^{(e)}} \sigma'^{T} \delta\dot{\varepsilon}\, dV + K \int_{V^{(e)}} \dot{\varepsilon}_v\, \delta\dot{\varepsilon}_v\, dV - \int_{S_F^{(e)}} \mathbf{f}\, \delta\mathbf{v}\, dS \right) = 0 \qquad (5.11)$$

Inside each element the velocity distribution is approximated by a linear combination of certain interpolation functions with the nodal velocities at the elements nodes. A linear function is used mostly because it yields a simple derivation to formulate the stiffness matrix and a lower degree of integration scheme can be used. Higher order interpolation functions are used when higher accuracy and flexibility in the element deformation are needed.

The discretization of the volume integrals corresponding to the first two terms in the left-hand side of Eqn. (5.11) for an 8-node hexahedral isoparamatric element is discussed in the rest of this section. The Cartesian coordinate system (x, y, z) is transformed into the natural coordinate system (ξ, η, ζ). The natural coordinate system is defined such that ξ, η, and ζ vary from -1 to 1 within each element. An arbitrary point (x, y, z) in an element can be expressed by

$$\mathbf{x} = N_I\, \mathbf{x}_I \qquad (5.12a)$$

$$\mathbf{x}^T = [x,y,z] \qquad (5.12b)$$

$$\mathbf{x}_I^T = [x_I, y_I, z_I] \qquad (5.12c)$$

where I the repetitive subscript refers to the summation of finite elements, i.e. I = 1, 2, . . 8 for a 3-D brick element

$$N_I = \frac{1}{8}(1+\xi_I\xi)(1+\eta_I\eta)(1+\zeta_I\zeta) \tag{5.13}$$

where $\mathbf{x}_I$ are the coordinates of the eight nodes of the element in consideration in the cartesian coordinate system and N_I are the interpolation functions (or the shape functions).

For isoparametric elements, the interpolation functions used for approximating the velocity distribution inside an element by the nodal velocities are given by

$$\mathbf{v} = N_I\,\hat{\mathbf{v}}_I \tag{5.15a}$$

$$\mathbf{v}^T = [v_x, v_y, v_z] \tag{5.15b}$$

$$\hat{\mathbf{v}}_I^T = [\hat{v}_x, \hat{v}_y, \hat{v}_z]_I \tag{5.15c}$$

where $\hat{\mathbf{v}}_I$ is the vector of the nodal (I-th node) velocity. Values of ξ, η, and ζ at the nodes of a 3-D brick element are given by

$$\begin{aligned} &\xi_1 = \xi_2 = \xi_3 = \xi_4 = -\xi_5 = -\xi_6 = -\xi_7 = -\xi_8 = 1 \\ &-\eta_1 = \eta_2 = \eta_3 = -\eta_4 = -\eta_5 = \eta_6 = \eta_7 = -\eta_8 = 1 \\ &-\zeta_1 = -\zeta_2 = \zeta_3 = \zeta_4 = -\zeta_5 = -\zeta_6 = \zeta_7 = \zeta_8 = 1 \end{aligned} \tag{5.16}$$

In Eqns. (5.2) and (5.3) σ' and $\dot{\varepsilon}$ are given by

$$\sigma' = \frac{2}{3}\frac{\bar{\sigma}}{\bar{\dot{\varepsilon}}}\dot{\varepsilon} \tag{5.17}$$

$$\dot{\varepsilon} = \mathbf{A}\,\mathbf{v} \tag{5.18}$$

where the components of σ', $\dot{\varepsilon}$ and $\mathbf{A}$ are defined by

$$\dot{\varepsilon}^T = \left[\, \dot{\varepsilon}_{xx},\ \dot{\varepsilon}_{yy},\ \dot{\varepsilon}_{zz},\ \dot{\gamma}_{xy},\ \dot{\gamma}_{yx},\ \dot{\gamma}_{zx} \,\right] \tag{5.19}$$

$$\sigma'^T = \left[\, \sigma'_{xx},\ \sigma'_{yy},\ \sigma'_{zz},\ \tau_{xy},\ \tau_{yx},\ \tau_{zx} \,\right] \tag{5.20}$$

and

$$\mathbf{A}^T = \begin{bmatrix} \frac{\partial}{\partial x} & 0 & 0 & \frac{1}{2}\frac{\partial}{\partial y} & 0 & \frac{1}{2}\frac{\partial}{\partial z} \\ 0 & \frac{\partial}{\partial y} & 0 & \frac{1}{2}\frac{\partial}{\partial x} & \frac{1}{2}\frac{\partial}{\partial z} & 0 \\ 0 & 0 & \frac{\partial}{\partial z} & 0 & \frac{1}{2}\frac{\partial}{\partial y} & \frac{1}{2}\frac{\partial}{\partial x} \end{bmatrix} \tag{5.21}$$

Substituting Eqn. (5.15a) into Eqn. (5.18) yields

$$\dot{\varepsilon} = \mathbf{A}\ N_I \hat{\mathbf{v}}_I = \mathbf{B}_I \hat{\mathbf{v}}_I \tag{5.22}$$

Where $\mathbf{B}_I$ is the matrix representation of the differential operator $\mathbf{A}$ acting on the interpolation matrix N_I and given by

$$\mathbf{B}_I^T = \begin{bmatrix} \frac{\partial N_I}{\partial x} & 0 & 0 & \frac{1}{2}\frac{\partial N_I}{\partial y} & 0 & \frac{1}{2}\frac{\partial N_I}{\partial z} \\ 0 & \frac{\partial N_I}{\partial y} & 0 & \frac{1}{2}\frac{\partial N_I}{\partial x} & \frac{1}{2}\frac{\partial N_I}{\partial z} & 0 \\ 0 & 0 & \frac{\partial N_I}{\partial z} & 0 & \frac{1}{2}\frac{\partial N_I}{\partial y} & \frac{1}{2}\frac{\partial N_I}{\partial x} \end{bmatrix} \tag{5.23}$$

The Jacobian matrix of the coordinate transformation is given by

$$\begin{bmatrix} \frac{\partial N_I}{\partial \xi} \\ \frac{\partial N_I}{\partial \eta} \\ \frac{\partial N_I}{\partial \zeta} \end{bmatrix} = \begin{bmatrix} \partial x/\partial \xi & \partial y/\partial \xi & \partial z/\partial \xi \\ \partial x/\partial \eta & \partial y/\partial \eta & \partial z/\partial \eta \\ \partial x/\partial \zeta & \partial y/\partial \zeta & \partial z/\partial \zeta \end{bmatrix} \begin{bmatrix} \frac{\partial N_I}{\partial x} \\ \frac{\partial N_I}{\partial y} \\ \frac{\partial N_I}{\partial z} \end{bmatrix} \tag{5.24}$$

$$\begin{bmatrix} \frac{\partial N_I}{\partial x} \\ \frac{\partial N_I}{\partial y} \\ \frac{\partial N_I}{\partial z} \end{bmatrix} = \mathbf{J}^{-1} \begin{bmatrix} \frac{\partial N_I}{\partial \xi} \\ \frac{\partial N_I}{\partial \eta} \\ \frac{\partial N_I}{\partial \zeta} \end{bmatrix} \tag{5.25}$$

and $\mathbf{J}^{-1}$ the inverse of the Jacobian matrix and is given by

$$\mathbf{J}^{-1} = \frac{1}{|\mathbf{J}|} \begin{bmatrix} \frac{\partial y}{\partial \eta}\frac{\partial z}{\partial \zeta} - \frac{\partial y}{\partial \zeta}\frac{\partial z}{\partial \eta} & \frac{\partial y}{\partial \zeta}\frac{\partial z}{\partial \xi} - \frac{\partial y}{\partial \xi}\frac{\partial z}{\partial \zeta} & \frac{\partial y}{\partial \xi}\frac{\partial z}{\partial \eta} - \frac{\partial y}{\partial \eta}\frac{\partial z}{\partial \xi} \\ \frac{\partial x}{\partial \zeta}\frac{\partial z}{\partial \eta} - \frac{\partial x}{\partial z}\frac{\partial z}{\partial \eta} & \frac{\partial x}{\partial \xi}\frac{\partial z}{\partial \zeta} - \frac{\partial x}{\partial \zeta}\frac{\partial z}{\partial \xi} & \frac{\partial x}{\partial \eta}\frac{\partial z}{\partial \xi} - \frac{\partial x}{\partial \xi}\frac{\partial z}{\partial \eta} \\ \frac{\partial x}{\partial \eta}\frac{\partial y}{\partial \zeta} - \frac{\partial x}{\partial \zeta}\frac{\partial y}{\partial \eta} & \frac{\partial x}{\partial \zeta}\frac{\partial y}{\partial \xi} - \frac{\partial x}{\partial \xi}\frac{\partial y}{\partial \zeta} & \frac{\partial x}{\partial \xi}\frac{\partial y}{\partial \eta} - \frac{\partial x}{\partial \eta}\frac{\partial y}{\partial \xi} \end{bmatrix} \tag{5.26}$$

where $|\mathbf{J}|$ is the determinant of the Jacobian matrix and is given by

$$|\mathbf{J}| = \frac{\partial x}{\partial \xi}\frac{\partial y}{\partial \eta}\frac{\partial z}{\partial \zeta} + \frac{\partial x}{\partial \zeta}\frac{\partial y}{\partial \xi}\frac{\partial z}{\partial \eta} + \frac{\partial x}{\partial \eta}\frac{\partial y}{\partial \zeta}\frac{\partial z}{\partial \xi} - \frac{\partial x}{\partial \zeta}\frac{\partial y}{\partial \eta}\frac{\partial z}{\partial \xi} - \frac{\partial x}{\partial \eta}\frac{\partial y}{\partial \xi}\frac{\partial z}{\partial \zeta} - \frac{\partial x}{\partial \xi}\frac{\partial y}{\partial \zeta}\frac{\partial z}{\partial \eta} \tag{5.27}$$

Inserting Eqn. (5.22) in Eqn. (5.3), the effective strain-rate is expressed by nodal velocities as

$$\dot{\bar{\varepsilon}} = \left(\frac{2}{3}\dot{\varepsilon}^T \dot{\varepsilon}\right)^{1/2} = \left(\frac{2}{3}\hat{\mathbf{V}}_I^T \mathbf{B}_I^T \mathbf{B}_J \mathbf{V}_J\right)^{1/2} \tag{5.28}$$

The volumetric strain-rate is given by

$$\dot{\varepsilon}_v = \dot{\varepsilon}_{kk} = \dot{\varepsilon}_x + \dot{\varepsilon}_y + \dot{\varepsilon}_z \tag{5.29}$$

For convenience, using the appropriate vector representation of the Kronecker delta the volumetric strain-rate becomes

$$\dot{\varepsilon}_v = \mathbf{c}\,\dot{\varepsilon} = \mathbf{c}\;\mathbf{B}_I\,\hat{\mathbf{V}}_J \tag{5.30}$$

where

$$\mathbf{c} = [\,1 \;\; 1 \;\; 1 \;\; 0 \;\; 0 \;\; 0\,] \tag{5.31}$$

Substituting Eqns. (5.15a), (5.28) and (5.30) into Eqn. (5.11) it is found that the variation $\delta\mathbf{v}$ is factored out by the variation of the nodal velocity components $\mathbf{v}$ resulting in

$$\sum_e \left(\delta\hat{\mathbf{v}}_I \left\{\int_{V^{(e)}} \frac{2}{3}\left(\frac{\bar{\sigma}}{\dot{\bar{\varepsilon}}}\right)\mathbf{B}_I^T\mathbf{B}_J\mathbf{v}_J\,dV + K\int_{V^{(e)}} \mathbf{c}^T\mathbf{B}_J^T\mathbf{c}\mathbf{B}_I\,\hat{\mathbf{v}}_J\,dV + \int_{S_F^{(e)}} N_I^T\,\mathbf{f}\,dS\right\}\right) = 0 \tag{5.32}$$

Because Eqn. (5.32) should be satisfied for any arbitrary variation $\delta\mathbf{v}$, the final equations to be solved become

$$\sum_e \left(\int_{V(e)} \frac{2}{3}\left(\frac{\bar{\sigma}}{\dot{\bar{\varepsilon}}}\right)\mathbf{B}_I^T\mathbf{B}_J\mathbf{v}_J\,dV + K\int_{V(e)} \mathbf{c}^T\mathbf{B}_J^T\mathbf{c}\mathbf{B}_I\hat{\mathbf{v}}_J\,dV + \int_{S_F^{(e)}} N_I^T\,\mathbf{f}\,dS\right) = 0 \tag{5.33}$$

The first term in Eqn. (5.33) has non-linearity since the flow stress depends on the strain-rate, strain, and temperature. Generally nonlinear solvers are used to obtain the solutions. The iteration control is discussed later.

Strain Calculation

The basic equation for effective strain in terms of velocity and effective strain-rate is is given by

$$\frac{\partial \bar{\varepsilon}}{\partial t} + \mathbf{u}\frac{\partial \bar{\varepsilon}}{\partial \mathbf{x}} = \dot{\bar{\varepsilon}}(\mathbf{u}) \tag{5.34}$$

Since drawing is a steady-state process, the first term becomes zero. For a given effective strain-rate field the total effective strain-rate is evaluated from Eqn. (5.34). As in the case of Eqn. (5.10b) the above equation can also be discretized by dividing the volume into, 8-node hexahedral isoparametric elements interconnected at N nodal points. Interpolation functions given by Eqn. (5.13) are used to approximate the value of total effective strain inside an element. The discretized form of Eqn. (5.34) is given by

$$\sum_e \left(\int_{V(e)} N_I \, \mathbf{u} \frac{\partial N_J}{\partial \mathbf{x}} \hat{\bar{\varepsilon}}_J \, dV - \int_{V(e)} N_I \, \dot{\bar{\varepsilon}} \, dV \right) = 0 \tag{5.35}$$

Eqn. (5.35) can be written in the vector form as

$$K_{IJ}(\mathbf{u}) \, \hat{\bar{\varepsilon}}_J = f_I(\mathbf{u}) \tag{5.36}$$

Traction Boundary Condition

Traction boundary condition exist at the interface between the die and the material being drawn. At the die workpiece interface, traction is imposed as constant shear friction

on the contact surface in the direction opposite to the relative velocity of the drawn material with respect to the die. Prescribed velocity is treated as an essential boundary condition. Therefore it is applied during the finite element discretization. Velocity of the material at the die material interface (and in the rest of the deforming material) is evaluated automatically in terms of nodal velocities and element shape functions.

Traction boundary condition is imposed in the form of nodal point forces. Constant shear friction is given by f=mk, where m is the friction factor and k is the shear strength of the material. As constant shear friction is dealt with locally, the dependency of local shear strength on the local strain in work hardening materials is taken into account. In case some region at the interface has no relative motion (neutral region), the first derivative of friction with respect to velocity becomes infinite in that region. To avoid singularity, constant shear friction is approximated by velocity dependent friction, which is given by

$$f = mk\left[\frac{2}{\pi}\tan^{-1}\left(\frac{v_r}{A}\right)\right] \tag{5.37}$$

where v_r is the relative velocity of the drawn material with respect to the die, and a small value of A is arbitrarily introduced for performing numerical calculations. The value of v_r/A should be equal to or larger than 10 [Kobayashi et al, 1989] to attain the friction value within 9% of the friction originally intended.

Numerical Integration

All volume and surface integrations were performed by applying the Gaussian quadrature formulas. For given functions f(x,y) and g(x,y,z), the Gaussian integration formulas are given by

$$\int_S f(x,y)\, dS = \int_x \int_y f(x,y)\, dxdy = \int_{-1}^{1} \int_{-1}^{1} f(\xi,\eta)\, |\mathbf{J}(\xi,\eta)|\, d\xi d\eta \tag{5.38}$$

$$\approx \sum_J^m \sum_I^n w_I w_J\, f(\xi_I,\eta_J)\, |\mathbf{J}(\xi_I,\eta_J \tag{5.39}$$

$$\int_v g(x,y,z)\, dV = \int_x \int_y \int_z h(x,y,z)\, dxdydz = \int_{-1}^{1} \int_{-1}^{1} \int_{-1}^{1} h(\xi,\eta,\zeta)\, |\mathbf{J}(\xi,\eta,\zeta)|\, d\xi d\eta d\zeta \tag{5.40}$$

$$\approx \sum_K^l \sum_J^m \sum_I^n w_I w_J w_K\, f(\xi_I,\eta_J,\zeta_K)\, |\mathbf{J}(\xi_I,\eta_J,\zeta_K)| \tag{5.41}$$

where $|\mathbf{J}|$ is the determinant of the Jacobian matrix of co-ordiante transformation and w_I are weight factors. The weight factors and co-ordinates of the integration points can be found in any textbook dealing with numerical methods.

The volume integrals related to the first term in Eqn. (5.33) were evaluated using 2x2x2 integration points. The volume integrations related to the second term in Eqn. (5.33) was done by using 1x1x1 integration points. This is known as reduced integration, and is used to avoid the possibility of over-constraint caused by a higher order integration scheme. The surface integrations related to the third term in Eqn. (5.33) were carried out using 3x3 integration points. The volume integrations in Eqn. (5.35) were done by using 2x2x2 integration points.

Iteration Control

After setting up the elemental equations, the global stiffness matrix is assembled in compact form (skyline) and solved by column reduction scheme. Eqns. (5.33) and (5.35) are coupled to each other, and the coupled iteration process is carried out as follows.

(i) Calculate the guess velocity field $\hat{\mathbf{v}}$ from Eqn. (5.33) by the direct iteration method. The simultaneous criteria were used to test for the convergence of the velocity equation. One criterion is the error norm of the velocity defined as $\|\Delta \mathbf{v}\| / \|\mathbf{v}\|$, where $\|\mathbf{v}\|$ is the Euclidean vector norm. The other criterion is the residual norm of the equations corresponding to the right hand side of Eqn. (5.33). Satisfaction of either of the two criteria is considered enough for convergence.

(ii) Using the guess velocity field from (i) calculate the velocity field by the Newton-Raphson method again form Eqn. (5.33).

(iii) Applying the velocity field and strain-rate ($\dot{\bar{\varepsilon}}$) field from step (ii), total effective strain is evaluated from Eqn. (5.35).

(iv) Update the effective strain of the elements

(v) Steps (ii), (iii) and (iv) are repeated until the convergence criteria for effective strain is satisfied. The criteria for convergence of effective strain is given by the error norm $\|\Delta \bar{\varepsilon}\| / N$.

CHAPTER VI

BAR DRAWING

Simulation Conditions

All the simulations in this study were performed for bars of rectangular cross-section. The stock entering the die is also of rectangular cross-section.

Material Properties

Annealed Al 2024 is used for the simulation. The flow stress-strain relation is given by $\bar{\sigma} = K(\bar{\varepsilon})^n$, where K = 386.8 MPa and n = 0.154. The stress-strain curve for Al 2024 is shown in Fig. 6.1.

Dimensions

For a given percentage area reduction, the dimensions of the die that can be varied are the die draft angle (2 x die semi-cone angle) and in turn the length of the die. The various die specifications for which simulations were performed are tabulated in Table 1.

Boundary Conditions

The material in the die is shown in Fig. 6.2. Taking advantage of symmetry only the top left quarter of the material in the die is used in the simulations. This is shown hatched in Fig. 6.2.

The material in the die moves axially in the X-direction with a uniform velocity. A constant shear friction factor (m) is applied to all the nodes touching the die surface.

TABLE I

SIMULATION CONDITIONS

No.	Dimensions at entrance (mm)	Dimensions at exit (mm)	Percentage reduction	Die draft angle (deg)	Die Length (mm)	Drawing Velocity (mm/sec)	Friction factor	Δ parameter
1	110.16 x 59.36	104.16 x 53.36	12.32	3.0	114.56	508	0.1	0.78
2	110.16 x 59.36	104.16 x 53.36	12.32	4.0	85.40	508	0.1	1.03
3	110.16 x 59.36	104.16 x 53.36	12.32	6.0	57.24	508	0.1	1.53
4	110.16 x 59.36	104.16 x 53.36	12.32	8.0	42.90	508	0.1	2.04
5	110.16 x 59.36	101.6 x 50.8	14.93	11.0	44.45	25	0.01	1.94
6	110.16 x 59.36	101.6 x 50.8	14.93	11.0	44.45	25	0.1	1.94
7	110.16 x 59.36	101.6 x 50.8	14.93	11.0	44.45	25	0.5	1.94
8	110.16 x 59.36	92.87 x 42.07	40.23	22.0	44.45	25	0.01	1.82
9	110.16 x 59.36	92.87 x 42.07	40.23	22.0	44.45	25	0.1	1.82
10	110.16 x 59.36	92.87 x 42.07	40.23	22.0	44.45	25	0.5	1.82
11	110.16 x 59.36	101.6 x 50.8	14.93	11.0	44.45	508	0.1	1.94
12	110.16 x 59.36	92.87 x 42.07	40.23	22.0	44.45	508	0.1	1.82

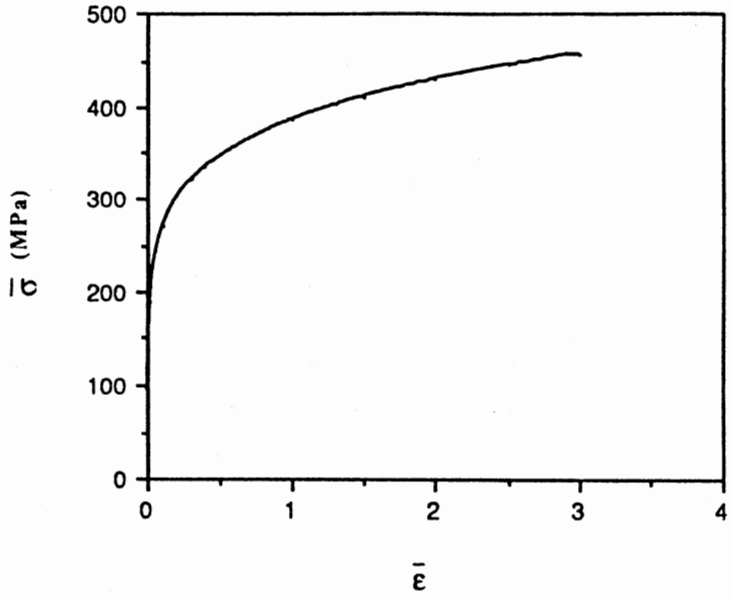

Figure 6.1 Stress-Strain Curve for AL 2024

Constant velocity boundary condition is imposed on the nodes at the exit. Along the planes of symmetry, the velocities normal to the drawing direction must vanish.

The semi die angle is represented by α. The boundary conditions applied for the analysis of drawing are shown in Fig. 6.3. The local co-ordiante system at the top surface of the die is represented by (x_t,y_t,z_t). This is obtained by rotating the global co-ordinate system about the y-axis by -90 degrees and then by (90 - α) degrees about the x-axis. Similarly the local co-ordinate system at the side face of the die is represented by (x_s,y_s,z_s), and is obtained by rotating the global co-ordinate system about the y-axis by -α. At the exit and the planes of symmetry the local co-ordinate system coincides with the global co-ordinate system. It should be noted that the z-axis is made normal to the die surface by rotating about the Y-axis (global) first and then about the X-axis (global).

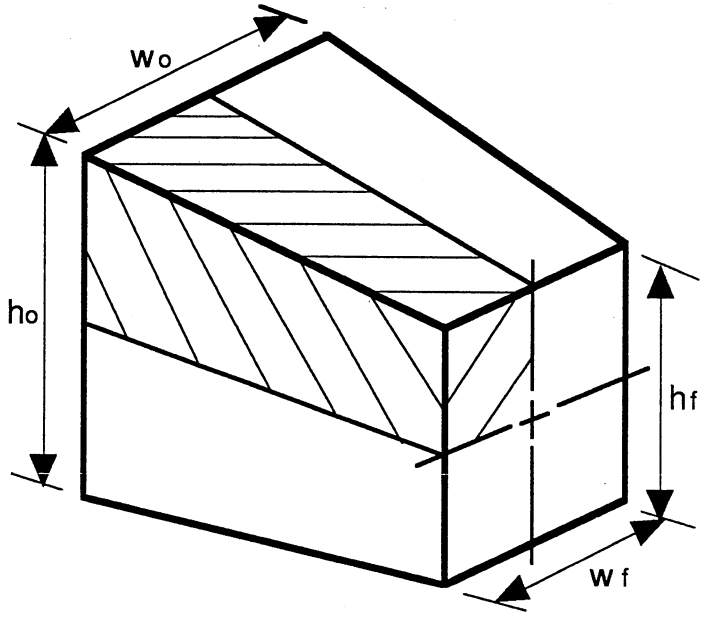

Figure 6.2 Material in the Die With the Quarter Used in the Simulations Shown Hatched

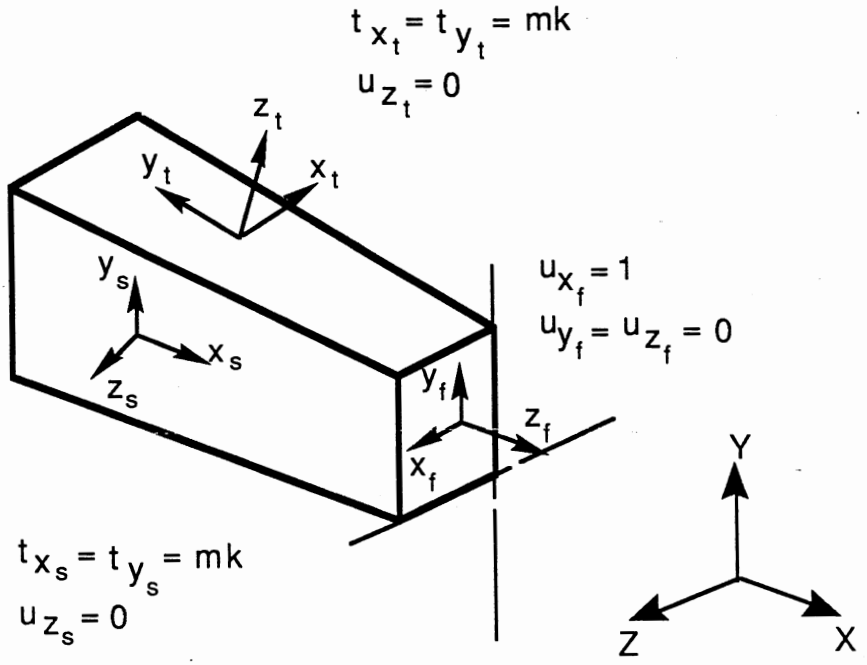

Figure 6.3 Boundary Conditions

Results and Discussion

The results obtained consist of velocity distributions, steady-state drawing loads, die pressure distribution, flow stress contours, average stress contours, effective strain-rate contours, total effective strain contours, and principal stresses. The mesh system used for the simulations is shown in Fig. 6.4. The control volume was discretized into 84 elements with 161 nodal points. The part of the control volume along the die corner is discretized into finer elements.

The iterations were performed until either the residual norm or the error norm $\|\Delta v\| / \|v\| \leq 0.0001$. On the average about 7 to 10 iterations were required for convergence.

Deformation Zone Geometry

The variation of steady-state drawing load with die angle was studied using the deformation-zone geometry. The shape of the deformation-zone has a strong influence on redundant work, frictional work, and forming forces in drawing, extrusion and rolling [Hosford and Caddell, 1983]. A single parameter, Δ, is used to characterize the deformation-zone geometry which is defined as

$$\Delta = \frac{h}{L} \tag{6.1}$$

where h is the mean thickness or diameter of the work metal and L is the contact length between tool and work metal. The Δ parameter was calculated for all the simulations and the result is shown in Table I. This shows that Δ increases with α for constant percentage reduction. This implies that the strain induced due to inhomogeneous deformation increases with α. Hence an increase in steady-state drawing load is expected as α increases for Simulation No. 1 - 4.

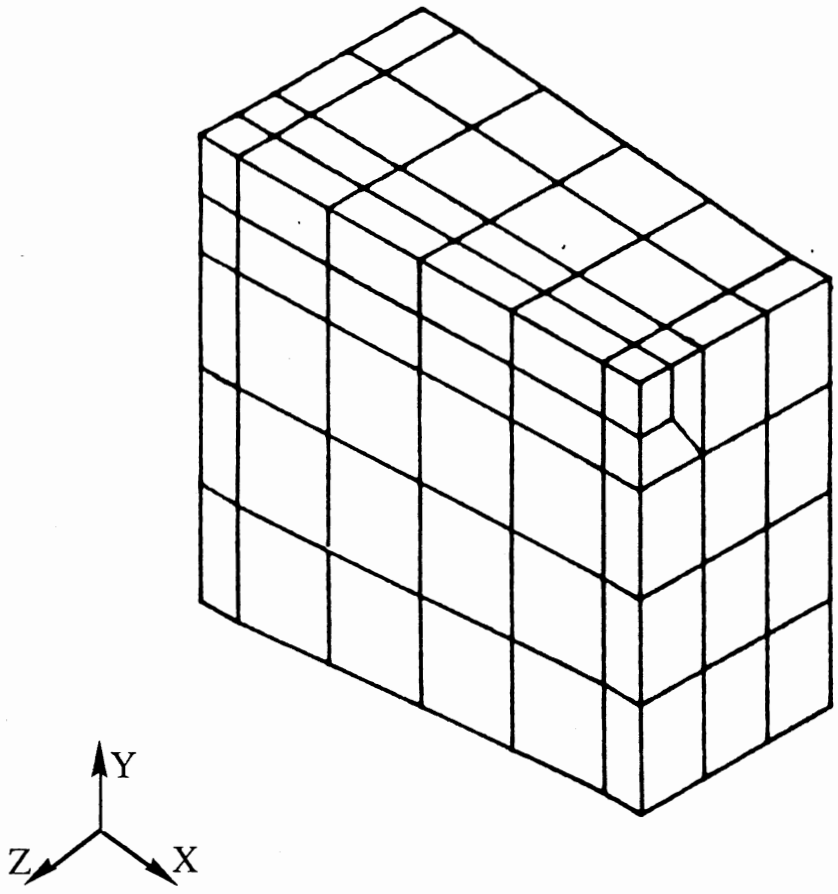

Figure 6.4 Mesh System Used for the Simulations (84 Elements, 161 Nodes)

Velocity Distribution

The velocity distributions have the same general trend for different friction conditions and die angles. A typical velocity distribution for simulation No. 4 (refer to Table 1) is shown in Fig. 6.5. The velocity has the maximum value at the die exit and decreases gradually towards the entrance of the die, as seen in Fig. 6.6. But for the exit where the velocity boundary condition is imposed the velocity is not uniform on any cross-section normal to the drawing direction. Velocity is maximum at the center of the rod and it decreases towards the edges in contact with the die. As expected the minimum velocity is at the die corner because the material is in contact with the two sides of the die which in turn results in a greater frictional force acting on the material. Fig. 6.6 shows the variation of velocity along the die axis and the die corner for simulation No. 4.

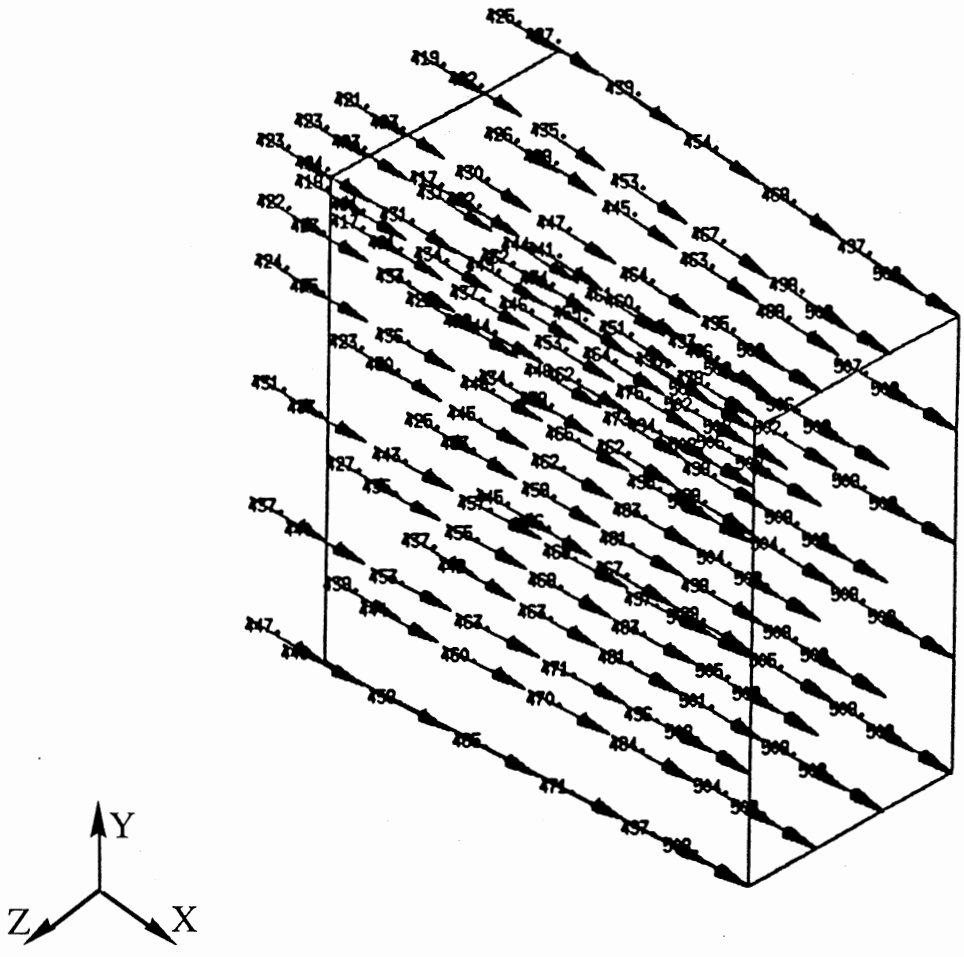

Figure 6.5 A Typical Velocity (mm/sec) Distribution (Simulation No. 4)

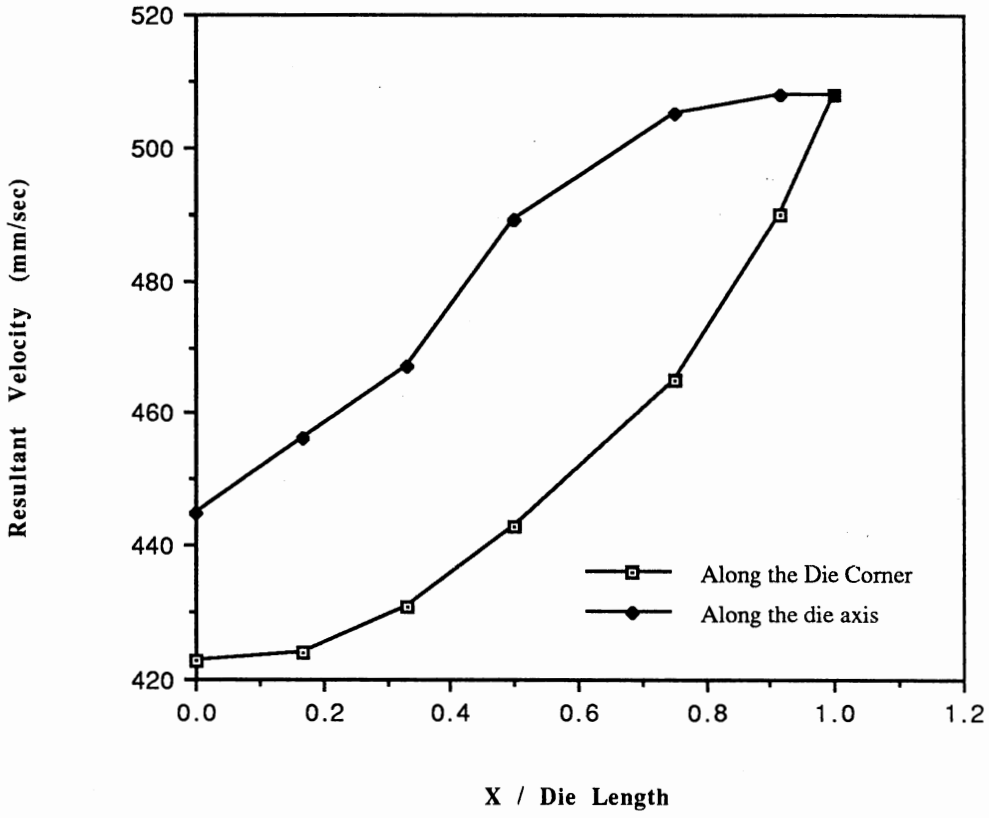

Figure 6.6 Velocity Distribution at the Die Axis and Die Corner (Simulation No. 4)

Steady-State Drawing Load

The variation of steady-state drawing load with die draft angle, friction factor (m) and drawing velocity is discussed. Steady-state drawing load as a function of die angle for a constant reduction is shown in Fig. 6.7. The drawing load decreases with the increase in die angle. This is because, increasing the die angle (for constant reduction) results in less area of contact and hence less frictional force to overcome. The steady-state drawing load was calculated using slab analysis [Hosford and Caddell, 1983] for comparison with the FEM result. The following equation was used to calculate the drawing load.

$$\frac{\sigma_d}{2k} = \frac{1+B}{B}[1- \exp(-B\varepsilon_h)] \tag{6.2}$$

where σ_d is the drawing stress, ε_h is the homogeneous strain; and $B = \mu \cot\alpha$ where μ is the friction coefficient, α is the semi-die angle. In this case (simulation No. 1 to 4) $\varepsilon_h = \ln(\frac{A_0}{A_e}) = 0.163$, where A_0 and A_e are the cross-sectional area at the entrance and exit,respectively, of the die and k is computed as

$$2k = \bar{\sigma} = 386.8\ (\bar{\varepsilon})^{0.154} = 262.9\ \text{MPa} \tag{6.3}$$

where $\bar{\varepsilon} = \frac{\varepsilon_h}{2} = 0.0815$. The result is shown in Fig. 6.7. This shows that the drawing load predicted by the slab analysis with $\mu = 0.1$ is about 30 % lower than that predicted by FEM simulation with friction factor m = 0.1 whereas with $\mu = 0.2$ the drawing load predicted by the slab analysis is considerably higher than that predicted by FEM simulation. With $\mu = 0.15$ the drawing load predicted by the slab analysis method agrees well with those predicted by FEM simulation.

The variation of steady-state load with the change in friction factor is shown in Fig. 6.8. Drawing load increases linearly with friction factor (m). Fig. 6.9 shows the variation

of drawing load with drawing velocity. From the plot it is clear that velocity has negligible effect on drawing load. This is because, aluminium, at room temperature, is strain hardening material and not strain-rate sensitive.

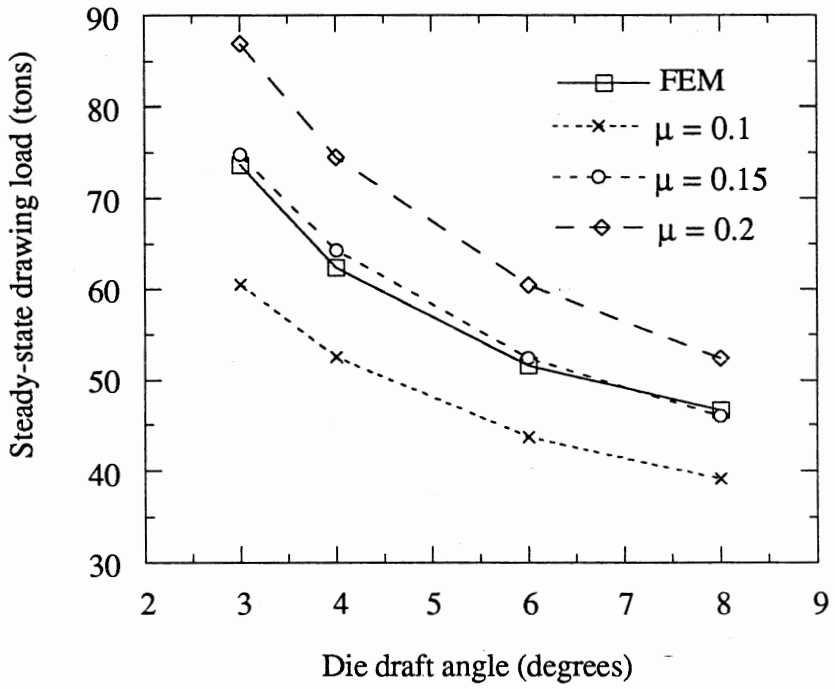

Figure 6.7 Variation of Steady-State Drawing Load as a Function of Die Draft Angle (Simulation No. 1 to 4)

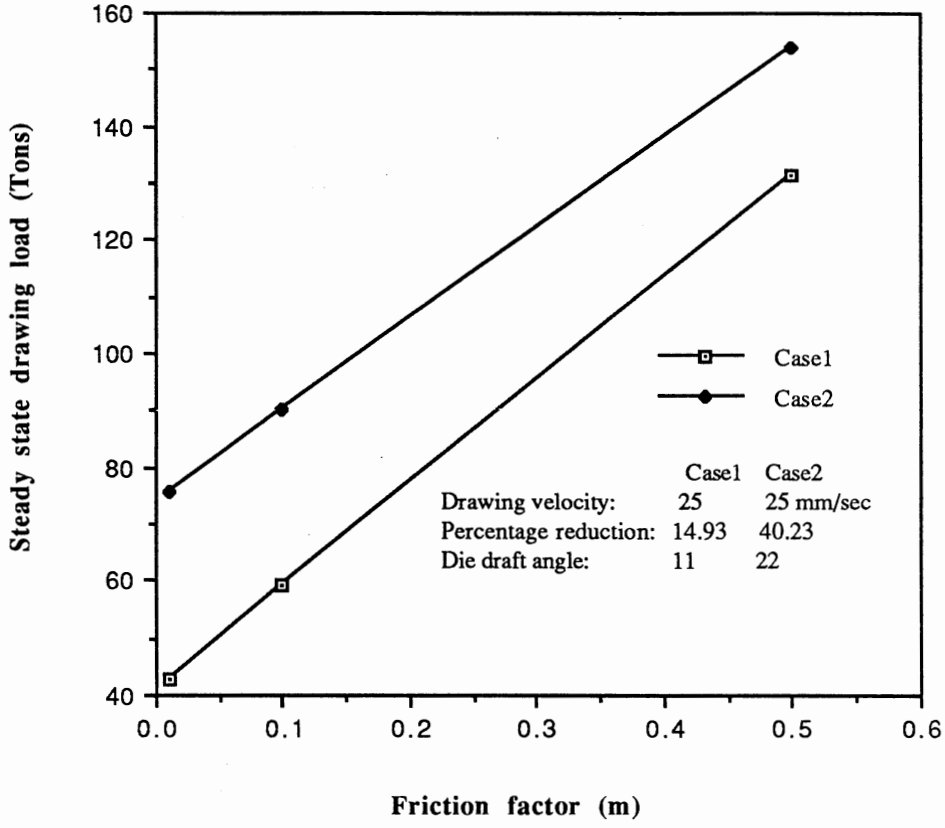

Figure 6.8 Variation of Steady-State Drawing Load With Friction Factor (Simulation No. 5 to 10)

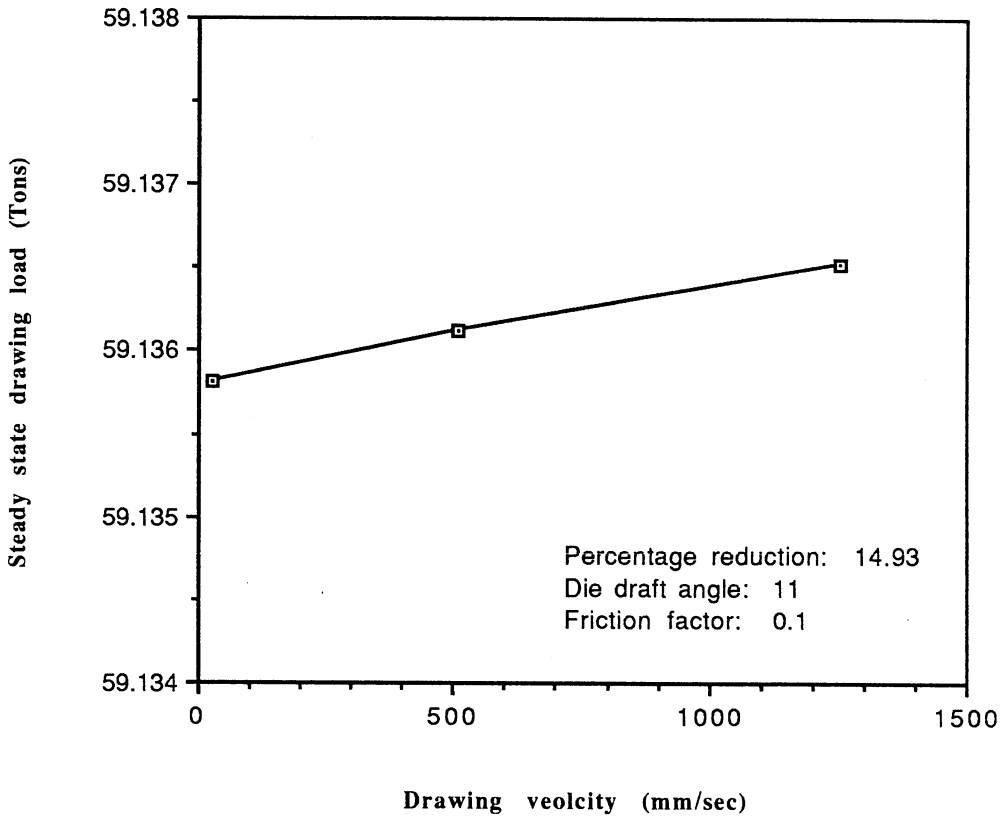

Figure 6.9 Variation of Steady-State Drawing Load With Drawing Velocity (Simulation No. 6 and 11)

Die Pressure Distribution

The die pressure distribution for simulation No. 1 is plotted in Fig. 6.10. The general trend is that the die pressure is the highest at the exit, decreasing towards the entrance and then increasing again near the entrance. In the direction normal to the drawing direction the die pressure is maximum at the line of symmetry and falls gradually towards the corner of the die. This is in agreement with experimental results [Wistreich, 1955]. Fig. 6.11 shows the variation of the maximum die pressure with die draft angle. Higher die draft angles produce greater maximum die pressures. The maximum die pressure is higher for frictionless dies than those with friction as shown in Fig. 6.12. Friction has effects similar to back pull, reducing the die loads, this again is in agreement with experimental results [Wistreich, 1955].

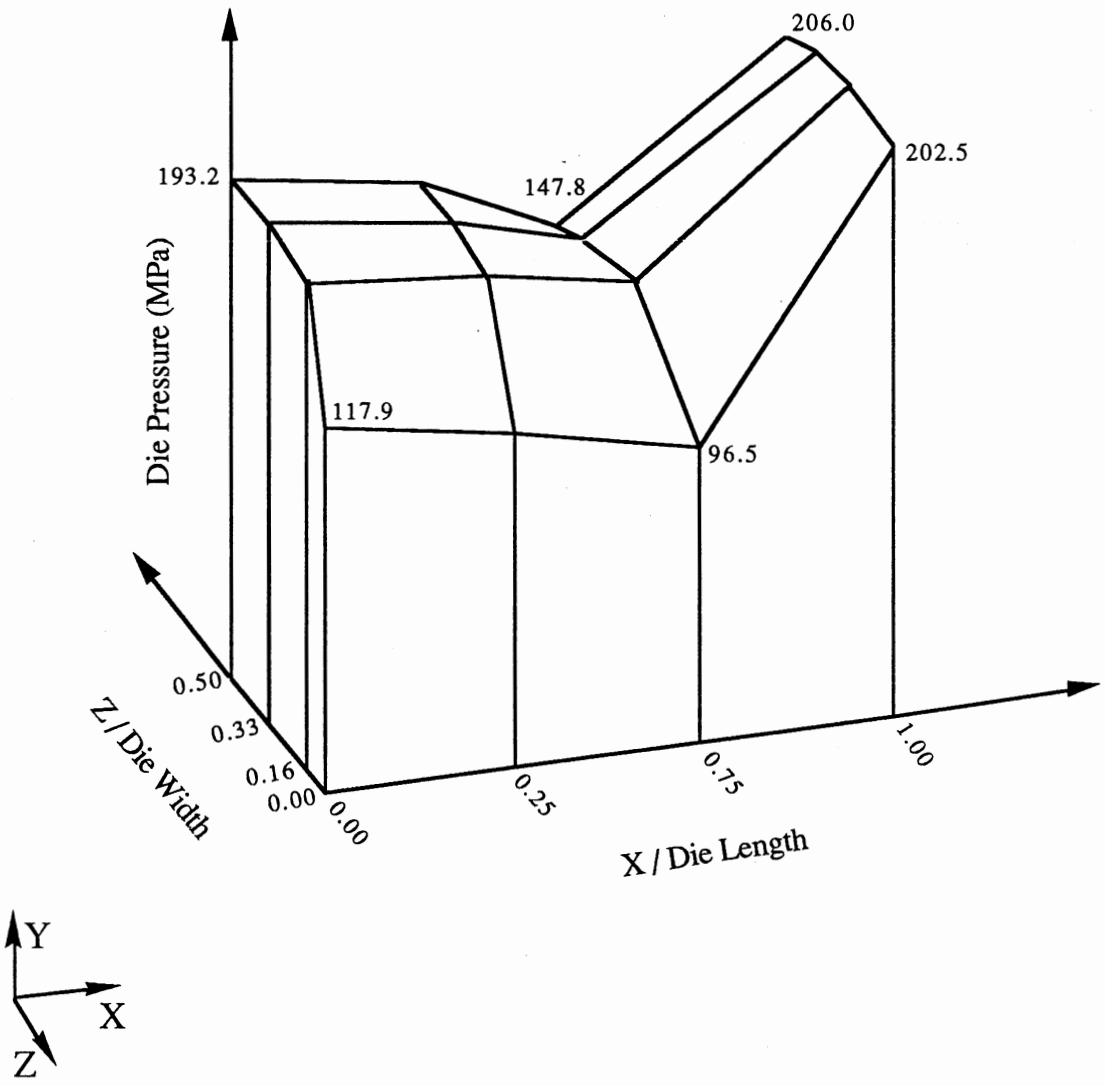

Figure 6.10 Typical Die Pressure Distribution on the Top Surface of the Die (Simulation No. 4)

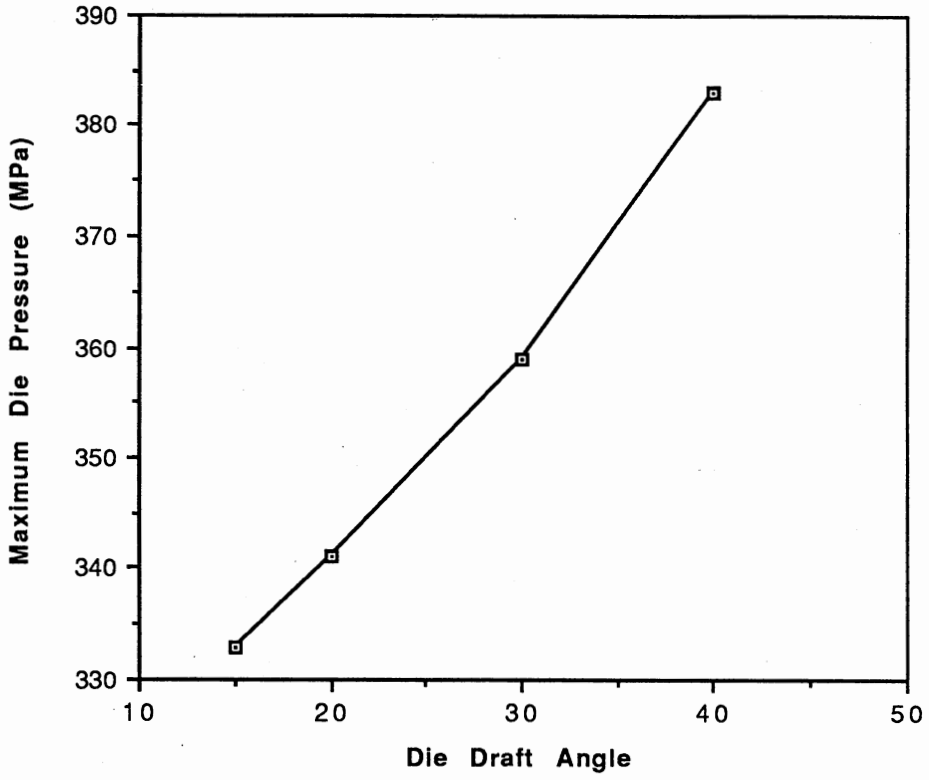

Figure 6.11 Variation of Maximum Die Pressure With Die Draft Angle

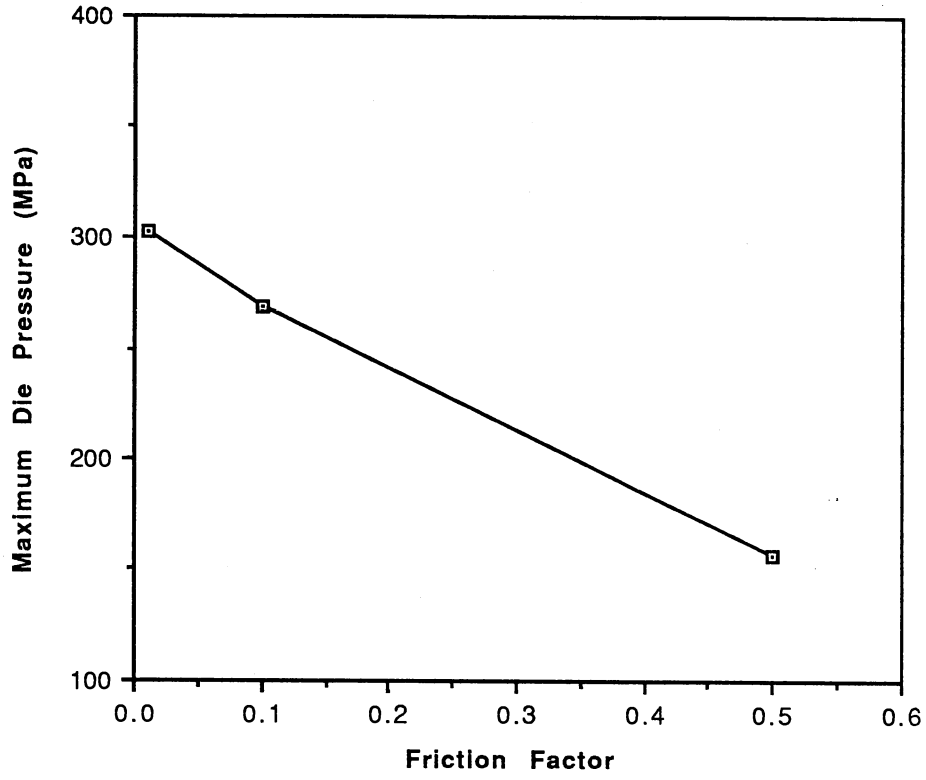

Figure 6.12 Variation of Maximum Die Pressure with Friction Factor
(Simulation No. 5 to 7)

Flow Stress Distribution

The flow stress contours with a velocity boundary condition of 508 mm/sec and a constant shear friction factor of 0.1 and a die angle of 8 degrees (simulation No. 4) are shown in Fig. 6.13. The flow stress is concentrated at the corners of the die. It has the lowest value at the entrance to the die. Also the stress decreases towards the center of the die. It was found that the flow stress distribution pattern is not affected by a change in the velocity boundary condition. This is explained by the fact that the flow stress of aluminium implemented for analysis is a function of strain at room temperature.

Mean Stress Distribution

Mean stress distributions for simulation No. 4 are shown in Fig. 6.14. It is highest at the corners. It is high along the edges of the die decreasing towards the planes of symmetry. On the planes of symmetry it decreases gradually from the exit towards the entrance. As expected average stress is compressive near the entrance and turns tensile near the exit.

Effective Strain-Rate Distribution

Effective strain-rate distribution for simulation No. 4 is shown in Fig. 6.15. It has the highest value at the corners and decreases towards the center and towards the entrance. At the entrance the effective strain-rate value is so low that it can be considered as almost rigid region.

Effective strain-rate contours have the same pattern as that of the flow stress contours at the die corners and at the die exit. Compared to the flow stress contours the effective strain-rate contours are concentrated not only at the corners of the die but also at the axis of the die at the exit. At the entrance to the die, unlike the average stress contours which run parallel to the edge of the die, the strain-rate contours move backwards.

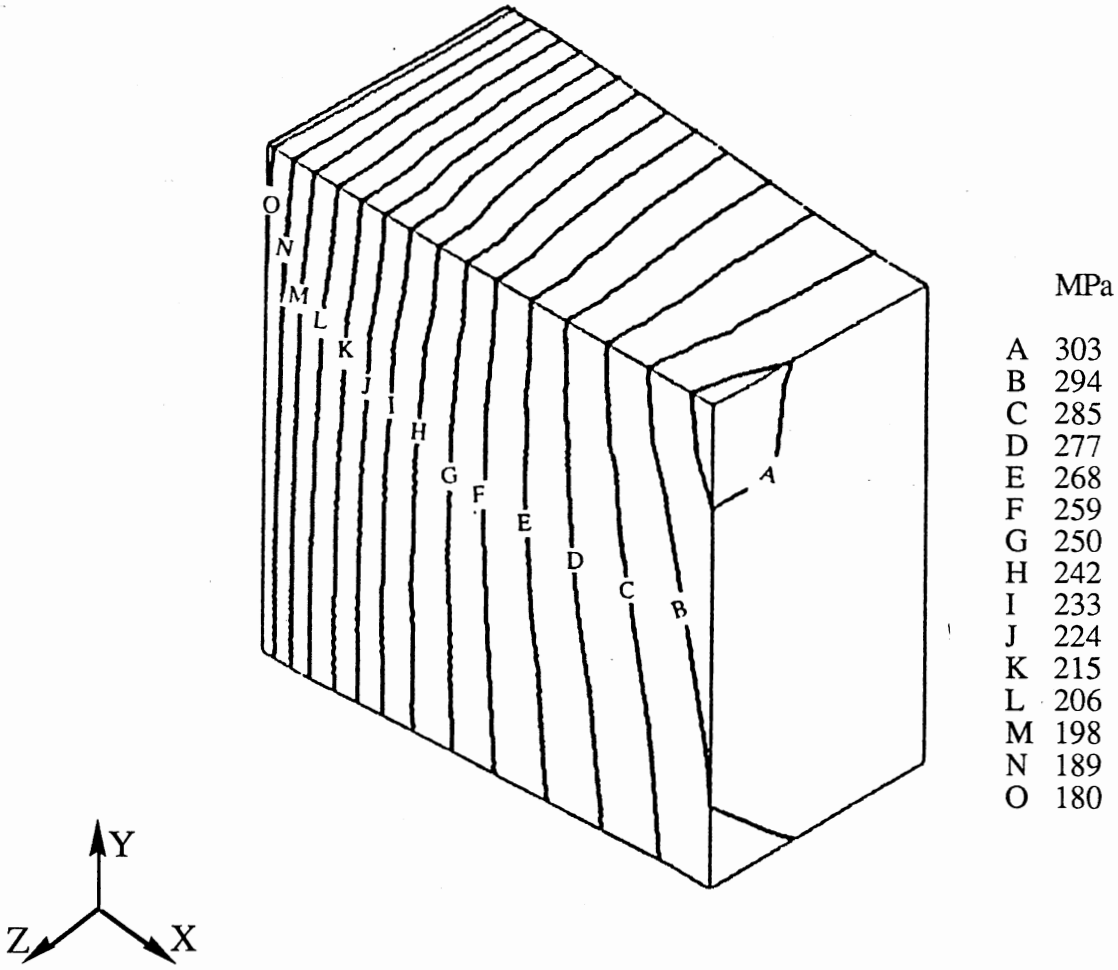

Figure 6.13 Flow Stress Contours for Simulation No. 4

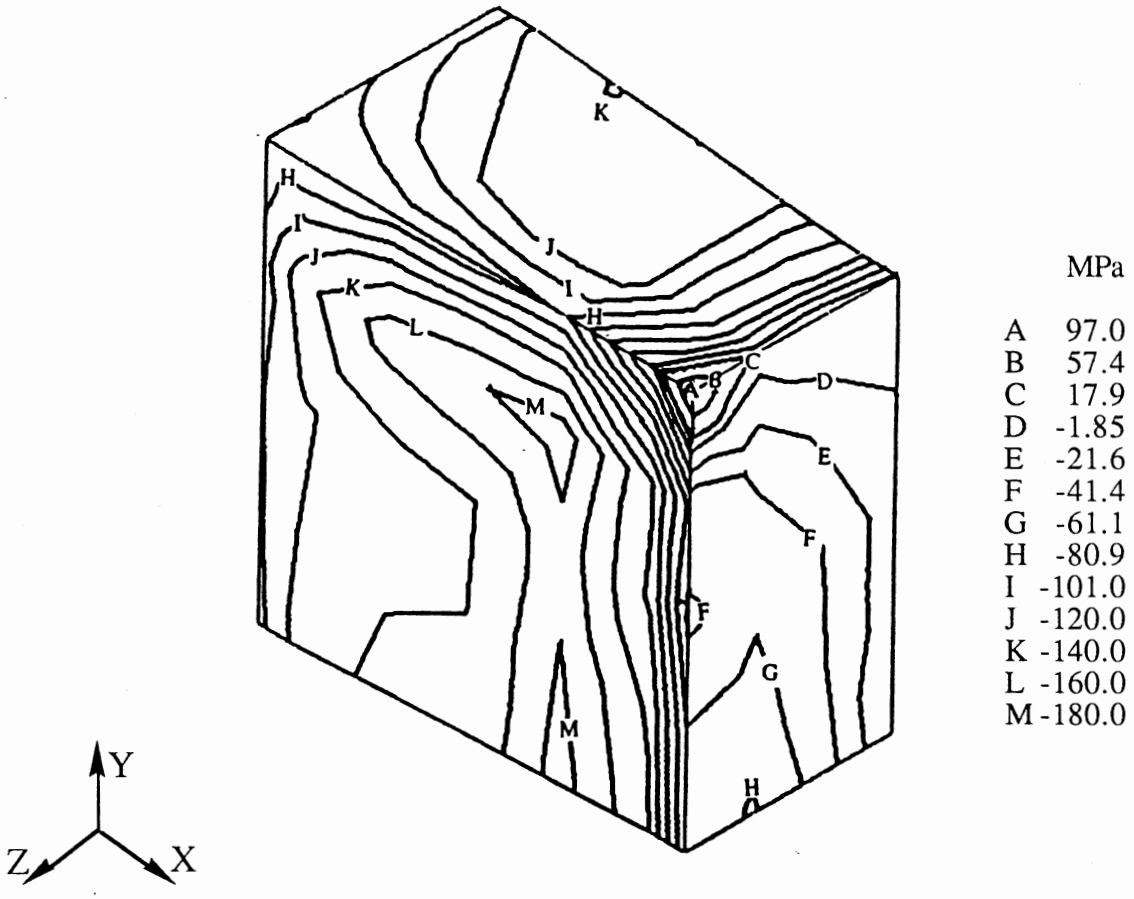

Figure 6.14 Mean Stress Contours for Simulation No. 4

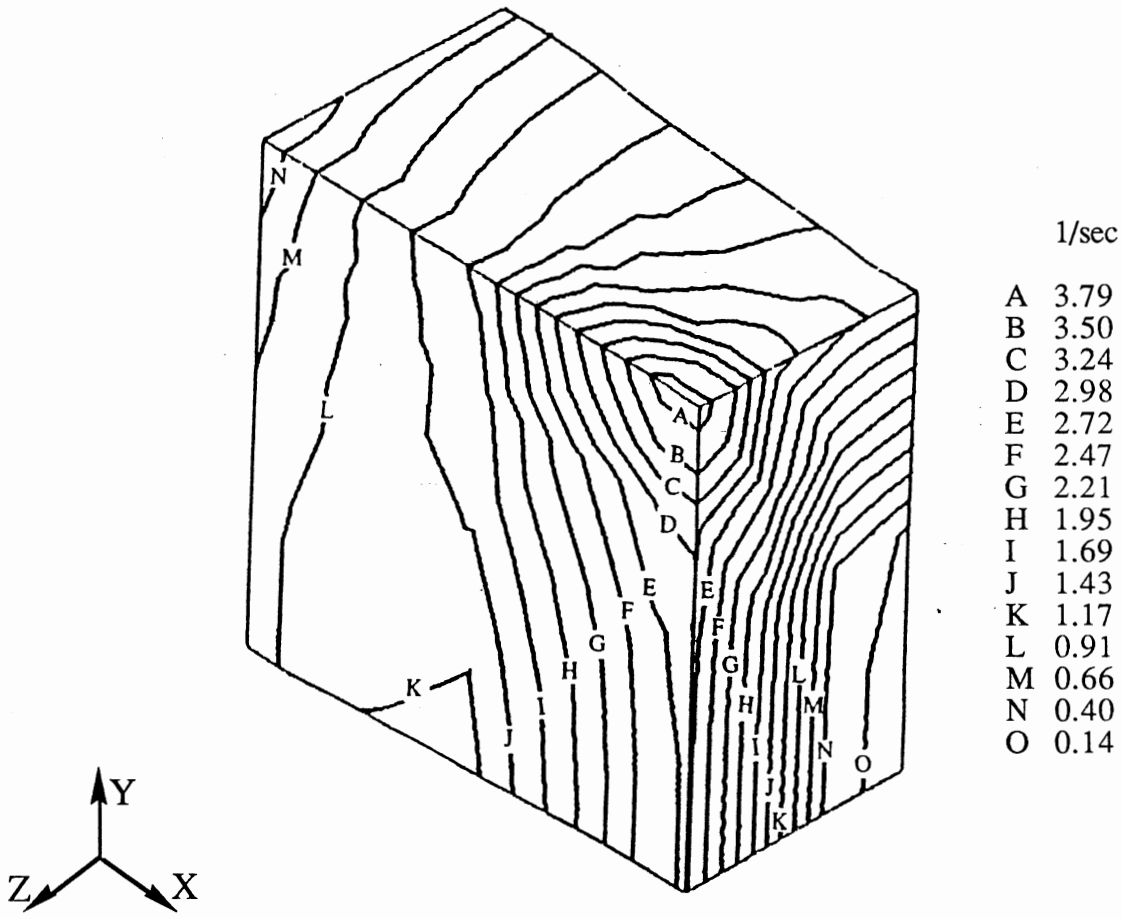

Figure 6.15 Effective Strain-Rate Contours for Simulation No. 4

Total Effective Strain Distribution

A typical example of total effective strain distribution is shown in Fig. 6.16. Total effective strain is also maximum at the corners of the die . At the exit it decreases gradually towards the center. The decrease towards the entrance is steeper. Across any cross-section normal to the drawing direction the total effective strain is higher closer to the die faces.

Principal Stresses

Finally, the directions and magnitudes of the major, intermediate and minor principal stresses are plotted in Fig. 6.17 for simulation number 4. The major principal stress component has the highest values at the exit and decreases very rapidly towards the entrance. The directions of the major principal stresses are not effected by the change in die angle and very negligibly by variation in friction factor. The magnitude of the major principal stresses increase with friction factor and decrease with increasing die angle. It is tensile throughout the deformation zone.

Microstructural Studies

Microstructural changes in four samples of cold drawn C1069 Si killed steel are examined. These samples are from the final series of passes, which in this case is a nine hole practice (nine die reductions). The as received rod (raw stock) is of 0.218 in. diameter and is drawn to 0.14 in. before final drawing (final passes). The first sample is as air patented processes wire (0.140 in. dia.) before the final series of drawing. Air patenting is a heat treatment process in which, thin wire austenitized, and then air cooled. Large diameter wires and rods are patented. Patenting is a heat treatment process in which, wire or rod is austenitized, quenched in a molten bath at a subcritical temperature, and then air cooled. Patenting is usually done before and in between cold drawing operations. The remaining samples are from the three consecutive passes of sample one. The diameters of

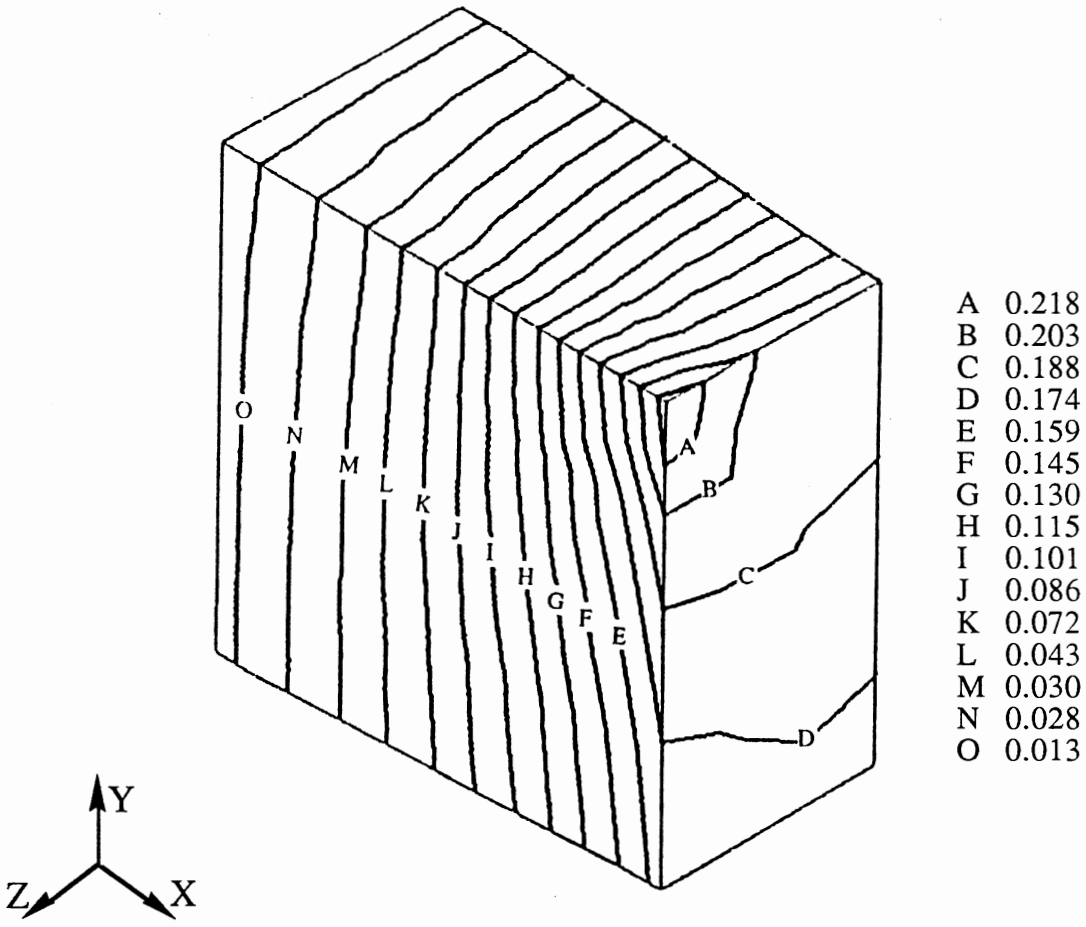

Figure 6.16 Total Effective Strain Contours for Simulation No. 4

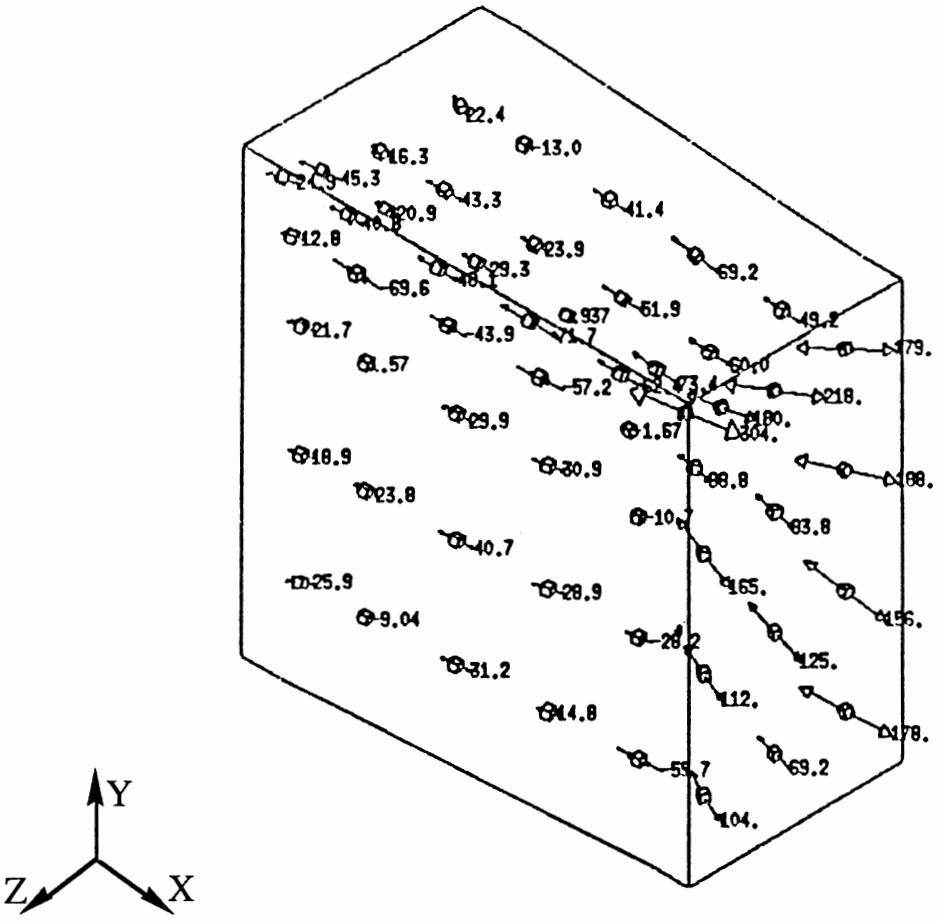

Figure 6.17 Major Principal Stresses (MPa) for Simulation No. 4

these samples are 0.119, 0.1, and 0.86 inches respectively. The drawing speed is proprietary and load measurements are not available.

Figs. 6.18 to 6.25 show the longitudinal and cross-sectional micrographs of the four samples. All samples were etched by using 2% nital. Air patenting results in a fine lamellar pearlite (mostly unresolved). This is seen as dark areas in Figs. 6.18 to 6.25. The lighter areas are ferrite, some of which are formed at prior austenite grain boundaries. In the figures showing the cross-sections it is noticed that as the diameter of the wire is reduced, the grain size becomes smaller. In the figures showing the longitudinal sections, pearlite deforms more and more with every pass. In Fig 6.25, pearlite appears as fine dark streaks. Thinner layers of pearlite result in a greater grain-boundary area per unit volume. This causes more plastic constraint to the normally deformable ferrite. With greater boundary area the strength of the material increases. Thinner layers of ferrite also increase the strength of the wire.

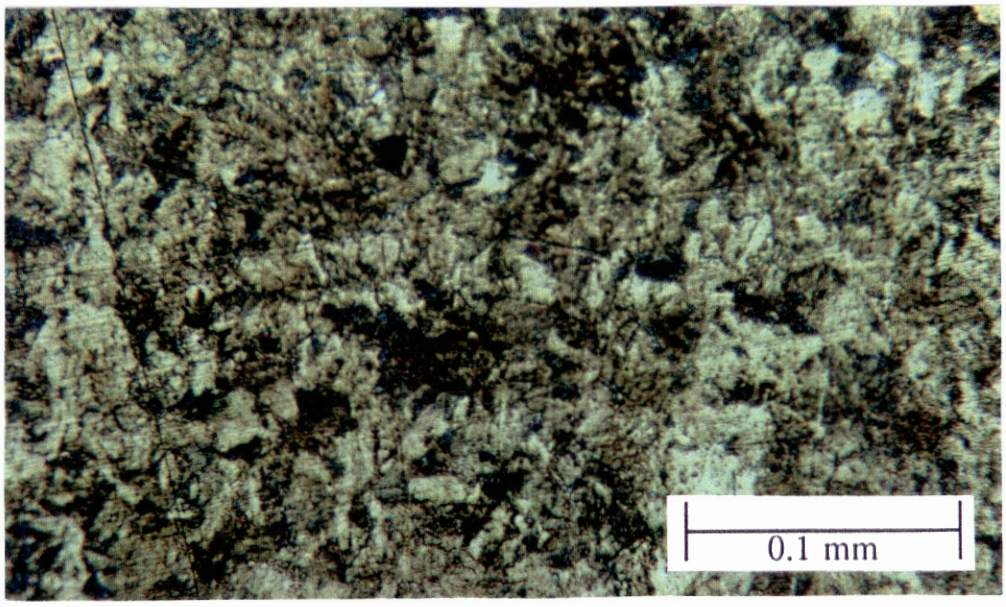

Figure 6.18 C1069 Steel Wire, as Patented of Diameter 0.14 in.
(Cross-Section, 385X)

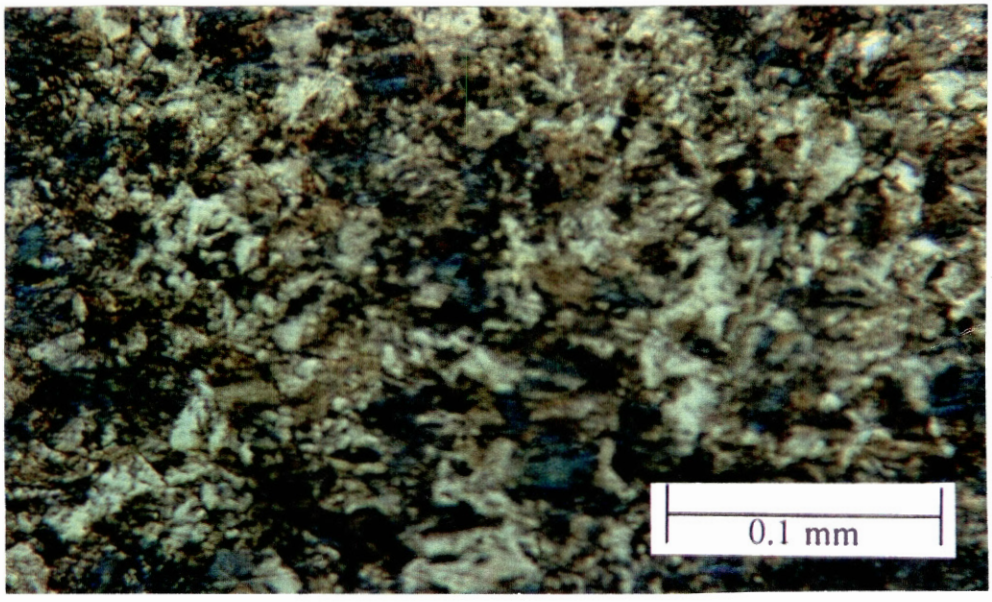

Figure 6.19 C1069 Steel Wire, as Patented of Diameter 0.14 in.
(Longitudinal Section, 385X)

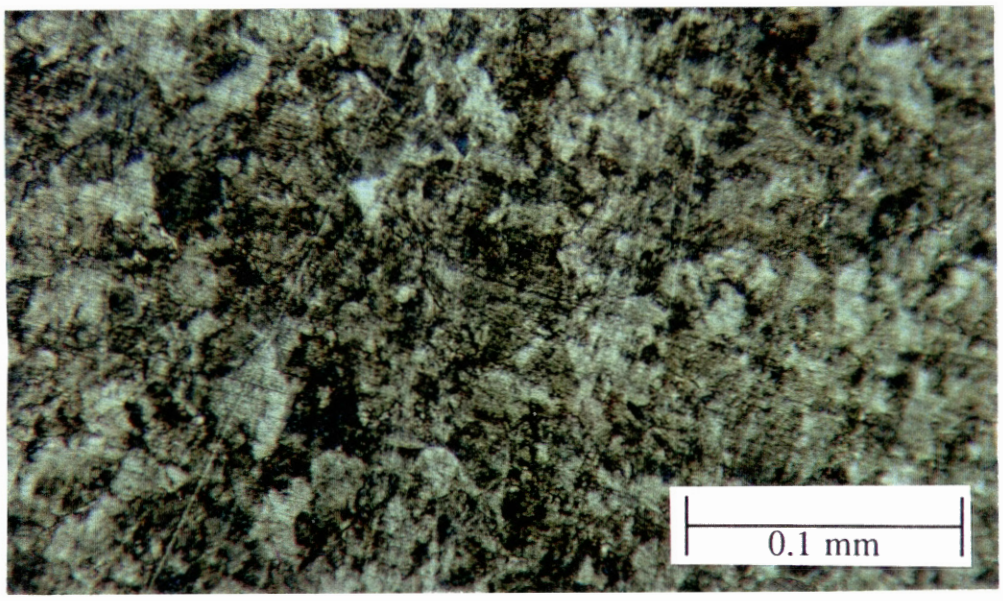

Figure 6.20 Same as Fig. 6.18, Cold Drawn to 0.119 in. Dia.
(Cross-Section, 385X)

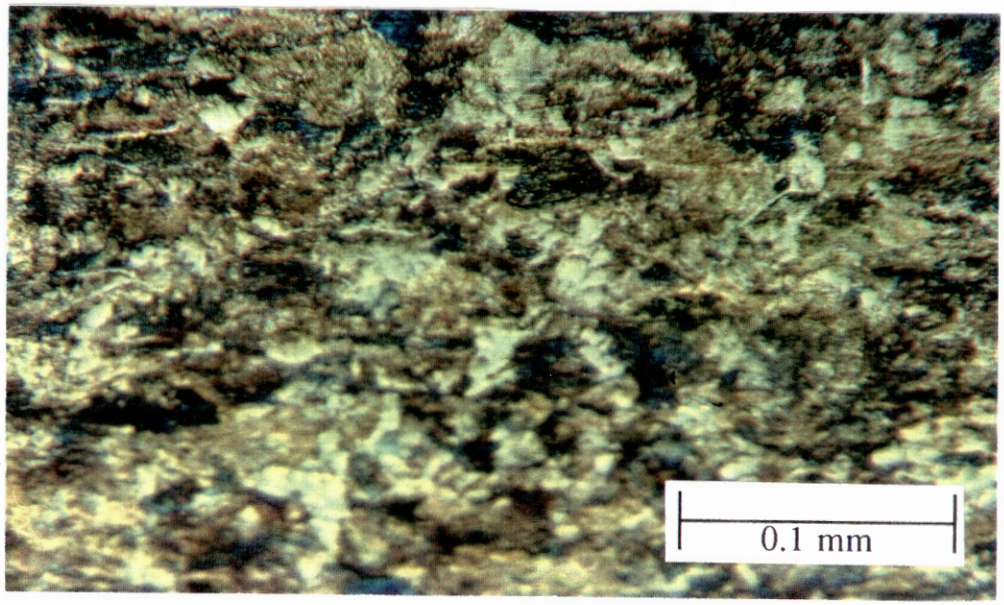

Figure 6.21 Same as Fig. 6.18, Cold Drawn to 0.119 in. Dia.
(Longitudinal Section, 385X)

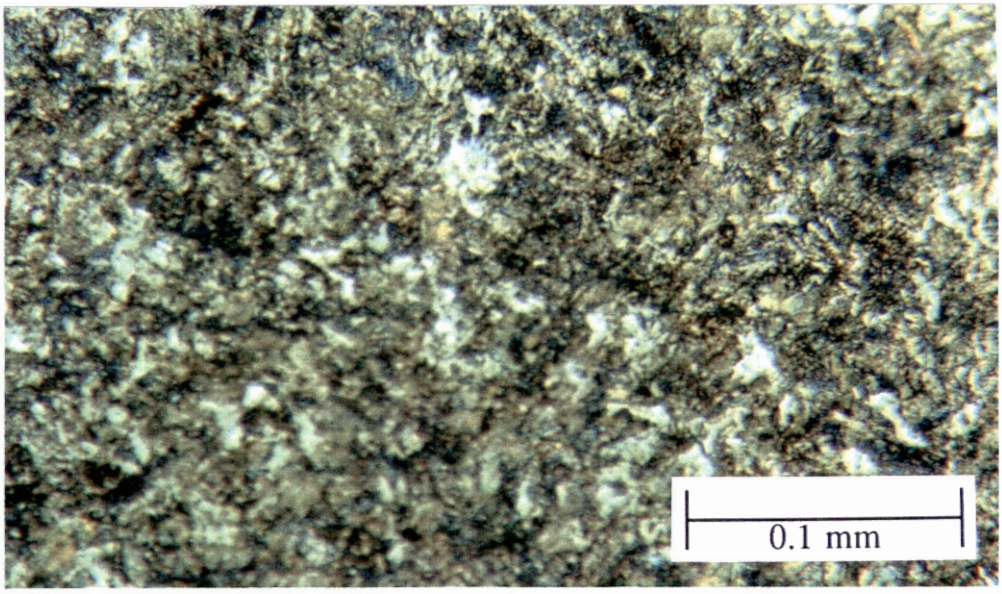

Figure 6.22 Same as Fig. 6.20, Cold Drawn to 0.1 in. Dia.
(Cross-Section, 385X)

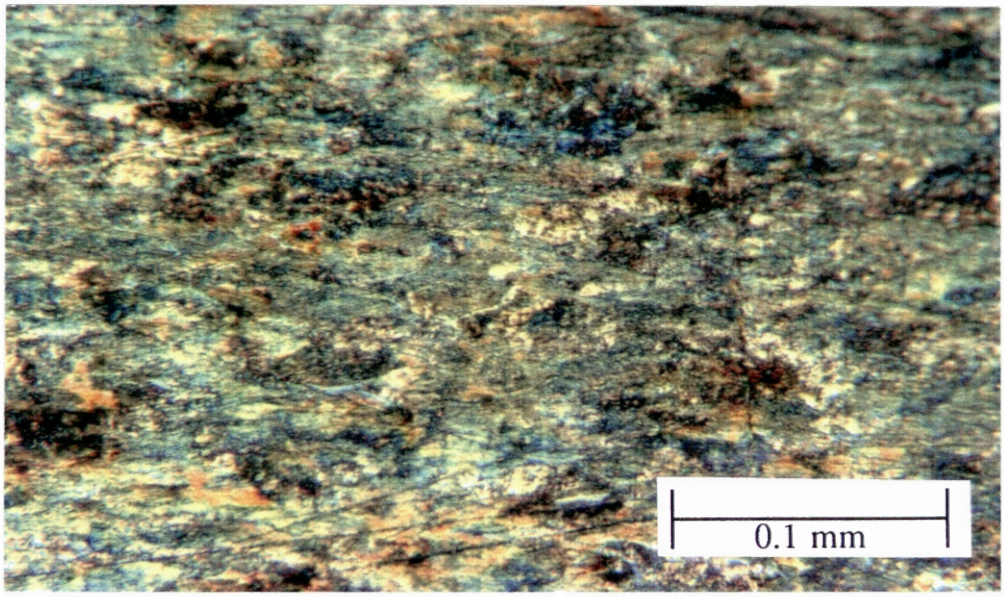

Figure 6.23 Same as Fig. 6.20, Cold Drawn to 0.1 in. Dia.
(Longitudinal Section, 385X)

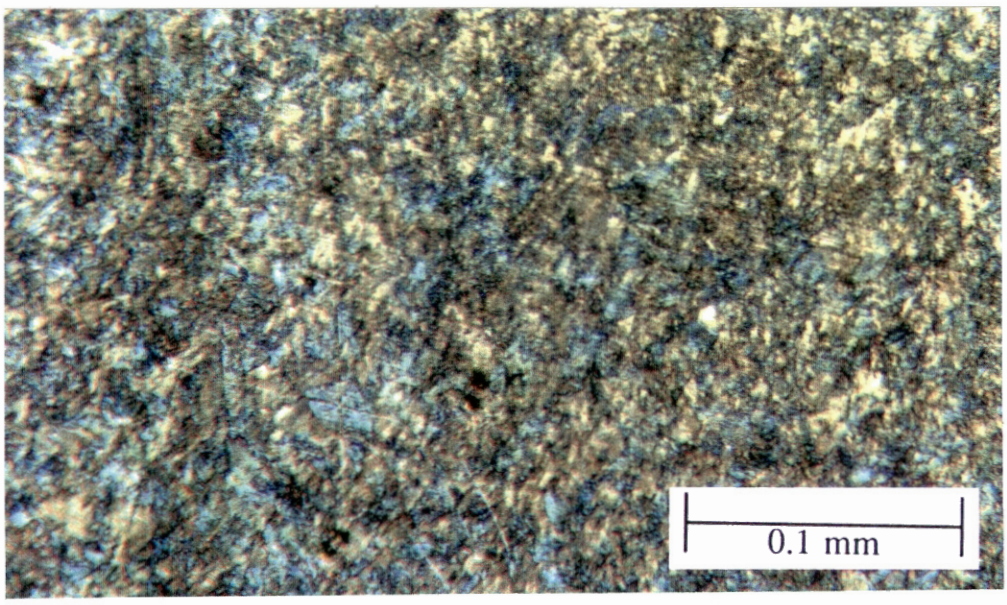

Figure 6.24 Same as Fig. 6.22, Cold Drawn to 0.086 in. Dia.
(Cross-Section, 385X)

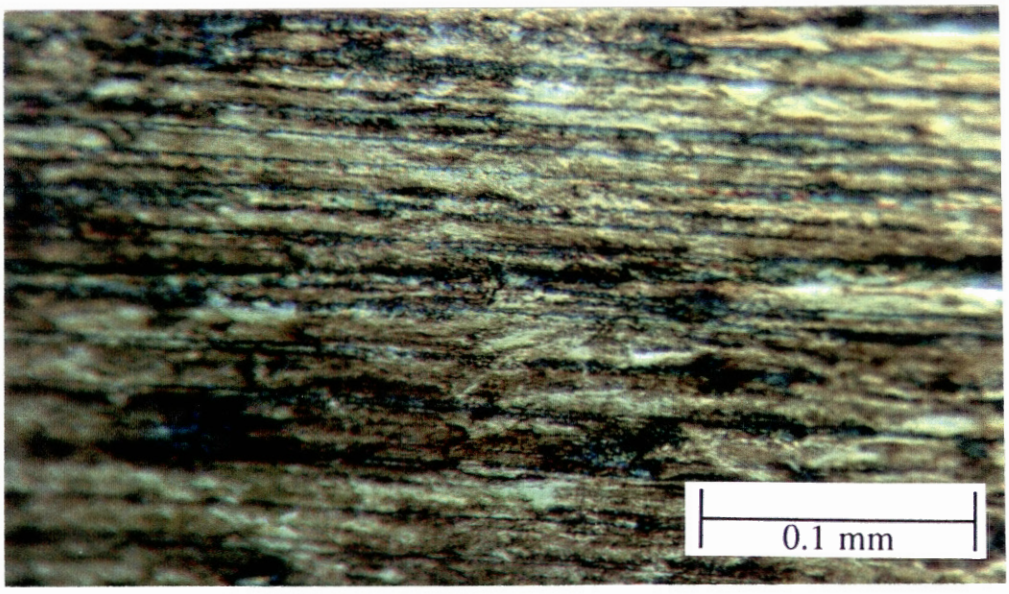

Figure 6.25 Same as Fig. 6.22, Cold Drawn to 0.086 in. Dia.
(Longitudinal Section, 385X)

CHAPTER VII

CONCLUSIONS AND RECOMMENDATIONS

The rigid-viscoplastic finite-element method has been successfully applied to the process of drawing rectangular bars. The finite element formulation and the calculation of total effective strain were discussed in detail. Since drawing is a steady-state process, a step-by-step analysis is not needed. Instead the total effective strains at the nodes are evaluated only once. The corresponding strain rates and flow stress values are solved for again. An iterative process was repeated until a desired converging solution was obtained.

Eight node brick elements were used to discretize the workpiece. Compared to the corner of the die the rest of the workpiece was discretized into coarser elements so as to reduce the computer time without sacrificing accuracy.

Velocity distributions were found to have the maximum value at the center of the rod and the minimum value at the corners of the die. Also velocity decreases from the exit of the die to the entrance of the die. Steady state drawing load decreases with larger die draft angles and increases with friction factor. Die pressure has the maximum value at the exit, decreases steeply towards the entrance and then increases gradually at the entrance. Flow stress, mean stress and effective strain-rate and the major principle stress are maximum at the corners of the die exit.

Its recommended to conduct experiments conditions similar to simulation conditions so that flow pattern, grain deformation, and hardness distribution can be correlated with strain rates, total effective strain etc. Additional changes have to be made to the program so that the drawing of more complex shapes can be simulated. The thermal model can also be

incorporated to study the effects of temperature. An expert system will be helpful to recommend process parameters and die design parameters based on the values of stress, strain-rates, material properties etc. from the existing program. A better pre- and post-processor need to be developed to use the simulation program more effectively.

REFERENCES

Aku, S. Y., R. A. C. Slater, and W. Johnson, "The use of Plasticine to Simulate the Dynamic Compression of Prismatic Blocks of Hot Metal," Int. J. Mech. Sci., 9, pp. 495-525, 1967.

Altan, T., S. Oh, and H. L. Gegel, "Metal Forming Fundamentals and Applications," American Society for Metals, 1983.

Andrews, K. R. F., G. l. England, and E. Ghani, "Classification of the Axial Collapse of Cylindrical Tubes under Quasi-Static Loading," Int. J. Mech. Sci., 25, No. 9/10, pp. 687-696, 1983.

ASM, Metals Handbook Forging and Casting, 5, 8th edition, pp. 41-47, American Society for Metals, 1970.

Atkinson, B., C. C. H. Card, and B. M. Irons, "Application of The Finite Element Method to Creeping Flow Problems," Trans. Inst Chem. Engrs., 48, pp. T276-T284, 1970.

Avitzur, B., "Metal Forming, Processes and Analysis," McGraw Hill, New York, 1968.

Chen, C. C. Finite-Element Analysis of Plastic Deformation in Metal-Forming Processes, Ph.D. Dissertation, Department of Mechanical Engineering, University of California, Berkeley, 1978.

Chen, C. C., and S. Kobayashi, "Deformation Analysis of Multi-Pass Bar Drawing and Extrusion," Annals of the CIRP, 27 1, pp. 151-155, 1978.

Chen, C. C., S. I. Oh, and S. Kobayashi, "Ductile Fracture in Axisymmetric Extrusion and Drawing, Part 1 Deformation Mechanics of Extrusion and Drawing," J. Engng. Indust., 101, pp. 23-35, 1979.

Chen, Fuh-kuo, "Applications of the Finite Element Method to the Plastic Deformation Analysis of Perforated sheet Metals and the Process Simulation of Shape Rolling," Ph.D. Dissertation, Department of Mechanical Engineering, University of California, Berkeley, 1989.

Cheng, Jung-Ho, and Noboru Kikuchi, "An Analysis of Metal Forming Processes Using Large Deformation Elastic -Plastic Formulations," Comput. Meths. Appl. Mech. Engrg., 49, pp. 71-108, 1985.

Chenot, J. L., "A Velocity Approach to Elasto-Plastic and Elasto-Viscoplastic Calculation by the Finite Element Method," J. Engng. Indust., 112, pp. 150-154, 1990.

Davis, E. A., and S. J. Dokos, "Theory of Wire Drawing," J. of Appl. Mech.," 11, Trans. ASME 66, pp. 192-198, 1944.

Dawson, R. D., and E. G. Thompson, "Finite Element Analysis of Steady-State Elasto-Viscoplastic Flow by the Initial Stress-Rate Method," Int. J. num. Meth. Engng., 12, pp. 47-57, 1978.

Drucker, D. C., and Prager W., "Soil Mechanics and Plastic Analysis or Limit Design," Quart. Appl. Math., 10, pp. 157-165, 1952.

Farren, W. S., and G. I. Taylor, "The Heat Developed During Plastic Extrusion of Metals," R. Soc. London, A107, pp. 422-451, 1925.

Frisch, J., and E. G. Thomsen, "An Experimental Study of Metal Extrusions at Various Strain Rates," J. Engng. Indust., Trans. ASME, 76, pp. 599-606, 1954.

Green, A. P., "On Unsymmetrical Extrusion in Plane Strain," J. Mech. Phys. Solids, 3, pp. 189-196, 1955.

Green, A. P., "Calculations on the Theory of Sheet Drawing," British Iron and Steel Research Association, Report MW/b/7/52, 1955.

Harper, S., A. R. Goreham, and A. A. Marks, "Some Modern Developments in Copper Wire Drawing," Metals and Materials, 4, pp. 335-339, 1970.

Hencky H., "Uber einige Statisch bestimmte Falle des Gleichgewichts in Plastischen Korpeln," Z. Angew. Math. Mech., 3, pp. 241-251, 1923.

Hill, R., "A Theoretical Analysis of the Stress and Strain in Extrusion and Piercing," J. Iron Steel Inst., 158 1, pp. 177-185, 1948.

Hill, R., and S. J. Tupper, "A New Theory of the Plastic Deformation in Wire-Drawing," J. Iron Steel Inst., 159, pp. 353-359, 1948.

Hosford, W. F. and R. M. Caddell, "Metal Forming Mechanics and Metallurgy", Prentice Hall Inc., 1983.

Iwatha, K., K. Osakada, and S. Fujino, "Analysis of Hydrostatic Extrusion by the Finite Element Method," J. Engng. Indust., 94, pp. 697-703, 1972.

Johnson, A. E., and N. E. Frost, "Rheology of Metals at Elevated Temperatures," J. Mech. Phys. Solids, 1, pp. 37-52, 1952.

Johnson, W., "Estimation of Upper Bound Loads for Extrusion and Coining Operations," Proc. Instn. Mech. Engrs, 173 1, pp. 61-72, 1959.

Johnson, W., and H. Kudo, "The Mechanics of Metal Extrusion," Manchester University Press, 1962.

Johnson, W., and P. B. Mellor, "Plasticity for Mechanical Engineers," Van Nostrand, London, 1962.

Kanazawa, K., and P. V. Marcal," Finite Element Analysis of the Steel Rolling Process, Applications of Numerical Methods to Forming Process," AMD, 28, pp.81, 1978.

Kawahara, M., and N. Takeuchi, "Mixed Finite Element Method for Analysis of Viscoelastic Fluid Flow," Computers and Fluids, 5, pp. 33-45, 1977.

Kobayashi, S., S. I. Oh, and T. Altan. Metal Forming and Finite-Element Method. Oxford University Press, 1989.

Korber, F., and A. Eichinger, "Die Grundlagen der bildsamen Verforming, "Mitt. K. W. Inst. Eisenforschung, 22, pp. 57, 1940.

Kudo, H., "An Upper-Bound Approch to Plane-strain Forging and Extrusion," Int. J. Mech. Sci., I, pp. 57-83, 1960.

Kudo, H., "An Upper-Bound Approch to Plane-Strain Forging and Extrusion - III," Int. J. Mech. Sci., 1, pp. 366-368, 1960.

Kudo H., "Study on Forging and Extrusion Processes: Part I - Analysis on Plane Strain Problems," Koku-kenkyu-sho Shuho, Tokyo University, Tokyo, Japan, 1: No.1, pp. 37-96, 1958.

Lange, Kurt, "Study Book of Forming Technology," Vol II - Massiuforming, Chapter 5, Springer-Verlag, Berlin-Heidelberg, New York, 1974.

Lange, Kurt, "Handbook of Metal Forming," McGraw-Hill Book Company, 1985.

Lee, C. H., and T. Altan, "Influence of Flow Stress and Friction Upon Metal Flow in Upset Forging of Rings and Cylinders," J. Engng. Indust., pp. 775-782, 1972.

Li, G. J., and S. Kobayashi, "Analysis of Spread in Rolling by the Rigid-Plastic, Finite Element Method," in Numerical Analysis of Forming Process, Edited by J. F. T. Pittman, O. C. Zienkiewiz, R. D. Wood, and J. M. Alexander, John Wiley & Sons, 1984.

Liu, J. Y., "An Analysis of Deformation Characteristics and Interfacial Friction Conditions in Simple Upsetting of Rings," J. Engng. Indust., 94, pp. 1149-1156, 1972.

Livesey, J. L., "Inertia Effects in Viscous Flows," Int. J. Mech. Sci., I, pp. 84-88, 1959.

Lynch, Frances De S., "A Finite Element Method of Viscoplastic Stress Analysis With Application to Rolling Contact Problems," Int. J. num. Meth. Engng., 1, pp. 379-394, 1969.

Maclellan, G. D. S., "A Critical Survey of Wire-Drawing Theory," J. of Iron and Steel Inst., 158, pp. 347-356, 1948.

Mori, K., and K. Osakada, "Simulations of Three-dimensional Rolling by the Rigid-plastic Finite Element Method," Proc. Num. Methods Ind. Forming Processes, Swansea, Pineridge Press, pp. 747, 1982.

Nayak, G. C., and O. C. Zienkiewicz, "Elasto-Plastic Stress Analysis. A Generalization for Various Constitutive Relations Including Strain Softening," Int. J. num. Meth. Engng., 5, pp. 113-135, 1972.

Oh, S. I., C. C. Chen, and S. Kobayashi, "Ductile Fracture in Axisymmetric Extrusion and Drawing," J. Engng. Indust., 101, pp. 36-44, 1979.

Oh, S. I., and S. Kobayashi, "An Approximate Method for a Three-Dimensional Analysis of Rolling," Int. J. Mech. Sci, 17, pp. 293-305, 1975.

Papsdorf, W., "Friction, Wear, and Lubrication in Wire Drawing," Stahl u. Eisen, 72, pp. 393, 1952.

Park, J. J., and S. Kobayashi, "Three-Dimensional Finite Element Analysis of Block Compression," Int. J. Mech. Sci, 26, No.3, pp. 165-176, 1984.

Park, J. J., and S. I. Oh, "Application of Three-Dimensional Finite Element Analysis to Metal Forming Processes," NAMRAC, pp. 296-303, 1987.

Perzyna, P., "Fundamental Problems in Viscoplasticity," Advan. Appl. Mech., 9, pp. 243-377, 1966.

Prager, W., "The Theory of Plasticity : A survey of Recent Achievements," Proc. Inst. Mech. Engrs., 169, Pt. 1 pp. 41-57, 169.

Prager, W., and P. G. Hodge, "Theory of Perfectly Plastic Solids'" Chapman and Hall, London, 1951.

Price III, S. H., and L. Vance, "Wiredrawing Dies: Industry Improvements," Wire J. Int., 21, pp. 63-67, 1988.

Ranger, A. E., "An Electrical Analogue for Estimating Die Temperatures During Wire Drawing," J. of Iron and Steel Inst., 185, pp. 383-388, 1957.

Rigby, G. L., and G. M. McNeice, "Further Limitations on General Hexahedron Finite Elements With Derivative Degrees of Freedom," Int. J. Num. Meth. Engng., 5, pp. 137-139, 1972.

Saches G., "Spanlose Forming der Metalle," Springer Varlag, Berlin, 1931.

Saches, G., and K. R. Van Horn, "Practical Metallurgy," American Socity for Metals, 1940.

Schey, J. A., "Tribology in Metalworking: Friction Lubrication, and Wear," ASM, Metals Park, Ohio, 1983.

Schreurs, P. J. G., F. E. Veldpaus, and W. A. M. Brekelmans, "Simulation of Forming Processes, Using the Arbitrary Eularian-Langrangian Formulation," Comput. Meths. Appl. Mech. Engrg., 58, pp. 19-36, 1986.

Shabaik, A. H., "Computer-Aided Viscoplasticity Solution to Axisymmetric Extrusion Through Curved Boundaries," J. Engng. Indust., 94, pp. 1225-1231, 1972

Siebel E., "Die Formgebung im bildsaman Zustande," Varlag Stahleisen, Dusseldorf, 1932

Shield, R. T., "Plastic Flow in a Converging Conical Channel," J. Mech. Phys. Solids, 3, pp. 246-258, 1955.

Shimazaki, Y., and E. G. Thompson, "Elasto Visco-Plastic Flow With Special Attention to Boundary Conditions," Int. J. num. Meth. Engng., 17, pp. 97-112, 1981.

Smets, J., and R. Mortier, "The Influence of Oxygen During Hot Rolling and Drawing of Continuous-Cast Rod," Wire J. Int., 17, Pt. 2 pp. 80-94, 1984.

Soyris, N., J. P. Cescutti, T. Coupez, G. Brachotte and J. L. Chenot, "Three Dimensional Finite Element Calculation of the Forging of a Connecting Rod," in Modelling of Metal Forming Processes, J. L. Chenot and E. Onate (eds), Kluwer Academic Publishers, 1988.

Su, Yea-Yang, "Analysis of the Factors Affecting the Drawability of Copper Rod," Wire J. Int., 15 Pt. 1, pp. 74-79, 1982.

Surdon, G.and J. L. Chenat, "Finite Element Calculations of Three-Dimensional Hot Forging," Int. J. Num. Meth. Engng., 24, pp. 2107-2117, 1987.

Thompson, E. G. , and H. M. Berman, "Steady-State Analysis of Elasto-Viscoplastic Flow During Rolling," in Numerical Analysis of Forming Processes, (Eds J. F. T. Pittman, R. D. Wood, J. M. Alexander and O. C. Zinkiewize), pp. J. Wiley & Sons, 1984.

Thomsen, E. G., and F. D. Negroni, "Strains in Multipass Drawing of Annealed Oxygen-Free Copper," J. of Engineering Materials and Technology, 110, pp. 361-363, 1988.

Thomsen E. G., Yang C. T., and Kobayashi S., "Mechanics of Plastic Deformation in Metal Processing," The Macmillan Company, New York, 1965.

William, P., "The Theory of Plasticity : A Survey of Recent Achievements," Proc. Inst. Mech. Engrs., 169, Pt. 1 pp. 41-57, 1955.

Wistreich, J. G., "The Fundamentals of Wire Drawing," Met. Rev., 3 10, pp. 97-142, 1958.

Wistreich, J. G., "Ringing in Wire Drawing Dies," J. Iron Steel Inst., pp. 162-164, 1951.

Wistreich, J. G., "Investigation of the Mechanics of Wire Drawing," Proc. Inst. Mech Engrs., 169, pp. 654-665, 1955.

Yang, C. T., "On the Mechanics of Wire Drawing," J. Engng. Indust., 83, pp. 523-530, 1961.

Yang, D. Y., C. M. Lee, and J. H. Yoon, "Finite Element Analysis of Stedy-State Three-Dimensional Extrusion of Sections Through Curved Dies," Int. J. Mech. Sci., 31 2, pp. 145-156, 1989.

Yu, Szu-wei, and E. G. Thompson, "A Direct Eulerian Finite Element Method for Steady State Elastic Plastic Flow," Numiform 89, pp. 95-103, 1989.

Zienkiewicz, O. C., and P. N. Godbole, "Flow of Plastic and Visco-Plastic Solids With Special Reference to Extrusion and Forming Process," Int. J. Num. Meth. Engng., 8 pp. 3-16, 1974.

Zienkiewicz, O. C., S. Valliappan, and I. P. King, "Elasto-Plastic Solutions of Engineering Problems 'Initial Stress', Finite Element Approch," Int. J. Num. Meth. Engng., 1, pp. 75-100, 1969.

Zienkiewicz, O. C., "The Finite Element Method," 3rd Edn., McGraw-Hill, New York, 1977.

APPENDIX

ROUTINES FOR CALCULATION OF EFFECTIVE STRAIN

All the programming was done in FORTRAN 77 on the CRAY Y-MP UNICOS operating system. The structure of the subroutines for the calculation of effective strain is shown in Fig. A.1. It should be noted that, in Fig. A.1, the calling sequence of the subroutines is shown and not the logical flow of the program. The dashed boxes indicate that the subroutines are called more than once for other calculations. A FORTRAN I/O device labelled 78 is used to input the data for applying the boundary condition of zero effective strain to the nodes at the back end of the die.

The global stiffness matrix is stored in the real band matrix form. The final equations are solved by calling the IMSL (International Mathematical and Statistical Library) routine LSLRB. The rest of this appendix lists the subroutines in Fig. A.1.

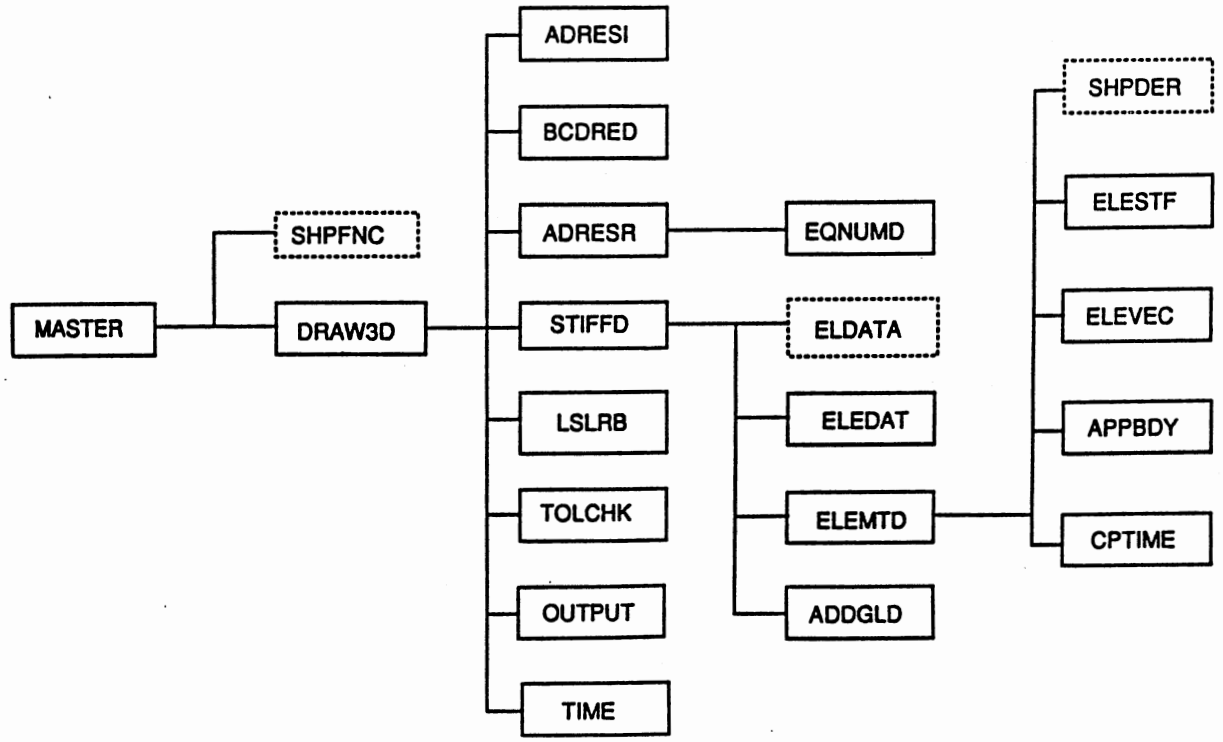

Figure A.1 Subroutine Structure for Calculation of Effective Strain

```
c---+----+----+----+----+----+----+----+----+----+----+----+----+----+--
c
      subroutine adresi(numnp,maxind)
c
c---+----+----+----+----+----+----+----+----+----+----+----+----+----+--
c
c     description
c       this routine determines addresses for md-series in common/adsind/
c
c       numnp  =  number of nodal points
c
c     output
c       common /adsind/
c
c     starting addresses
c       md1 : boundary condition codes for nodes
c       md2 : equation numbers in the global system to be solved
c
      implicit integer*4 (i,j,k,l,m,n), real*8 (a-h,o-z)
c
      common /adsind/ md1,md2,mdlast
      common /inout/ inpt,mssg
c
c  calculates addresses /adsind/
c
      md1    =  1
      md2    =  md1 + numnp
      mdlast =  md2 + numnp
c
      write(77,*) 'addresses for array nard'
      write(77,*) 'md1 = ',md1,' md2 = ',md2,' mdlast = ',mdlast
      if(mdlast.gt.maxind) goto 100
      return
c
  100 write(mssg,2010) mdlast
      stop
c
 2010 format(  46h stop because common/adsind/ size is too small,/,
     +         33h minimum size for input phase is ,i10)
c
      end
c---+----+----+----+----+----+----+----+----+----+----+----+----+----+--
c
      subroutine adresr(nel,nonp,numnp,numel,maxred)
c
c---+----+----+----+----+----+----+----+----+----+----+----+----+----+--
c
c     description
c       this routine determines addresses for kd-series in
c       common/adsred/
c
c     input (from common /mcd1/)
c       numel  =  number of elements
c       numnp  =  number of nodal points
c
c     output
c       common /adsred/
c
```

```
c    starting addresses
c      kd1 : solution vector
c      kd2 : elemental stiffness matrix
c      kd3 : elemental load vector
c      kd4 : global load vector
c      kd5 : global stiffness matrix
c
     implicit integer*4 (i,j,k,l,m,n), real*8 (a-h,o-z)
c
     common /adsred/ kd1,kd2,kd3,kd4,kd5,kdlast
     common /blind/  nard(1)
c
     common /band/  neleqd,neqd,nbw
      common /inout/ inpt,mssg
     common /adsind/ md1,md2,mdlast
c
     dimension nel(1)
c
c  calculates addresses /adsred/
c
     kd1    =  1
     kd2    =  kd1 + numnp
     kd3    =  kd2 + nonp*nonp
     kd4    =  kd3 + nonp
c
     call eqnumd(nard(md1),nel,numel,nard(md2),numnp)
c
     kd5    =  kd4 + neqd
     kdlast =  kd5 + neleqd
c
     write(77,*) 'addresses for array ad'
     write(77,*) 'kd1 = ',kd1,' kd2 = ',kd2,' kd3 = ',kd3
     write(77,*) 'kd4 = ',kd4,' kd5 = ',kd5,' kdlast = ',kdlast
c
     if(kdlast.gt.maxred) goto 100
     return
c
  100 write(mssg,2010) kdlast
      stop
c
 2010 format(  46h stop because common/adsred/ size is too small,/,
    +         33h minimum size for input phase is ,i10)
c
     end
c---+----+----+----+----+----+----+----+----+----+----+----+----+----+----+--
c
     subroutine appbdy(ppd,qqd,nonp)
c
c---+----+----+----+----+----+----+----+----+----+----+----+----+----+----+--
c
c    description
c      this routine specifies the initial effective strain values
c      to the elemental stiffness matrix
c
c      ppd    =  element stiffness matrix
c      qqd    =  element load      vector
c      elefst =  total effective-strain at the nodes of each element
c                from /elbc/
```

```
c      melbcd =  boundary condition codes of nodes from /elbc/
c      nonp   =  number of nodes of an element
c
      implicit integer*4 (i,j,k,l,m,n), real*8 (a-h,o-z)
c
     common /elbc/ melbcd(8),neleqn(8),elefst(8),efsr
c
     dimension  ppd(nonp,1),qqd(1)
c
      do 100      i =  1,nonp
c
     if(melbcd(i).eq.1) then
c
c  finds out eq. no. and eliminate.
c
         do  50  n =  1,nonp
        qqd(n)   =  qqd(n) - ppd(n,i)*elefst(i)
   50     continue
       endif
c
  100 continue
c
      return
      end
c---+----+----+----+----+----+----+----+----+----+----+----+----+----+--
c
     subroutine bcdred(mbcd,numnp,efst)
c
c---+----+----+----+----+----+----+----+----+----+----+----+----+----+--
c
c     description
c       this routine reads boundary conditions
c
c     note: the unit number of the "steady state info" file is "78"
c          ( opened by "subroutine allopn.for" which reads the unit
c             number from the file "d.mymap")
c
      implicit integer*4 (i,j,k,l,m,n), real*8 (a-h,o-z)
     character*60 trash
c
     common /adsind/ md1,md2,mdlast
      common /inout/inpt,mssg
     common /bcd1/tolrce
c
     dimension mbcd(1),efst(1)
c
      do 100 i = 1,numnp
  100  mbcd(i) = 0
c
      do 150 i = 1,10
       read(78,*) trash
  150  continue
c
     read(78,*) tolrce
     read(78,*) numbc
c
      do 200 i = 1,numbc
       read(78,*)np,mbcd(np),efst(np)
```

```
 200  continue
c
      return
      end
c---+----+----+----+----+----+----+----+----+----+----+----+----+----+--
c
      subroutine cptime(ifirst,timexx)
c
c---+----+----+----+----+----+----+----+----+----+----+----+----+----+--
c
c     description
c       this routine is a system dependent routine which is used to
c       determine the cpu time since the beginning of the job.
c
      implicit integer*4 (i,j,k,l,m,n), real*8 (a-h,o-z)
     real tarray(2)
      data timein /0.0/
c
c     some systems require an initialization call
c
      if(ifirst.eq.1) goto 20
c*r   call lib$init_timer
c**   call second(timein)  on cray
     call second(timein)
c** the following two lines for unix
c**   call etime(tarray)
c**   timein = tarray(2)
      return
c
   20 continue
c*r   call lib$stat_timer(2,itime)
c*r   timexx = itime/100.0
c**   call second(tmp)
     call second(tmp)
c** the following two lines for unix
c**   call etime(tarray)
c**   tmp = tarray(2)
      timexx=tmp-timein
      return
      end
c---+----+----+----+----+----+----+----+----+----+----+----+----+----+--
c
      subroutine draw3d(itol,iflagd)
c
c---+----+----+----+----+----+----+----+----+----+----+----+----+----+--
c
c                        draw3d
c
cc---+----+----+----+----+----+----+----+----+----+----+----+----+----+--
c      (Analysis of large plastic incremental deformation during the
c       drawing process - three dimensional application)
c        Date              February 1, 1990
c       Coded by        Vasudeva Prasad Ravi (405)744-7466
c                       (graduate student)
c                        Oklahoma State University
c                       Department of Mechanical & Aerospace Engineering
c                        Stillwater, OK 74078
c
```

```
c    <description>
c
c     draw3d is a fem code for three dimensional simulations
c     of the cold drawing process.
c
c     <some important features of draw3d are>
c     1. the code is based on rigid-viscoplastic finite element
c        formulation.
c     2. 8-node linear hexahedral isoparametric elements are used.
c     4. the code is modularized for versatility

c     <sponsorship>
c     This research was done under the guidance of
c                        Dr.Y. C. Shiau
c                       Oklahoma State University
c                     Department of Mechanical and Aerospace Engineering
c                       Stillwater, OK 74078
c     Technical questions regarding the program may be directed
c     to Dr. Y. C. Shiau orVasudeva Prasad Ravi at the above address
c
c     <history>
c     The theoretical basis used in this program was originally
c     developed by
c                        Professor    Shiro Kobayashi
c                       Department of Mechanical Engineering
c                        University of California
c                        Berkeley, CA 94720
c     and his coworkers.
c
      implicit integer*4 (i,j,k,l,m,n), real*8 (a-h,o-z)
c
     parameter(maxred = 120000, maxind = 10000)
c
     common /blred/ ad(maxred)
     common /blind/ nard(maxind)
c
      common /ads3/ m1,m2,m3,m4,m5,m6,mlast
     common /adsred/ kd1,kd2,kd3,kd4,kd5,kdlast
      common /eldt/ nonp,ndf,int1,int2,mxst,lel,lendf
      common /inout/inpt,mssg
      common /mcd1/ numnp,numel,nstep,itmax,numtr,numdie
      common /blin/ nar(1)
c
     common /adsind/ md1,md2,mdlast
     common /band/  neleqd,neqd,nbw
     common /bcd1/tolrce
c
c  in case more memory space is needed, increse dimensions of
c  common/blind/ and common/blred/, by changing the parameters
c  "maxred" & "maxind", accordingly.
c
c  initialize blank common/blind/ and common/blred/
c
      if (iflagd .eq. 0) then
c
        do 300 i  =  1,maxred
  300   ad(i)     =  0.0
c
```

```
      do 400 i  =  1,maxind
 400    nard(i)   =  0
c
       call adresi(numnp,maxind)
c
       call bcdred(nard(md1),numnp,ad(1))
c
       call adresr(nar(m5),nonp,numnp,numel,maxred)
c
       iflagd = 1
c
     else
c
       m = kd5-1
       do 500 i  =  1,neleqd
         ad(m+i) = 0.0
 500     continue
       m = kd4-1
       do 600 i  =  1,neqd
         ad(m+i) = 0.0
 600     continue
     endif
c
     m = kd4 -1
     do 22 i = 1, neqd
 22   continue
     call stiffd(nonp)
      write(77,*)'solving the global stiffness matrix ....'
     lda = 2*nbw + 1
     call lslrb(neqd,ad(kd5),lda,nbw,nbw,ad(kd4),1,ad(kd4))
     call tolchk(itol,ad(kd4),ad(kd1),nard(md2),numnp,tolrce,
     +            nonp,numel)
c
     return
     end
c---+----+----+----+----+----+----+----+----+----+----+----+----+----+--
c
     subroutine eldata(n,idrec)
c
c---+----+----+----+----+----+----+----+----+----+----+----+----+----+--
c
c    description
c      this routine transfers values from blank common to /elft/,
c      or vice versa.
c
c    n     =  element number
c    idrec =  1,  from blank common and /blin/  to  /elft/
c             2,  from /elft/  to  blank common and /blin/
c
     implicit integer*4 (i,j,k,l,m,n), real*8 (a-h,o-z)
c
      common /ads1/ n1,n2,n3,n4,n5,n6,n7,n8,n9,n10,n11,nlast
     common /ads2/ k1,k2,k3,k4,k5,klast
      common /ads3/ m1,m2,m3,m4,m5,m6,mlast
     common /eldt/ nonp,ndf,int1,int2,mxst,lel,lendf
     common /elft/ xyz(3,8),vg(3,8),vl(3,8),trn(9,8),
    +             sts(8),eps(8),teps,nbcd(3,8),nf(8),
    +             lrz(3,8),nel(8),matr
```

```
c
      common /blin/ nar(1)
      common        a(1)
c
      if(idrec.gt.1) goto 500
c
      ndf2     = ndf*ndf
c
      matr     = nar(m6 + n - 1)
      teps     =  a(n11+ n - 1)
c
      k        =  m5 + (n - 1)*nonp
c
      do 100 i  =  1, nonp
c
      nn       =  nar(k)
      nel(i)   =  nn
      nc       =  nar(m2 + nn - 1)
      nf(i)    =  nc
      np       =  (nn- 1)*ndf
c
      do  50 j  =  1, ndf
      xyz(j,i)  =  a(n1 + np)
      vg(j,i)   =  a(n2 + np)
      vl(j,i)   =  a(n3 + np)
      nbcd(j,i) =  nar(m1 + np)
      lrz(j,i)  =  nar(m3 + np)
   50 np        =  np + 1
c
      if(nc.eq.0)  goto 100
c
      np       =  (nc- 1)*ndf2
c
      do  70 j  =  1, ndf2
      trn(j,i)  =  a(n6 + np)
   70 np        =  np + 1
c
  100 k        =  k  + 1
      return
c
  500 continue
c
      np       =  (n - 1)*mxst
c
      do 550  i =  1, mxst
      a(n9 +np) =  sts(i)
      a(n10+np) =  eps(i)
  550 np       =  np + 1
c
      return
      end
c---+----+----+----+----+----+----+----+----+----+----+----+----+----+--
c
      subroutine eledat(n)
c
c---+----+----+----+----+----+----+----+----+----+----+----+----+----+--
c
c     description
```

```
c      this routine transfers values of mbcd and neqnum from
c       common/blind/ to common/elbc/
c
c     n     =   element number
c
      implicit integer*4 (i,j,k,l,m,n), real*8 (a-h,o-z)
c
      common /ads3/ m1,m2,m3,m4,m5,m6,mlast
      common /eldt/ nonp,ndf,int1,int2,mxst,lel,lendf
      common /adsind/ md1,md2,mdlast
      common /ads1/ n1,n2,n3,n4,n5,n6,n7,n8,n9,n10,n11,nlast
c
      common        a(1)
      common /blin/  nar(1)
      common /blind/ nard(1)
      common /blred/ ad(1)

c
      common /elbc/ melbcd(8),neleqn(8),elefst(8),efsr
c
      k       =  m5 + (n - 1)*nonp
c
      do 100 i  =  1, nonp
      nn      =  nar(k)
      np      =  (nn- 1)
      melbcd(i) =  nard(md1 + np)
      neleqn(i) =  nard(md2 + np)
      elefst(i) =  ad(1+np)
  100 k       =  k  + 1
c
      k1      =  n10 + (n-1) * mxst + (mxst-1)
      efsr    =  a(k1)
c
      return
      end
c---+----+----+----+----+----+----+----+----+----+----+----+----+----+--
c
      subroutine elemtd(ppd,qqd,nn)
c
c---+----+----+----+----+----+----+----+----+----+----+----+----+----+--
c
c     description
c       this routine calculates elemental stiffness matrix and load
c        vector.
c
c       calculated by gaussian quadrature
c
c     input
c       nn     =  element number
c
c     output
c       ppd    =  element stiffness matrix
c       qqd    =  element load      vector
c
      implicit integer*4 (i,j,k,l,m,n), real*8 (a-h,o-z)
c
      common /cptm/ tmcp(20),ncnt(5)
      common /eldt/ nonp,ndf,int1,int2,mxst,lel,lendf
```

```
      common /elft/ xyz(3,8),vg(3,8),vl(3,8),trn(3,3,8),
     +              sts(8),eps(8),teps,nbcd(3,8),nf(8),
     +              lrz(3,8),nel(8),matr
      common /tap2/ qdx(3,8,9),dxj(9)
      common /scrh/ ha(72),pa(216)
      common /elbc/ melbcd(8),neleqn(8),elefst(8),efsr
c
      dimension ppd(1),qqd(1)
c
c  int1=2 and int2=1 from common/eldt/
c
      intt1 = int1*int1*int1
      intt2 = int2*int2*int2
      intt  = intt1 + intt2
c
c  initializes ppd and qqd matrix.
c
      leld = nonp*nonp
c
      do  10  i = 1, leld
   10 ppd(i)    = 0.0
      do  20  i = 1, nonp
   20 qqd(i)    = 0.0
c
      call shpder(nn,xyz)
c
      call elestf(ppd,qdx(1,1,1),ha(1),vg(1,1),nonp,ndf,intt1,intt)
c
      call elevec(qqd,ha(1),efsr,nonp,intt)
c
      call appbdy(ppd,qqd,nonp)
c
      return
      end
c---+----+----+----+----+----+----+----+----+----+----+----+----+----+--
c
      subroutine elestf(ppd,qdx,ha,vg,nonp,ndf,intt1,intt)
c
c---+----+----+----+----+----+----+----+----+----+----+----+----+----+--
c
c     description
c       this routine generates the elemental stiffness matrix ppd
c
c     input
c       qdx   =  derivatives of shape functions
c       ha    =  values of the shape functions at the integration points
c       vg    =  nodal velocity components in the global coordinate system
c       nonp  =  number of nodal points in an element
c       ndf   =  number of degrees of freedom
c
c     output
c       ppd   =  elemental stiffness matrix
c
      implicit integer*4 (i,j,k,l,m,n), real*8 (a-h,o-z)
c
      dimension ppd(nonp,nonp),qdx(ndf,nonp,intt),ha(nonp,intt),
     + vg(ndf,nonp),wf(8)
c
```

```
c  wf: weighting factor (= 1*1*1)
      data wf / 8*1.0 /
c
      do 100 int = 1,intt1
      do 100 i = 1,nonp
      do 100 j = 1,nonp
      sum = 0
      do 110 k = 1,ndf
      sum = sum + vg(k,j)*qdx(k,j,int)
 110  continue
      ppd(i,j) = ppd(i,j) + sum*ha(i,int)*wf(int)
 100  continue
c
      return
      end
c---+----+----+----+----+----+----+----+----+----+----+----+----+----+--
c
      subroutine elevec(qqd,ha,efsr,nonp,intt)
c
c---+----+----+----+----+----+----+----+----+----+----+----+----+----+--
c
c     description
c       this routine calculates the elemental load vector
c
c     input
c       ha   =  values of the shape functions at the integration points
c       efsr  =  effective strain rate at the center of the element
c       nonp =  number of nodal in an element
c
c     output
c       qqd  =  elemental load vector
c
      implicit integer*4 (i,j,k,l,m,n), real*8 (a-h,o-z)
c
      dimension qqd(nonp),ha(nonp,intt)
c
c     wf  = weighting factor (= 2*2*2)
      data wf /8.0/
c
      do 100 i = 1,nonp
 100  qqd(i) = wf*ha(i,intt)*efsr
c
      return
      end
c---+----+----+----+----+----+----+----+----+----+----+----+----+----+--
c
      subroutine eqnumd(mbcd,nel,numel,neqnum,numnp)
c
c---+----+----+----+----+----+----+----+----+----+----+----+----+----+--
c
c     description
c       this routine decides equation number of nodal variables
c       and determines the band width of the stiffness matrix.
c
c     input
c       mbcd     =  boundary condition codes
c       nel      =  element connectivity
c       numel    =  number of elements
```

```
c      numnp    = number of nodal points
c
c     output
c      neqnum   = equation numbers
c      neleqd   = number of components in global stiffness matrix
c                (neleq = neq*(1+2*nbw))
c      neqd     = number of equations
c      nbw      = band width of the stiffness matrix
c
      implicit integer*4 (i,j,k,l,m,n), real*8 (a-h,o-z)
c
      common /eldt/ nonp,ndf,int1,int2,mxst,lel,lendf
     common /band/ neleqd,neqd,nbw
c
     dimension  mbcd(1),neqnum(1),nel(nonp,1)
c
c  initializes neqnum and assigns/counts equation no
c
      neqd     = 0
c
      do 100  n =  1,numnp
       neqnum(n) = 0
       if(mbcd(n).ne.1) then
         neqd     = neqd + 1
         neqnum(n)   = neqd
       endif
 100  continue
c
c  determines the band width of the stiffness matrix
c
      nbw = 0
      do 200 k =1,numel
        do 200 i =1,nonp
          do 200 j =1,i
           nb = iabs(nel(i,k) - nel(j,k))
           if (nb .gt. nbw) nbw = nb
 200  continue
     neleqd = neqd*(1+2*nbw)
c
      write(77,*) 'number of comp in glo stiff mat (neleqd) = ',neleqd
      write(77,*) 'number of equations (neqd) = ',neqd
c     write(77,*) 'band width of the stiffness matrix (nbw) = ',nbw
c
      return
      end
c---+----+----+----+----+----+----+----+----+----+----+----+----+----+--
c
      subroutine master
c
c---+----+----+----+----+----+----+----+----+----+----+----+----+----+--
c
c     description
c
c       this routine is the master module to control step solution
c       procedure consisting of
c
c         1.  k-series address determination
c         2.  velocity solution
```

```
c       3. checking the boudary condition
c       4. determining step size
c       5. update process condition
c        6. print out the solution
c
      implicit integer*4 (i,j,k,l,m,n), real*8 (a-h,o-z)
c
      common /ads1/ n1,n2,n3,n4,n5,n6,n7,n8,n9,n10,n11,nlast
      common /ads2/ k1,k2,k3,k4,k5,klast
      common /ads3/ m1,m2,m3,m4,m5,m6,mlast
      common /cptm/ tmcp(20),ncnt(5)
      common /eldt/ nonp,ndf,int1,int2,mxst,lel,lendf
      common /mcd1/ numnp,numel,nstep,itmax,numtr,numdie
      common /mcd2/ dtmax,dsmax
c
      common /blin/ nar(1)
      common        a(1)
c
      dtmx     = dtmax
c
      nst      = a(1) + 1
      ned      = a(1) + nstep
c
      mflag    = 0
      if(nst.eq.1) mflag = 1
c
c  evaluate shape functions and derivatives
c
      call shpfnc
c
c  step iteration starts from here.
c
      do 1000 nrt =  nst,ned
c
  100 a(1)       =  nrt
      call cptime( 1,tmcp(11))
c
c  cleans boundary condition for nodes to be seperated from dies.
c
c     call modbcs(nar(m1),nar(m2),a(n4),numnp,ndf)
c
  200 nrr        =  nrt - nst
c
c  determines k-series address.
c
      call adres2(nrr)
c
 c  set up local coord. systems
 c
      call trnmat(a(n1),a(n6),a(n7),nar(m1),nar(m2),numnp,ndf)
c
c  impose die velocity to touching nodes in terms of local coord.
c
      call dievel(a(n3),a(n6),nar(m1),nar(m2),numnp,ndf)
c
c  obatains one step solution.
c
      iflagd = 0
```

```
      itol   = 0
      nrtt   = 0
c
 999  continue
      write(77,*) 'executing nonlin ... . . . .'
c
      call nonlin(mflag)
      nrtt    = nrtt + 1
c
      write(77,*) 'out of nonlin'
      write(77,*) 'iteration no. ',nrtt
c
c*c testing
      write(77,*)'itol = ',itol
      write(77,*) 'executing draw3d ... . . . .'
     call draw3d(itol,iflagd)
     write(77,*) 'out of draw3d'
      write(77,*)'itol = ',itol
c
c*c
      call outmdl(nrtt)
c*c
      if (nrtt .eq. 4) goto 1000
      if (itol .eq. 0) goto 999
      if (itol .eq. 1) goto 1000
c
c  checks boundary conditions whether nodes should be seperated.
c
      call cptime( 1,tmcp(19))
     call chkbcs(a(n5),a(n6),a(n7),nar(m1),nar(m2),numnp,ndf,mflag)
c*** temporary aborted (1-27-89) ********* resumed on (2-24-89) ***
      if(mflag.ne.0) go to 200
c
      if(dsmax.ge.1.0d+09) goto 300
c
c  finds the maximum strain-rate.
c
      call stnmax(a(n10),stnmx,numel,mxst)
      tmin1 = dsmax/stnmx
c
  300 continue
c
c  determines time step.
c
      call chkstp(a(n1),a(n2),nar(m1),nar(m2),dtmx,tmin,numdie,
     +            numnp,ndf)
c
      if(dsmax.gt.1.0d+09) goto 350
      if(tmin .gt.  tmin1) tmin = tmin1
c
  350 odds  = dtmx - tmin
c
c  updates wopkpiece -  geometry, strain,
c         dies      -  stroke, force,
c
      call postpr(a(n1),a(n2),a(n5),a(n6),a(n10),a(n11),nar(m1),
     +            nar(m2),tmin,nrt,mxst,ndf)
c
```

```
      call cptime( 1,tmcp(20))
      tmcp(7)    =  tmcp(7) + tmcp(20) - tmcp(19)
      ncnt(5)    =  ncnt(5) + 1
c
      tmcp(3)    =  tmcp(3) + tmcp(20) - tmcp(11)
      ncnt(1)    =  ncnt(1) + 1
c
      a(2)       =  a(2)    + tmin
      dtmx       =  abs(odds)
      if(dtmx.lt.1.0d-05) goto 500
      mflag      =  1
      go to 100
  500 dtmx       =  dtmax
c
c  prints/stores the step solution.
c
      call outmdl(nrt)
c
      call cptime( 1,tmcp(15))
      tmcp(4)    =  tmcp(4) + tmcp(15) - tmcp(20)
      ncnt(2)    =  ncnt(2) + 1
c
 1000 continue
c
      return
      end
c---+----+----+----+----+----+----+----+----+----+----+----+----+----+--
c
      subroutine shpder(nn,xyz)
c
c---+----+----+----+----+----+----+----+----+----+----+----+----+----+--
c
c     description
c       this routine calculates derivatives of shape functions
c       and determinants of jacobian matrix
c
c     input
c       nn  =  element number
c       xyz =  nodal point coordinates of the element
c
c     output
c       common /tap2/
c
      implicit integer*4 (i,j,k,l,m,n), real*8 (a-h,o-z)
c
      common /eldt/ nonp,ndf,int1,int2,mxst,lel,lendf
      common /inout/inpt,mssg
      common /scrh/ ha(72),pa(3,8,9)
      common /tap2/ qdx(3,8,9),dxj(9)
c
      dimension xyz(3,1)
      dimension rj(3,3),xj(3,3)
c
      int        =  int1*int1*int1 + int2*int2*int2
c
      do 1000 it  =  1, int
c
      do  100 i   =  1, ndf
```

```
      do  100 j   =  1, ndf
      xj(i,j)     =  0.0
cdir$ shortloop
      do 100  k   =  1,nonp
      xj(i,j)     =  xj(i,j) + pa(i,k,it)*xyz(j,k)
  100 continue
c
c  evaluate dj - determinant of jacobian matrix
c
      dj        =   xj(1,1)*xj(2,2)*xj(3,3) + xj(1,2)*xj(2,3)*xj(3,1)
     +            + xj(1,3)*xj(2,1)*xj(3,2) - xj(3,1)*xj(2,2)*xj(1,3)
     +            - xj(2,1)*xj(1,2)*xj(3,3) - xj(1,1)*xj(2,3)*xj(3,2)
c
      dxj(it)   =  dj
      if(dj.lt.1.0e-09) goto 1500
c
c  inverse of jacobian matrix
c
      rj(1,1)   = (xj(2,2)*xj(3,3)-xj(2,3)*xj(3,2))/dj
      rj(1,2)   = (xj(3,2)*xj(1,3)-xj(1,2)*xj(3,3))/dj
      rj(1,3)   = (xj(1,2)*xj(2,3)-xj(1,3)*xj(2,2))/dj
      rj(2,1)   = (xj(3,1)*xj(2,3)-xj(2,1)*xj(3,3))/dj
      rj(2,2)   = (xj(1,1)*xj(3,3)-xj(3,1)*xj(1,3))/dj
      rj(2,3)   = (xj(2,1)*xj(1,3)-xj(1,1)*xj(2,3))/dj
      rj(3,1)   = (xj(2,1)*xj(3,2)-xj(3,1)*xj(2,2))/dj
      rj(3,2)   = (xj(3,1)*xj(1,2)-xj(1,1)*xj(3,2))/dj
      rj(3,3)   = (xj(1,1)*xj(2,2)-xj(2,1)*xj(1,2))/dj
c
c  evaluates  qdx  from  pa and rj.
c
      do  200  j   =  1,nonp
      do  200  i   =  1,ndf
      qdx(i,j,it)  =  0.0
cdir$ shortloop
      do 200   k   =  1,ndf
      qdx(i,j,it)  =  qdx(i,j,it) + rj(i,k)*pa(k,j,it)
  200 continue
c
 1000 continue
c
      return
c
 1500 continue
c
c  dj is zero or negative
c
      write(mssg,1010) dj,it,nn
      stop
c
 1010 format(//,50h program stops because of negative jacobian value ,
     +  e15.7,/, 4h at ,i2,37h -th integration point of element no.,i5)
      end
c---+----+----+----+----+----+----+----+----+----+----+----+----+----+--
c
      subroutine shpfnc
c
c---+----+----+----+----+----+----+----+----+----+----+----+----+----+--
c
```

```
c    description
c      this routine evaluates values of linear shape functions and
c      their derivatives at integration points in terms of natural
c      coordinate system.  this routine is set up for for nine
c      integration points for eight node linear hexahedral element.
c      nine integration points consist of eight regular points and
c      center point.
c
c    input
c      data pt
c
c    output
c      common /scrh/
c
     implicit integer*4 (i,j,k,l,m,n), real*8 (a-h,o-z)
c
     common /scrh/ ha(72),pa(216)
     common /eldt/ nonp,ndf,int1,int2,mxst,lel,lendf
c
     dimension pt(3,3)
c
     data  pt/ 0.0d0           , 0.0d0           , 0.0d0           ,
    +        -0.5773502691896d0, 0.5773502691896d0, 0.0d0           ,
    +        -0.7745966692415d0, 0.0d0           , 0.7745966692415d0/
c
     data  int1/2/, int2/1/
c
     kint      = 0
c
     do  100 i  =  1, int1
     t         =  pt(i,int1)
c
     do  100 j  =  1, int1
     s         =  pt(j,int1)
c
     do  100 k  =  1, int1
     r         =  pt(k,int1)
c
     kint      =  kint + 1
c
     na        =  (kint - 1)*nonp + 1
     nb        =  (na   - 1)*ndf  + 1
c
     call hexadr(r,s,t,ha(na),pa(nb))
c
  100 continue
c
     do  200 i  =  1, int2
     t         =  pt(i,int2)
c
     do  200 j  =  1, int2
     s         =  pt(j,int2)
c
     do  200 k  =  1, int2
     r         =  pt(k,int2)
c
     kint      =  kint + 1
c
```

```
      na        = (kint - 1)*nonp + 1
      nb        = (na   - 1)*ndf  + 1
c
     call hexadr(r,s,t,ha(na),pa(nb))
c
  200 continue
c
      return
      end
c---+----+----+----+----+----+----+----+----+----+----+----+----+----+--
c
      subroutine stiffd(nonp)
c
c---+----+----+----+----+----+----+----+----+----+----+----+----+----+--
c
c     description
c       this routine assembles global stiffness matrix and load vector
c
      implicit integer*4 (i,j,k,l,m,n), real*8 (a-h,o-z)
c
     common /adsred/ kd1,kd2,kd3,kd4,kd5,kdlast
     common /blred/  ad(1)
      common /mcd1/ numnp,numel,nstep,itmax,numtr,numdie
c
      do 1000 n =  1, numel
c
c  move element information to common /elft/ and /elbc/
c
     call eldata(n,1)
     call eledat(n)
c
c  elemental stiffness matrix.
c
     call elemtd(ad(kd2),ad(kd3),n)
c
c**    write(77,*) 'elemental stiffness matrix for element ',n
c**    m = kd2 -1
c**    do 99 i = 1,64
c**      write(77,*) 'ad(',m+i,') = ',ad(m+i)
c** 99   continue
c
c  add to the global stiffness matrix
c
     call addgld(ad(kd2),ad(kd3),ad(kd4),ad(kd5),nonp)
c
 1000 continue
c
      return
      end
c---+----+----+----+----+----+----+----+----+----+----+----+----+----+--
c
      subroutine tolchk(itol,snew,sold,neqnum,numnp,tolrce,nonp,numel)
c
c---+----+----+----+----+----+----+----+----+----+----+----+----+----+--
c
c     description
c       this routine checks the solution to see if it meets a
c      pre-determined tolerance
```

```
c
c     snew : new solution vector
c     sold : old solution vector
c
c     output
c       itol = set to "1" if tolerance is met
c            = set to "0" if tolerance is not met
c
      implicit integer*4 (i,j,k,l,m,n), real*8 (a-h,o-z)
c
      common        a(1)
      common /blin/ nar(1)
      common /ads3/ m1,m2,m3,m4,m5,m6,mlast
      common /ads1/ n1,n2,n3,n4,n5,n6,n7,n8,n9,n10,n11,nlast
c
     dimension snew(1), sold(1), neqnum(1)
c
      sum = 0.0
      do 100 i = 1,numnp
       k = neqnum(i)
         if (k .ne. 0) then
c*c          write(77,*)'new = ',snew(k),' old = ',sold(i)
          sum = sum + (snew(k) - sold(i))**2
          sold(i) = snew(k)
         endif
 100  continue
c
        write(77,*)'sum = ',sum
      tol = sqrt(sum)
      write(77,*)'tol = ',tol
      write(77,*)'tolrce = ',tolrce
      if (tol .lt. tolrce) itol = 1
c
c calculate the value of the total effective strain at the
c center of each element and put it in the original array
c i.e in a(n11).
c
      jj        = n11 - 1
      do 200 n   = 1,numel
        teps     = 0.0
        k        = m5 + (n - 1)*nonp - 1
          do 300 i = 1,nonp
            ii     = nar(k + i)
            teps   = teps + sold(ii)
 300        continue
        a(jj+n)  = teps/8.0
        write(77,*)'teps(',n,') = ',a(jj+n)
 200  continue
c
      return
      end
```

VITA

Vasudeva Prasad Ravi

Candidate for the Degree of

Master of Science

Thesis : STEADY-STATE VISCOPLASTIC ANALYSIS OF METAL FLOW DURING COLD DRAWING

Major Field : Mechanical Engineering

Biographical :

Personal Data : Born in India, June 5, 1967, son of Janardhana Choudhary Ravi and Radha Kumari Ravi .

Education : Received Bachelor of Engineering in Mechanical Engineering from the Osmania University, Hyderabad, India, in April, 1988; completed requirements for the Master of Science degree at Oklahoma State University in May, 1992.

Professional Experience : Teaching Assistant, CAD/CAM and Interactive Graphics Research Facility, Oklahoma State University, August, 1988, to March, 1992; Research Assistant, Manufacturing Processes and Materials Research Group, Oklahoma State University, August, 1989, to March, 1992.